Alessandro Burini

Vineyard Precision Farming by means of Satellite Data: Optical and Polarimetric Radar Data Safeguarding the Frascati d.o.c. Area

---

Geoinformation Ph.D. Program

Tor Vergata University
Rome, Italy

June 2009

Tor Vergata University
Rome, Italy

Computer, Systems and Production Engineering

GeoInformation Ph.D. Thesis

Vineyard Precision Farming by means of Satellite Data: Optical and Polarimetric Radar Data Safeguarding the Frascati d.o.c. Area

Candidate

Ing. Alessandro Burini ....

Mentor

Prof. Domenico Solimini ....

June 2009

"Considerate la vostra semenza:
fatti non foste a viver come bruti
ma per seguir virtute e canoscenza"
(Dante Alighieri)

Acknowledgements

La domanda a cui rispondere è: "cosa è rimasto di questi anni?". Matrici di scattering? L'ennesima "alzataccia" per capire se il vignaiolo ha deciso di arare, concimare, vendemmiare, potare, ecc ...? Il mal di pancia dopo essermi mangiato una cassa d'uva durante le "ground truth measurements"? Oppure il mal di testa causato da una bottiglia di Frascati ("Poggio Regillo" per la precisione)?

Sarebbe anche doveroso cercare di rispondere a "che cosa ho imparato?" IDL, ENVI e tutti i vari tool di telerilevamento? Ad aprire qualsiasi formato di dato mi venisse fornito?

Mi sono rimasti tanti ricordi, tante persone per cui è valsa la pena provare a tirare avanti sempre e comunque. Alcuni sono passati, altri sono dei buoni amici. Credo sia questa la cosa importante.

Ho imparato a risolvere problemi, a non scoraggiarmi quando non funziona niente e a rimboccarmi le maniche quando il lavoro è proprio più grande di quanto preventivato. Ho imparato a misurare le persone e a frenare l'entusiasmo, anche se non ho ancora capito perchè abbia dovuto dosare la voglia di fare. Ho imparato che con un sorriso anche il più amaro dei bocconi va giù e che delle volte è proprio inutile chiedere il permesso... meglio fare senza pensarci troppo e trovarti una buona scusa nel caso le cose vadano nel verso sbagliato!

E così ecco l'ultima fatica che prende forme, giorno dopo giorno, notte dopo notte, fino al momento in cui arriva il tanto desiderato e temuto giorno della resa dei conti. Ed è prima di affrontare questo giorno che voglio ringraziare le persone che nel bene o nel male, volenti o meno, sono state compagne di viaggio.

Un posto speciale va a Maria Grazia, un'anima bella che con la sua semplicità ha saputo ascoltarmi nei momenti più scuri e supportarmi quando ad andare avanti non ce la facevo proprio. Un ringraziamento per tutti questi anni va alla mia famiglia, delle persone splendide che, vicine o lontane, hanno sempre fatto sentire il loro calore... Mamma, Papà e Luca.

A Cosimo, compagno di ventura, va un abbraccio affettuoso per i momenti passati durante questi anni. Un pensiero anche ad Antonio e Federico, e ai colleghi dell'EoLab di Tor Vergata, specialemente ad Emanuele e Lino, che dall'esame di dottorato fino ad oggi si sono trovati sulla mia stessa barca (delle volte sembrava più un gommone rattoppato!).

Grazie a tutti di cuore.

I would like to acknowledge Prof. Domenico Solimini for the availability and support always provided during the whole course of this PhD work. The professionalism of Luigi Fusco (ESA) and Ralf Horn (DLR) during the "Bacchus-DOC" project is gratefully acknowledged.

Contents

Abstract

Some decades of observations have demonstrated the usefulness of space-borne optical sensors in agriculture. Progress in spatial, spectral, and temporal resolutions brought in by recent satellites, like QuickBird and Ikonos, Spot-5 or Kompsat-2 is resulting beneficial to precision farming practices (Arkun et al., 2005). Imagery from space spots spatial and temporal anomalies of crop vigor and biomass and allows timely remedial treatments (Johnson, 2004). Likewise, the crop response to the adopted local agronomic strategies is revealed (Johnson et al., 2004), while preserving the capability of monitoring land use at regional level. In several developed countries, customized services, such as grid soil sampling, yield mapping, variable rate application of fertilizers and pesticides, are now available (Srinivasan, 2006).

Especially in the last decade, some premium-wine producers approached space remote sensing technology with the main intent of enhancing the quality of their product. Indeed, while the cellar practices are being increasingly controlled and automated, on the field the operations mainly rely on individual skills of personnel and the quality of grapes remain subject to climatic variability. Leaf Area Index (LAI) of vines is related to fruit ripening rate, disease incidence and grape quality (Winkler, 1958) and the phenological state is crucial for the timing of the correct cultivation practices and of harvest (Moran et al., 1997). Soil Moisture Content (SMC) maps provide additional information for managing pesticides and fertilizations or, where allowed, for watering. Such parameters can be monitored by space-borne sensors and effectively handled by Geographic Information Systems (GIS) (Pearson et al., 1997a). Hence, space Earth Observation technology begins to look an attractive element of the wine producing chain.

Since 2000, an airborne hyperspectral system (ITRES, 1996) has been deployed in Australia as a support to the wine industry (Cochrane, 2000). Several experiments took place in California, U.S.A., to assess the serviceability of optical images from Unmanned Aerial Vehicle (UAV) (Johnson et al., 2003), or from space Johnson et al. (2004). In Europe, airborne remote sensing has been proposed for the detection of dead vine trees Chanussot et al. (2005). In Italy, an experiment was carried out in 2005 in the Franciacorta wine producing area based on the retrieval of the Normalized Vigor Index (NVI) from multispectral images acquired by IKONOS Brancadoro et al. (2006)

The potential of SAR images in monitoring the development and conditions of vegetation has been investigated in a number of studies e.g., Brisco and Brown (1998), Ferrazzoli (202),Toan et al. (1997), Della Vecchia et al. (2008). Specific analyses of radar images of vineyards are scarce in literature and manly focused on the effect of the periodicity in rows and vine supporting structures (Lewis et al., 1999). Indeed, the radar sensitivity to tree biomass stems from the different volumes of woody matter which affect the wave-plant-soil interaction mechanisms. In their development cycles, crops like maize, sunflower, colza, or alfalfa, considerably change the number, dimensions and shapes of the scattering elements, thus modifying their radar return. The situation is different when the plants have a stable woody structure which is only slightly modified by developing twigs, leaves and fruits. In this case, monitoring biomass evolution by radar is made difficult by the small variations of backscattering with respect to a strong, almost saturated (at least at C-band) background. Measurements on vineyards are even more difficult, given the high number of poles and metallic wires supporting the runners. For given radar frequency, polarization and observation angle, the backscattering depends on several parameters, including slope of the imaged vineyard, soil roughness, soil moisture content, weeds, cultivation aspect, geometry of supporting structures, plant type and state, and, finally, on the fruit biomass.

In an attempt to gain some insight on the potential of SAR in monitoring vineyards, and, especially, grape biomass, several experiments have been

carried out by means of different sensors, both optical and Radar, at several frequencies, ground resolutions and different polarimetric mode. Moreover, ground observations have been carried out to better understand the complex interaction between SAR and vineyards. After a first presentation of the state of the art on vineyard precision farming, several experiments by means of radar instruments will be presented and results critically discussed. Finally, a precision farming system prototype is presented.

Chapter 1

Introduction and State of Art

This chapter introduces the state of the art in precision farming by means of satellite data. In particular, several techniques, in the optical and microwave domain, will be considered. The reader will find a short overview of the precision farming systems and techniques available in the literature. An outline and a summary of the PhD study will conclude the chapter.

1.1 Precision Agriculture: An Overview

Agriculture dominates the worlds land use decisions. The urgent need for doubling farm production over the next 25 years on less land with less water through further intensification would inevitably involve substantial social, economic, and environmental costs. Identification of tools to minimize such costs through enhanced productivity and economic profits while simultaneously conserving the environment is, therefore, crucial. Precision agriculture (PA) is one of such tools catching worldwide attention since the early 1990s. PA is defined and termed in many ways, but the underlying concept remains the same. It is known as precision farming, information-intensive agriculture, prescription farming, target farming, site specific crop management, variable rate management, variable rate technology (VRT), farming by soil, grid soil sampling agriculture, grid farming, Global Positioning Systems (GPS) agriculture, farming by the inch, farming by the foot, and so on. In simple terms, PA can be defined as **a holistic and environmentally friendly strategy in which farmers can vary input use and cultivation methods** (including application of seeds, fertilizers, pesticides, and water, variety selection, planting, tillage, harvesting) **to match varying soil and crop conditions across a field**. A few other definitions of PA are given as follows.

- Careful tailoring of soil and crop management to fit the different conditions found in each field (Johannsen, 1996).

- Information gathering, management planning, and field operations that improve the understanding and management of soil and landscape resources so the cropping inputs of management practices are utilized more efficiently than with conventional one-fits-all strategies (Kitchen et al., 1996).

- Farmers use GPS technology involving satellites and sensors on the ground and intensive information management tools to understand variations in resource conditions within fields. They use this information to more precisely apply fertilizers and other inputs and to more accurately predict crop yields (Agriculture Committee, 2000).

- Application of technologies and principles to manage spatial and temporal variability associated with all aspects of agricultural production (Pierce and Nowak, 2000). In other words, it is nothing but doing the right thing, at the right time, in the right place, in the right way. It applies to virtually every aspect of agriculture, from planting to harvest.

These definitions suggest that there are at least three elements critical to the success of PA: **information, technology, and management**.

1.1.1 Basics of Precision Agriculture

It has been long recognized that crops and soils within a field and/or region are both spatially and temporally variable. Growers tried to manage such variability to a limited extent mainly by intuition. Developments in geospatial information and communication technologies especially in the late twentieth century have made it possible, however, to manage such variability much more precisely than before. Precision Agriculture, therefore, differs from conventional farming as it involves determining variation more precisely and linking spatial relationships to management actions, thereby allowing farmers to look at their farms, crops and practices from an entirely new perspective, thereby leading to :

1. reduction in costs,
2. optimization of yields and quality in relation to the productive capacity of each site,
3. better management of the resource base
4. protection of the environment. Precision Agriculture also provides a framework of information with which farmers can make rational management decisions (Srinivasan, 2001a,b). In the future, Precision Agriculture may even enable us to trace farm products to their genetics and environmental conditions thereby providing a significant degree of control over food quality and safety.

Field adoption of Precision Agriculture may be represented as a five-step cyclical process including data collection, diagnostics, data analysis, precision field operations, and evaluation (Figure 1.1). The Precision Agriculture system can be considered, therefore, the agricultural system of the twenty-first century, as it symbolizes a better balance between reliance on traditional knowledge and information- and management-intensive technologies. While the approach of Precision Agriculture is information-intensive and encompasses several technologies, application of its principles per se requires neither large scale operation nor heavy equipment. Because of

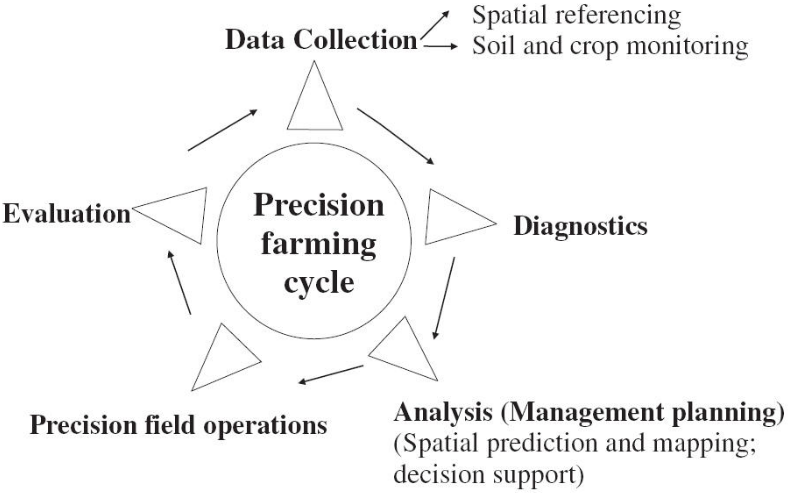

Figure 1.1: Precision Farming and its components, (Srinivasan, 2006).

its focus on technology use, some people consider Precision Agriculture as nothing but using information technologies to turn data into decisions. It is worth noting, however, that there are several opportunities and ways in which Precision Agriculture concepts and principles can be applied in diverse agronomic settings. Thus Precision Agriculture must be viewed more of a management approach rather than a prescriptive technology.

1.1.2 Tools for Implementation of Precision Agriculture

To achieve the ultimate goal of optimizing productivity and profitability in each unit of land, three basic requirements must be met:

1. Ability to identify each field location,
2. Ability to collect, interpret, and analyze data at an appropriate scale and frequency,

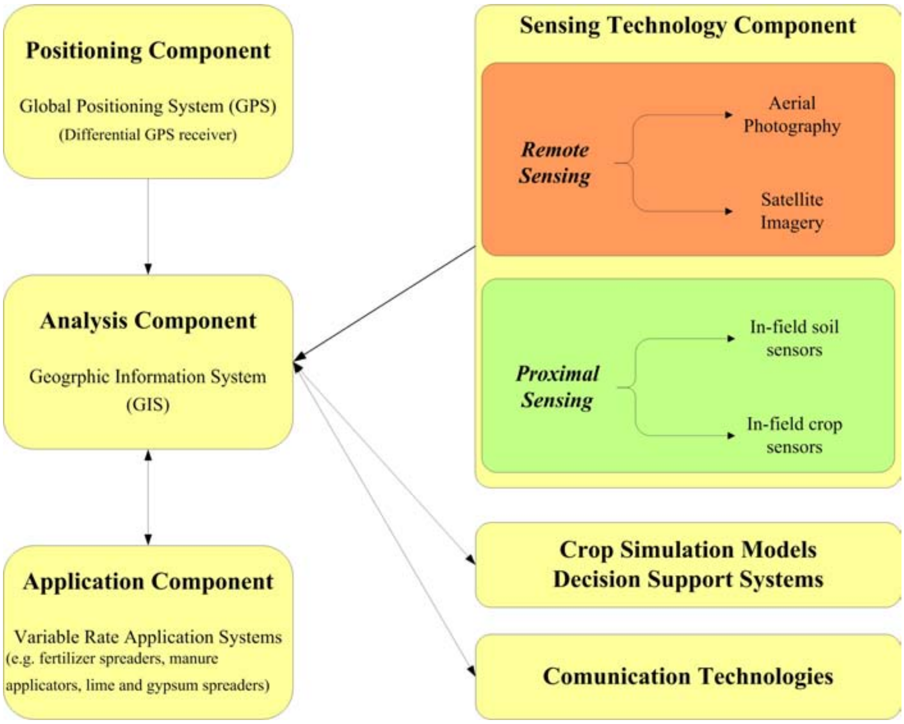

Figure 1.2: Tools for implementation of precision agriculture, (Srinivasan, 2006).

3. Ability to adjust input use and farm practices to maximize benefits from each location.

Global Positioning Systems (GPS), geographic information systems (GIS), remote and proximal sensing, variable rate technology (VRT) and decision support systems (DSS) are employed to meet these needs (Figure 1.2). In addition, new devices (e.g., GIS-enabled personal digital assistants,GPS-equipped yield and quality monitors), communication (e.g., Internet) and data compression technologies are useful for efficient collection and delivery of data, services, and products.

GPS

GPS is a world wide radio-navigation system formed from a constellation of 24 satellites and their ground stations, which provides geospatial accuracy to farm practices by enabling farmers to identify each field site. With the decision by the U.S. government to turn off selective availability (an artificial error introduced into the satellite data to reduce the positional accuracy to 100 meters) effective May 1, 2000, GPS accuracy has considerably improved to about 20 meters. However, differential GPS (GPS receiver used along with a ground reference station) is necessary to get accuracy of 1-3 m critical for yield mapping, crop scouting, and variable input applications. A series of maps with each field identified with the crop grown in each season can help in tracking crop rotations in a region from year to year. Recently, GPS auto-guidance (automatic steering for application equipment) is attracting attention in the United States, Australia, Brazil, and South Africa as a measure to save labor.

GIS

GIS is a software application for computerized data storage, retrieval, and transformation and is used to manage and analyze spatial data relating crop productivity and agronomic factors. Data may be derived for different fields from various sources including existing digital maps, data digitized from maps and photographs, topographic surveys, soil or crop sampling, and sensor data with location information derived by using GPS. GIS can display analyzed data in maps that allow(1) better understanding of interactions among yield, fertility, pests, weeds, and other factors, and (2) decision making based on such spatial relationships. A GIS for Precision Agriculture contains base maps such as land ownership, crop cover, soil type, topography, N, P, K, and other nutrient levels, soil moisture, pH, etc. Data on rotations, tillage, nutrient, and pesticide applications, yields, etc., is also stored. GIS is used to create fertility, weed and pest intensity maps, and for making prescription maps that show recommended application rates of farm chemicals at various field locations.

Remote Sensing

Low-flying aircraft and satellites have become a major source of spatial data due to reduction in both cost and time of image acquisition and delivery. Although the use of remote sensing in agriculture is several decades old, improvements in spatial, spectral, and temporal resolutions of recent satellites (e.g., IKONOS, QuickBird, etc ...) and systems such as airborne videography, and recent developments in new hyper-spectral sensors are increasingly becoming useful to determine size, location, and cause of variation. Imagery can show all fields in a region and spot anomalies related to crop vigor and biomass much earlier than ground inspections, thereby improving the efficiency of crop scouting in large fields and allowing prompt remedial treatments. Temporal changes in vigor, as determined from $NDVI$ (defined in 1.1) analysis of images acquired at critical times, can be used to characterize spatial and temporal dynamics of crop performance and predict crop yields. Upon integration of imagery with other data layers in a GIS, maps can be prepared. GPS receivers can then be used to locate weak spots and apply corrective measures. Likewise, images of different crops planted in rotation can reveal distinct crop vigor responses due to agronomic strategies adopted in previous crops. Imagery can also be used to monitor land use changes at regional level. In the microwave domain, many theoretical and experimental studies have demonstrated the sensitivity of microwave backscattering to vegetation characteristics and efforts are under way to exploit SAR observations for vegetation monitoring. The radar sensitivity to vegetation originates form different volumes of biological matter which affect the wave-plant-soil interaction mechanisms. Backscattering generally depends on the type of plant and by its development stage. Indeed, in their development cycles, crops like maize, sunflower, colza or alfalfa, considerably change the number, dimensions and shapes of the scattering elements, thus modifying their radar signature and return. Geometrical features of cultivations, including distances between rows and between single plants, as well as row orientation and terrain slope with respect to the observing direction, can also dramatically change the features of the imaged areas. Given the number of variables which affect the radar images, sophisticated tools are required to satisfactorily characterize wine producing areas, which are usually complex, fragmented and hilly. Moreover, to perform their task, the discriminating algorithms must be fed with a maximum number of measured pieces of information, hence polarimetric radar measurements are needed, possibly in an interferometric configuration. The sensitivity of radar returns to the vegetal matter hints at the feasibility of measuring vegetation biomass and, possibly, fruit biomass. Although strong limitations are still present.

Proximal Sensing

Technologies employing electronic in-field crop and soil sensors to quantify variability in crop and soil conditions are also in development. Soil sensors for testing *pH*, *EC* (electrical conductivity), *N content* and organic matter are currently in use in North America. Likewise crop sensors for determining *N status* (chlorophyllmeter),water stress, disease or weed problems, grain moisture levels (useful in optimizing harvest operations and storage and/or drying requirements), and protein are also in use. The 10 Hydro-N sensor to measure plant N, which was developed in Germany in the mid-1990s, is now in use in several parts of Europe. Research on plant disease sensors and other sensors is in progress. Such sensors provide quick and cost-effective ways to identify spatial variability, as they can collect data at a level of intensity not economically feasible with physical sampling and laboratory analysis. Yield monitors are another group of proximal sensors. Indeed, yield monitoring and mapping are the most widely used Precision Agriculture components today. Yield monitors for corn, wheat, potatoes, peanuts, and soybeans have been already developed while the monitors for cotton, sugar beets, sugar cane, onions, etc., are in advanced stages of development.

VRT

VRT[1] provides on-the-fly delivery of field inputs. A GPS receiver is mounted on a truck so that a field location can be recognized. An in-vehicle computer with the input recommendation maps controls the distribution valves to provide a suitable input mix by comparing to the positional information received from the GPS receiver. VRT systems are either map-based or sensor-based. VRT has been largely used for applying N, P, K, lime, pesticides and herbicides. Variable rate seeders and variable rate irrigation systems are currently being studied. Systems such as manure applicators, which enable precise application of animal wastes, are also in development.

Communication Technologies

Communication technologies, e.g. Internet (World Wide Web) or Wireless Link, offer capability to send, receive, and aggregate information at much lower costs than ever before. For example, transmitting a remotely sensed image of a field with crop stress zones, or digital photos of problem areas via the Internet can enable the grower to take prompt in-season remedial measures. Likewise, posting to the Web sites of crop yield maps in different rotations over two to three years enables crop consultants to examine and evaluate them in preparing appropriate recommendations. In this context, image compression technologies will be increasingly useful.

---

[1] Variable Rate Technology

Crop Model and Digital Data Systems

These provide an integrated framework for assessing the degree of sustainability of a farming system. They can be used for understanding yield variability in both space and time so as to optimize production, indicate future trends, and prescribe suitable actions to minimize environmental impact. Process-oriented crop simulation models integrate the effects of temporal and multiple stress interactions on crop growth processes under different environmental and management conditions. Use of models with GIS permits mapping of adaptation zones for individual crops and rotation systems and help in targeting sustainable practices to defined regions. Recent advances in Web-based GIS can provide access to spatial analysis of cropping systems through the Web in a scalable, threaded format. In several developed countries, customized services in Precision Agriculture such as grid soil sampling, yield mapping, variable rate application of fertilizers and pesticides are now offered through the private sector. Custom services can decrease the cost and increase the efficiency by distributing capital costs for specialized equipment over more land and by using the skills of Precision Agriculture specialists more effectively. (Srinivasan, 2006).

Having as a reference the schema reported in Figure 1.2, several remote sensing techniques for vine precision farming will be analyzed and discussed, emphasizing their potentialities in a modern farming system.

1.2 Satellite and Vineyards

In the last 10 years, the viticulture approached space technology with a growing interest in merging the producers'need and the research topic. The fast development of space borne sensors' technology, with an higher spatial resolution, opened new fronter for the vine precision farming.

The vine farming is strictly connected to its environment, with a strong link between the product quality and its geographic position. The rising of such new instruments suggested to the most updated and advanced vine producer to investigate the potential of products'quality enhancement related to the use of such techniques. Moreover, the presence of new and free geographic platforms, such as Google Earth, brought the interest of market close to satellites and their commercial application, bringing to the vine precision farming a fresh investors' interest.

Nowadays, the *"art"* of wine making is closer to an industrial process than to a farming one, with several parameters to be monitored by different skilled experts, creating one of the most rich and complex farming system of the world. It is well known that **vineyard leaf area** is related to fruit ripening rate, disease incidence and fruit and types of wine (Winkler, 1958), that a **soil moisture** map can provide information about the pesticides' and fertilizations' management or that a good **water management** can improve the product quality and drastically reduce the costs, particularly in very sunny areas. Moreover, the vine **phenological state** is crucial for a correct practices'timing (Moran et al., 1997) and its monitoring plays a key role in a precision farming system.

Such parameters can now be monitored by new space-borne and airborne sensors and easily handled thanks to the most modern computing technology, as the geographic information systems (GIS) (Pearson et al., 1997b). Remote sensing, in conjunction with purpose specific data processing algorithms, can provide a solution for the production of such informations using captured image data, providing a reliable vine management system. For example, in the viticulture industry precision crop management can be used to target harvesting strategies according to crop condition. The premium wine market requires grape quality information at harvest to isolate the good quality grapes from the lesser ones during the grape crush and storage. Grape quality assessment is usually done on a block-by-block basis, which currently does not take into account the variability of the quality of grapes within each block. If this variation is identified and mapped within a given block, then it is possible to apply precision harvesting techniques and thus improve the overall value of that harvest since the high quality grapes usually carry a value that is substantially greater than the lesser quality for the same quantity.

As another example of the application of precision crop management, the premium wine market may require information to meet certain export labeling standards limiting the cross varietal mixture of grapes. The mixture of the off-types can be identified and mapped within a vineyard block using remote sensing, and the application of precision harvesting can ensure the varietal purity at the crush by avoiding the harvesting of those rows and sections of vines in that block.

In the following paragraphs, several scenarios will be critically analyzed and discussed; each case of study will be shown, emphasizing the relationship between the proposed technique, the environment and its market. There is a strong link between these three factors: each wine quality is strictly linked to a region (orography and tradition) and to a market and no precision farming system can leave aside this complex scheme.

1.3 The Italian Case of Study: The Franciacorta Experience

The Italian scene for vine farming is particularly complex, due to the topographic and economic scenario; the mean area of each vine parcel is quite small related to the mean value of the rest of the world and the field management is made by in-situ measurements, following the traditional way of producing wine. Generally speaking, the scenario is quite different, where the information provided by satellites is carefully used to manage large areas, to optimize the irrigation and the agricultural timing practices. Anyway, also the Italian wine market, because of the presence of new foreign competitive wine producing countries, is looking for new solutions for field management: remote sensing as a data input layer of a precision farming system is becoming reality. (Brancadoro and Favilla, 2002).

One of the first and most important Italian experiments of vineyard precision farming by means of satellite data has been done during the fall of 2005, in the Franciacorta wine producing area, between the hills surrounding Brescia and the Iseo Lake. The aim of the experiment was to test the capability of high resolution space borne optical sensors, such as IKONOS, in vine parameters estimation and its accuracy assessment. The acquisition campaign was planned during the end of June 2005 over an area of about 500 Ha; the selected period was overlapping the maximum leaf vigor of the vine, when the plant is ready to store the water into the grapes and the leaves are at the top of their photosynthetic level. Besides the space campaign, a ground truth campaign was prepared in order to collect some in-situ measurements to correlate with the satellite images; all over the 10 selected test parcels, measurements were collected at at least 5 points (Figure 1.3) for the following parameters:

- parcel's yield
- Brix Index (Figure 1.5)
- Must Total Acidity Level (Figure 1.6)

1.3.1 The Franciacorta Methodology

The methodology used is based on the extraction from the IKONOS dataset of the IVN index (Normalized Vigour Index) and its correlation with the in-situ measurement points (Brancadoro et al., 2006). The index is related to crop vigor, vegetation amount or biomass, resulting from inputs, environmental, physical and cultural factors affecting crops. The IVN index can be calculated considering the NDVI normalized by the plant density (Figure 1.4):

$$NDVI = \frac{NIR - RED}{NIR + RED} \tag{1.1}$$

$$IVN = \frac{NDVI}{PlantDensity} \tag{1.2}$$

The collected ground measurements and the IKONOS data has been integrated into a G.I.S.[2] system; brix and acidity indexes have been processed over the whole area by means of a very simple linear regression.

---

[2] Geographic Information System

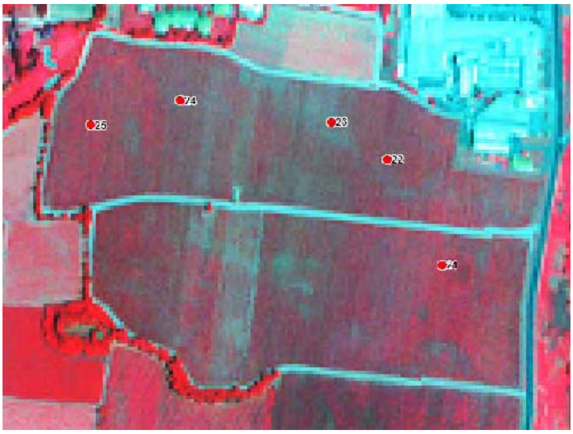

Figure 1.3: Overview over a vine parcel with measurement points, (Brancadoro et al., 2006).

1.3.2 Analysis and Results

The methodology proposed in the Franciacorta experiment is very simple, easy to use and fast during the processing phase. Otherwise, it is quite expensive in terms of ground data management because of the presence of a ground measurement campaign to "calibrate" the simple linear model. Moreover, an update and precise vine cadaster has to be present to provide information about the plant density of each analyzed parcel. The input can be summarized as :

- vine cadaster
    - Plant Density
    - Parcel Boundary
    - Vine structure (tent, row, . . .)
    - grape quality
- IKONOS data level 1A

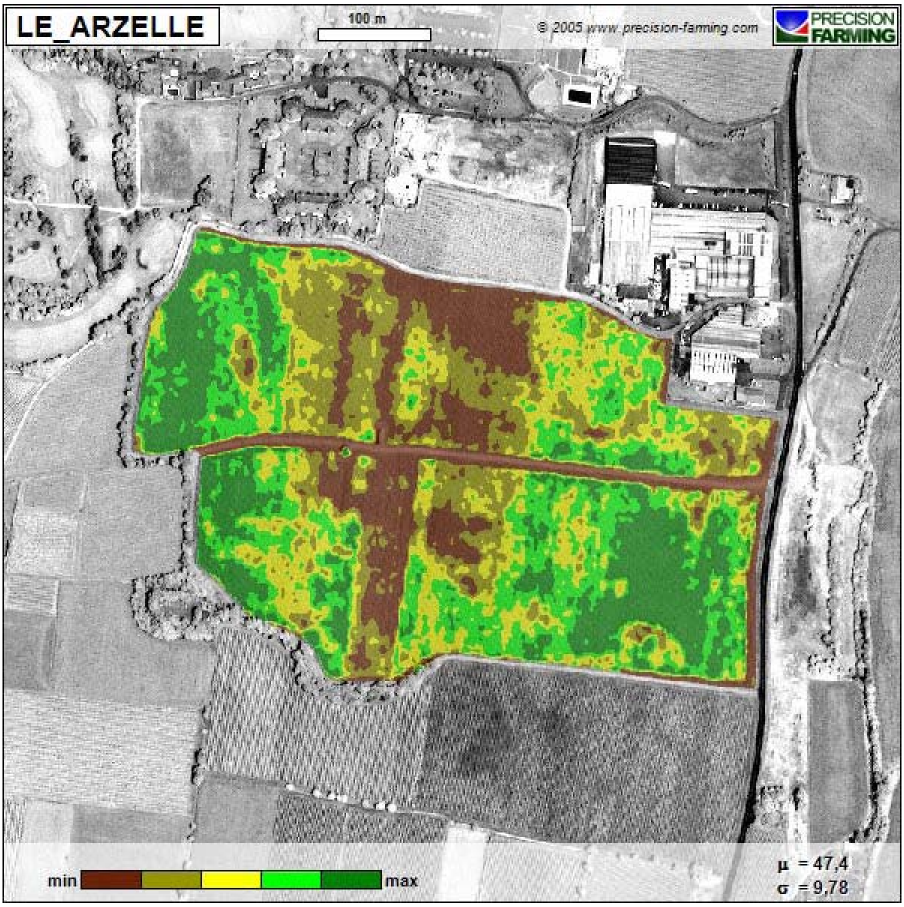

Figure 1.4: example of IVN index over "Le Arzelle" parcel, (Brancadoro et al., 2006).

- Ground measurement campaign

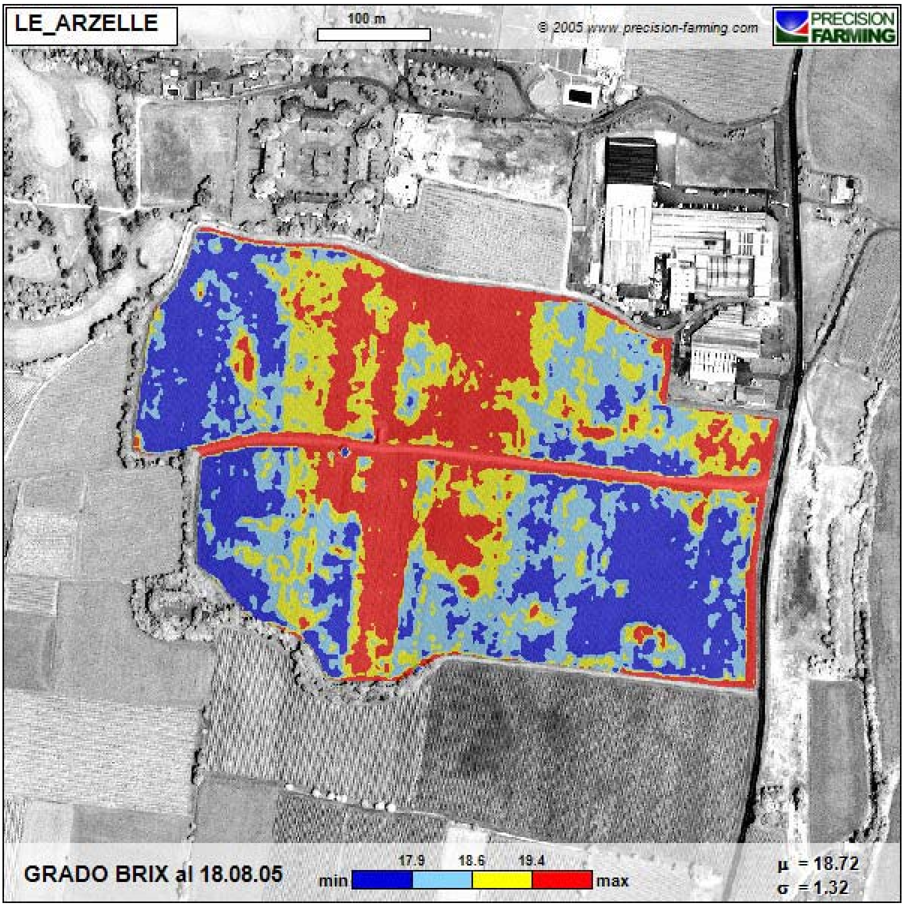

Figure 1.5: example of Brix Index over ”Le Arzelle” parcel, (Brancadoro et al., 2006).

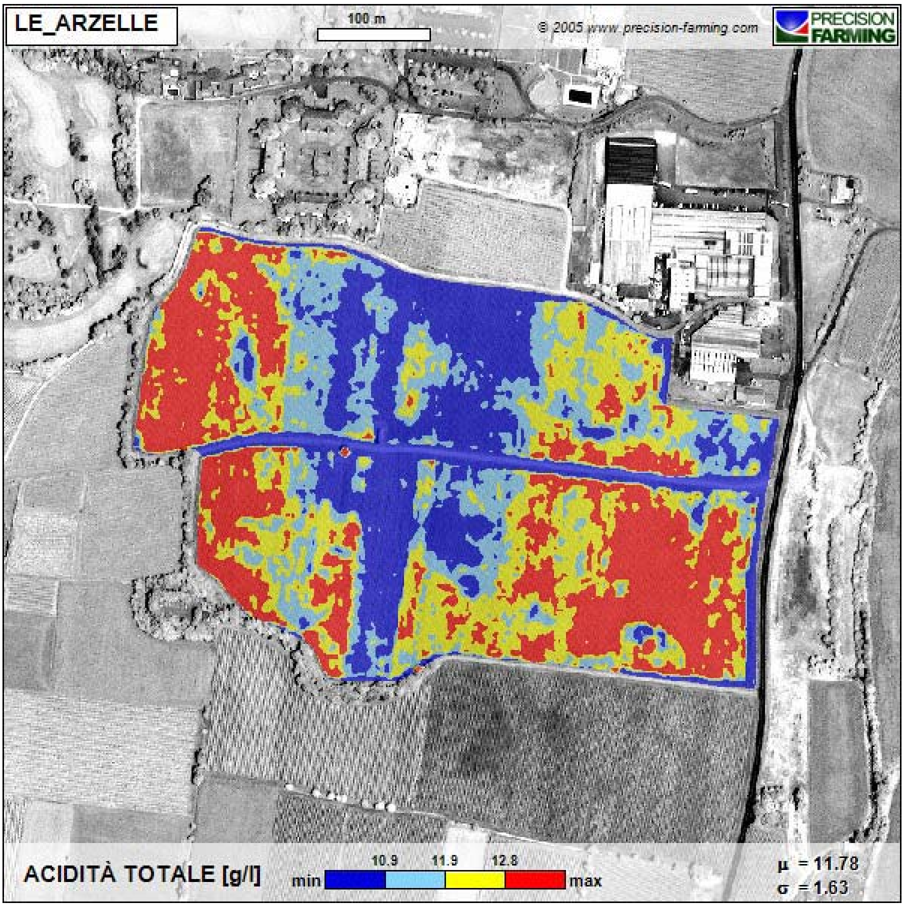

Figure 1.6: example of must total acidity over "Le Arzelle" parcel, (Brancadoro et al., 2006).

1.3.3 Vine Monitoring Parameters

During the growing season, several biological parameters have to be monitored in order to assess a good product quality level, wine making is one of the most complex farming process and it involves several professional profiles, from chemist to the sales manager. During the Franciacorta campaign three important biological parameters have been correlated to the satellite data, their prediction or extensive measure is crucial in a competitive market, where quality is playing a key role in success (Kamp and Lynch, 2008).

Must Acidity Index

Acids occur naturally during the growing of grapes and as part of the **fermentation** process. Wines show lower levels of acid when there are hot growing seasons or when the grapes come from hotter viticultural regions. Conversely, cooler regions or cooler growing seasons produce wines with higher acid levels. In the proper proportion, acids are a desirable trait and give the wine character, much as a dash of vinegar or lemon juice heightens the flavor of many foods. Too much acid leaves a sharp, tart taste in the mouth, while too little makes wine seem flat and lifeless. The three predominant acids in wine are tartaric, malic, and citric, all of which are intrinsic to the grape. Tartaric acid is the principal acid in grapes and is a component that promotes a crisp flavor and graceful aging in wine. A moderate amount of a wine's acid comes from malic acid, which contributes fruitiness, and a small amount comes from citric acid. Wine also contains minute to trace amounts of other acids, which are produced during fermentation, including: acetic, butyric, capric, caproic, caprylic, carbonic (in sparkling wines), formic, lactic, lauric, propionic, and succinic. The least desirable acid in wine is acetic acid, which, when present in more than a nominal amount, gives wine a sour or vinegar taste . Volatile acids (such as acetic and butyric) are those that can be altered-for instance, they can evaporate. Fixed acids are fruit acids (such as malic and tartaric) that are organic to the grape. Total acidity, also called titratable acidity, is the sum of the fixed and volatile acids, which is determined by a chemical process called titration. *Total acidity* is expressed either as a percentage or as grams per liter. The proper acid level of a wine varies, with sweeter wines generally requiring somewhat higher levels to retain the proper balance. Some labels make note of a wine's acidity. For dry Table Wine the acceptable range is usually 0.6 to 0.75 percent; for sweet wine it's 0.7 to 0.85 percent. In some areas (usually warm growing regions where acidity is lower) like California, natural grape acids can legally be added to wine to increase the acidity. This acid adjustment process is called acidulation. In a well-made wine, acidity will not be noticeable.

Brix Index

Named for A. F. W. Brix, a nineteenth-century German inventor, the Brix scale is a system used in the United States to measure the sugar content of grapes and wine. The Brix (sugar content) is determined by a Hydrometer, which indicates a liquid's Specific Gravity (the density of a liquid in relation to that of pure water). Each degree Brix is equivalent to 1 gram of sugar per 100 grams of grape juice. The grapes for most Table Wine have a Brix reading of between 20 to 25 at harvest. About 55 to 60 percent of the sugar is converted into Alcohol. The estimated alcohol that a wine will produce (called potential alcohol) is estimated by multiplying the Brix reading by 0.55. Therefore, a 20 Brix will make a wine with about 11 percent alcohol.

Yield

A term used in grape-growing and winemaking circles to express the productivity of a set amount of vineyard land. Yield is a way of comparing the relative productivity of different grape varieties in different locations. In Europe and South America, it's expressed in Hectoliters per Hectare. It's generally agreed that lower yields produce higher-quality wines and that the higher the yield, the more diluted the resulting wine will be. With that in mind, one of the criteria for meeting Italian *Denominazione di Origine Controllata* (DOC) regulations is permissible yield. Each DOC area has a maximum allowable yield, depending on the grape variety and quantity of land. Yields are kept down by pruning the vines so that there's an optimum ratio between fruit production and vegetative growth (important for the next year's production). As more is learned about viticultural techniques, higher yields are being achieved without loss of quality. However, it still holds true that higher yields from the same set of vines grown the same way will dilute the concentration in the grapes. Some vineyards in Germany's Rhine and Moselle district can yield 100 hectoliters per hectare without loss of quality. On the other hand, in Spain much of the vineyard land is very arid and can't be densely planted because the vines won't get enough moisture. This climate, plus rather antiquated viticultural practices, limits yields in most parts of Spain where the average is around 23 hectoliters of grapes per hectare. In California's coastal areas, where higher quality wines are made, growers expect 3 to 6 tons per acre (equivalent to 40 to 80 hectoliters per hectare), depending on the location and grape variety.

1.4 A New Rising Wine Market: The Australian Experience

One of the most promising wine market of the world is the Australian one, with fairly good quality products and relative low prices. During the last 10 years, the Australian wine scenario invested a lot in new space technologies in order to reduce the production'costs and improving also the mean product's quality level. Moreover, the Australian scenario is particularly suitable for space technology, thanks to its huge territory and its orography.

Australia produces a full range of favored wine styles, from full-bodied reds and deep, fruity whites through to sparkling, dessert and fortified styles. In global terms, Australia was ranked sixth in the list of world wine producers in 2005, producing 1.4 billion liters of wine: it is consistently one of the top 10 wine-producing countries in the world. Being such a large country with almost every climate and soil type, Australia is one of the few wine producers to make every one of the major wine styles.

Wine grape growing and wine making are carried out in each of the six states and two mainland territories of Australia. The principal production areas are located in the south-east quarter of the Australian continent, in the states of South Australia, New South Wales and Victoria. Wineries in South Australias Barossa Valley, in the Hunter River region north of Sydney in New South Wales and in Victoria played a major role in the development of the industry and continue to be important sources of fine wines. However, wine is produced in over 60 regions, reflecting the wide range of climates and soil types that exist across the continent. These areas include Mudgee, the Murrumbidgee River and Murray River valleys (New South Wales); the Southern Vales, Clare Valley and Riverland (South Australia); and Rutherglen and the Yarra Valley (Victoria). The states of Western Australia, Tasmania and Queensland have smaller wine industries, which have grown rapidly in volume, quality and reputation. The region near Australias national capital, Canberra, has a recognized cool-climate wine industry.

Even if the Australian wine Story started in the 17^{th} century, only during the last 11 years, from 1996 to 2008, that saw spectacular growth in exports, following rapidly increasing appreciation of Australian wines overseas. Major wine producers from abroad have invested in Australian wineries, and Australian companies have taken controlling interests in wineries in countries such as France and Chile.

In 2006–2007, sales of Australian wine totaled approximately 1.23 billion liters: 449 million liters were sold domestically and 786 million liters were exported. Australian wine exports were worth $2.87 billion, which represented an increase of 4.4 % over the previous year.

Wine production is a significant industry in Australia. It directly employs 28000 people in both wine making and grape growing and generates related employment in the retail, wholesale and hospitality industries.

Australias reputation as one of the most technologically advanced wine-producing nations owes much to the industrys emphasis on research and development. Key research and development sources include the Australian Wine Research Institute, the Commonwealth Scientific and Industrial Research Organization, the National Wine and Grape Industry Center, state departments of agriculture and universities.

1.4.1 The *AIMS* solution

The Australian territory seems to be perfect for new technologies'testing and the young wine market is strongly looking for new solutions to improve its competitiveness; the huge area of each single parcel is not negligible from a costs'management point of view and data collection during the growing season is awfully expensive. Because of these reasons, several enterprises are providing different solutions for vineyard's management, such as *AIMS (Ball Advanced Imaging & Management Solution)*, that suggests an hyper-spectral airborne high resolution based system for vineyard' monitoring and management.

Generally speaking, the application of satellite imagery to precision crop management (PCM) for high value crops is limited due to restrictions in spectral and spatial resolutions, and time-at-overpass constraints. In contrast, high spectral and spatial resolution airborne sensors enable timely acquisition of imagery (i.e. during optimum growth periods) for the assessment of the health and vigor of plantations. *AIMS* proposes a sensor, CASI-2, with an high spatial resolution (0.60 m up to 5.0 m in un-pressurized aircraft), enabling the capture of fine features in plantations such as the vine rows in a vineyard. The super-spectral sensor has got a sub-metric resolution (0.5 - 0.7 m) with a spectral resolution between 6 and 11.8 nm distributed on 18 bands, covering a spectral window between 447 to 937 nm. The data acquisition plan usually overlaps the maximum plant's vigor status because during this period (topically June-July, but it is linked to the field's latitude) the correlation between the remote sensed and in-situ measurements is maximum.

As the methodology shown in Chapter 1.3, also for *AIMS* the processing starts using the *NDVI* index; the processing chain is emphasized by the incidence angle correction, radiometric calibration and acquisition time in order to have a common benchmark for multi-temporal data using. The ability to more precisely characterize the spectral reflectance of the biophysical properties of the plants at different stages of phenology is crucial and *AIMS* choose an hyper-spectral solution.

1.4.2 The Processing Chain

Airborne digital data is acquired using a CASI-2 sensor mounted in a fixed wing twin-engine light aircraft. A band set in the visible-near infra red (VNIR) portion of the electromagnetic spectrum is configured and programmed into the sensor unit. The band set is designed to characterize the spectral properties of the vineyard (the device is application dependent and requires prior knowledge about the target in question).

The CASI-2 imagery utilized acquired with a ground resolution of 0.70 meters and programmed to capture 18 narrow spectral bands in the VNIR. Ball AIMS used a band set that was specifically designed for viticulture image data capture, with the spectral bands positioned between 447 and 937nm. The bandwidths for the 18 bands ranged between 6 to 11.8nm.

1.4.3 Baseline Processing

Following data acquisition, each flight line is radiometrically and geometrically corrected. Radiometric correction converts pixel digital numbers (brightness values) to spectral radiance units by applying pre-determined calibration parameters to the CCD[3] array in the CASI-2 sensor (ITRES, 1996). This is an important factor for the application of advanced image processing since the effectiveness of image classification or analysis of the image data relies on the radiometric uniformity of the image, especially if an atmospheric correction is required to be applied.

The CASI-2 utilizes a high performance position and orientation system (Applanix POS/AV 310) to collect attitude (roll, pitch, yaw) and position data simultaneously with image data. The system provides dynamically accurate, high-rate measurements of the full kinematic state of the aircraft. The positional data is differentially corrected using a base station. The processed position and attitude data is then used in a proprietary geo-correction process which applies geometric correction to each flight strip and geo-references the data to a standard coordinate system to an accuracy of within 3-5 pixels. If available, a digital elevation model is utilized to create

---

[3] Charge-Coupled Device

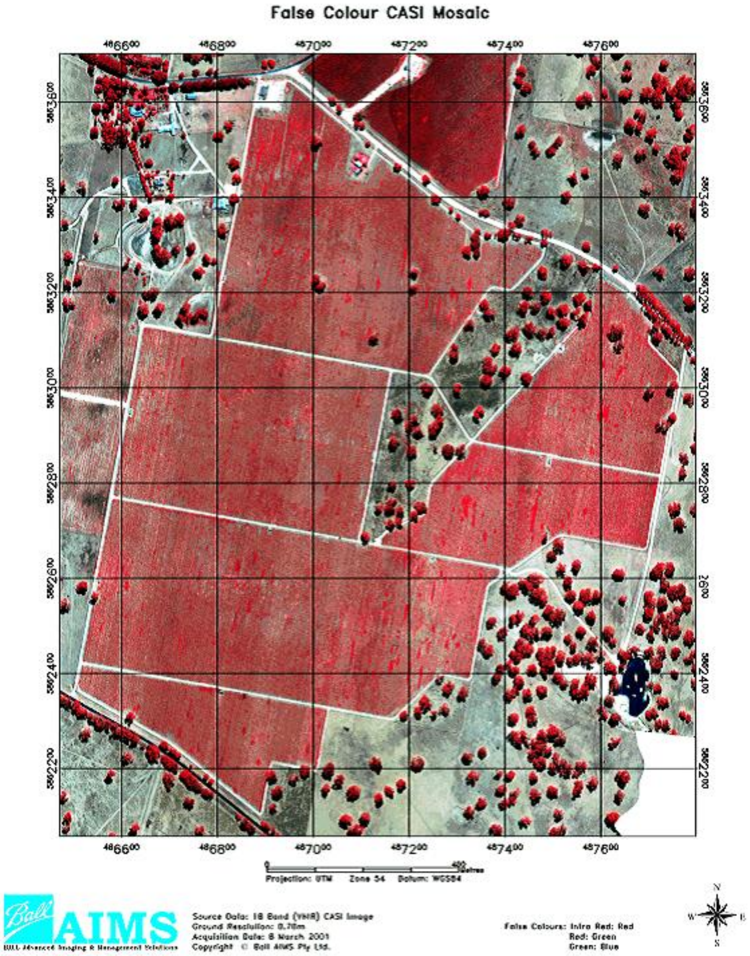

Figure 1.7: The CASI-2 false colour image mosaic of a vineyard in Coonawarra after radiometric and geometric corrections, (Arkun et al., 2005).

the ortho-rectified image strips, which eliminates the positional inaccuracies that result from the terrain height variations. This further improves the level of achievable positional accuracies.

The resultant radiometrically and geometrically corrected image strips are then mosaicked to produce a seamless image tile that is geo-referenced and hence is suitable for advanced processing (Figure 1.7).

1.4.4 Atmospheric Correction

The mosaic image is then atmospherically corrected using the empirical line calibration method (ELM), converting sensor radiance units to estimates of ground reflectance. Two spectrally contrasting pseudo invariant features (PIFs) bracketing the range of reflectance values from vegetation targets are used to develop prediction equations applied for calibration. The spectral characteristics of these targets, which are free from the effects of the atmosphere, are then measured with *a field spectrometer* and using the same target features in the image, are enforced on the radiometrically corrected image data to perform a low cost atmospheric correction.

The correction is applied to the full mosaic with the assumption that there is no significant variation of the atmospheric effects across the image. Following atmospheric correction, an independent validation of the atmospheric correction is undertaken using other spectrally flat features in the image such as gravel and bitumen road surfaces at known locations and measured reflectances.

Vineyard and Vine Row Definition

Each vineyard block is defined in a vector layer, on a post to post basis with access tracks or headlands and other features being excluded. All algorithms are applied at the block level that constitutes a vineyard management area, which exclude other features. For the greenness index to provide optimal results, the desired vineyard conditions are:

- Absence of strong ground cover growth between vine rows;

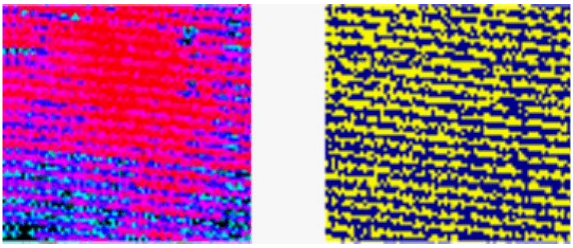

Figure 1.8: Vine row extraction from an area of weed/grass infestation. The NDVI vineyard segment is shown on the left; and the extracted vine row mask from the same segment on the right (yellow: vine rows, blue: background). (Arkun et al., 2005).

- Vine canopies are fully developed and spread across the trellising;
- Vine understory free of weeds and grass;
- Uniform structural and morphological existence of the vine rows (eg. vine row spacing, trellising etc.)

Vine rows are isolated from the rest of the imagery using a combination of band math, band ratio and NDVI thresholding designed to exploit the spectral differences between the vines and non-vines including weeds and grasses. This removes the background data attributable to weeds, grass, soil, rock and litter and provides a mask for the vine rows (Figure 1.8). The combination of these algorithms then produces an image that helps to confine the analysis to vine plants only.

This is important to ensure any subsequent processing to assess the health and vigor of the vines is not attenuated by the existence of non-representative plants and vegetation (or soils/shadows etc.). The NDVI imagery is then truncated using this mask and the mean vine NDVI value is substituted in the inter-rows to remove the variability attributable to the background noise (eg. weeds, grasses). This provides NDVI values more representative of the vine-canopy condition throughout the vineyard.

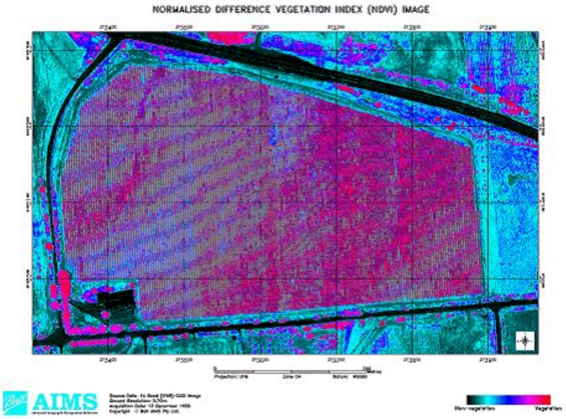

Figure 1.9: The normalized difference vegetation index (NDVI) image. Plants are shown in pink-red and non-plant in blue-black, (Arkun et al., 2005).

1.4.5 Greenness Index

Vine vigor grading is based on the NDVI ratio, which is used as a surrogate indication of bio-physical status and productivity. In healthy crops the index is positive having a maximum value of 1.0. General patterns of vine growth variability evident within the raw NDVI image (Figure 1.9) are more readily quantified into management units (or regions) in the graded image (Figure 1.10).

The greenness index is based on a smoothed form of the NDVI image, that has had inter vine row variability removed. Two results from the same data set are produced, firstly a relative greenness index image, and secondly an absolute greenness index image. The relative greenness image grades the smoothed NDVI values such that each grade covers equal area. This enables the mapping of greenness variability throughout the vineyard. In contrast, the absolute greenness image has the function of assessing the greenness conditions of a given vineyard in relation to any other vineyard both in temporal and spatial terms. This is made possible by the application

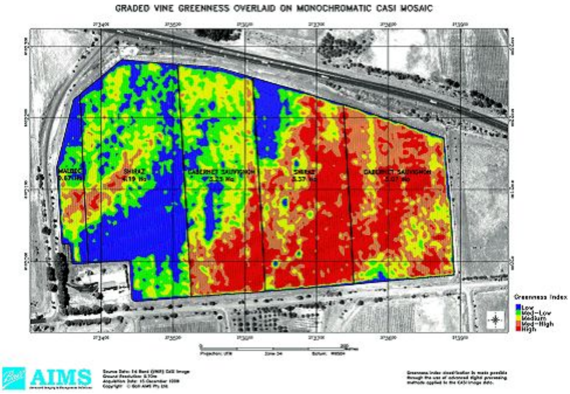

Figure 1.10: Five class relative greenness index image overlaid on a monochromatic CASI mosaic. Each plantation within the block is labeled with grape variety and area. (Arkun et al., 2005).

of atmospheric correction to the imagery which then defines all imagery in terms of spectral reflectance. Smoothed NDVI values are segmented through a histogram equalization process and binned to invariant thresholds to provide like comparisons on a temporal basis enabling longitudinal change monitoring. The number of grades to be applied can be nominated by the client in keeping with their application requirements.

A number of smoothing algorithms are applied to the transformed image to generalize the NDVI data on a local area basis, producing spatial regions more easily identified in terms of management units than is possible with the un-smoothed data. Integration of the smoothed data with the spectral data is completed for visual impact and spatial orientation for the interpreter. Graded vine blocks are typically overlaid on a geo-referenced gray scale image (client nominated map or grid datum and projection system) and show discreet vine rows for in-situ referencing on a row-by-row basis for the end user. The overlaying can be performed on any color imagery the client may request (i.e. true/false color etc).

1.4.6 Variety Mapping

Vine variety mapping is performed by the combination of two supervised classification techniques spectral matching and maximum likelihood method. The hyper-spectral nature of the data set is central to the success of the varietal discrimination since 18 narrow bands create a more complete and discrete spectral signature for each variety than a four band image of low spectral resolution.

The classification of plant species is not a trivial task due to several species having quantitatively similar spectra and the significant spectral variation within a species. The spectral separability is described by a few variables affecting the visible wavelengths, namely chlorophyll a, chlorophyll b, carotenoids, and xanthophylls, while the number and configuration of cells and cell structures within the leaf are influential in the NIR (Cochrane, 2000). Hence the high spatial and spectral resolution of the CASI-2 imagery enables the discrimination of the vine varieties using the segregated vine-canopies. It also allows the use of spectrographic methods to be applied on a pixel-by-pixel basis using either library spectra or image-derived spectra.

The two methods of supervised classification were applied to the 18 band image data resulting in a single layer of classification for each. These were then combined to form a single classified image enhancing the overall classification result (Figure 1.11).

On a large scale, the varietal mapping enables the regional mapping of vine varieties, which can be used for planning or inventory purposes. At the individual block scale, clusters of misplantings or off-types can be identified which help to avoid un-intended grape mix at harvest. In Figure 1.11 Shiraz misplantings have been discriminated within a Cabernet Sauvignon plantation.

1.4.7 Gap Identification

Identification of intra-row vine gaps is achieved through the application of textural analysis combined with filtering methods. The technique is based on the processing of the NDVI vineyard data. The vine gap identification

Figure 1.11: Five class relative greenness index image overlaid on a monochromatic CASI mosaic. Each plantation within the block is labeled with grape variety and area, (Arkun et al., 2005).

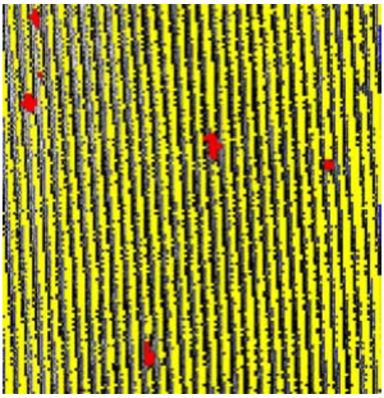

Figure 1.12: Vine row gap identification (enlargement) overlaid on a monochromatic CASI background (yellow: vine rows, red: vine row gaps). (Arkun et al., 2005).

(Figure 1.12) enables the quantification of the number and the extent of the vine gaps within a given vine block, which can then be converted into total area of missing vines. This can be used to assess the potential for re-planting or other management changes and the benefit of such choices, allowing the management to make informed decisions about vineyard improvement.

1.4.8 Temporal Comparisons

Temporal comparisons of the greenness index can be made to assess changes in the vineyard condition as a result of implemented management practices. This is made possible by atmospherically correcting the image data and converting it to spectral reflectance values. The absolute greenness index images can be used for periodic change detection, whilst the relative greenness imagery can be used to track the spatial nature of the variability across a block from season to season.

1.4.9 Analysis of the Australian case of study

As it is shown in the previous sections, the methodology proposed by *AIMS* is well-established and service-oriented; *AIMS* put an emphasis on the pre-processing and calibration of the input data, to create a reliable multi-temporal dataset and a stable monitoring system. Indeed, during the growing season, the vine has be measured several times and a stable instrument is a base for a precision farming and monitoring system. Because of the regional behavior of the vine, the *AIMS* method is designed to provide solutions for a typical Australian vineyard, with huge and uniform parcels, where an airborne-based system has got an advantageous benefit/cost ratio. The costs of each overflight is considered profitable also for a single farmer, because of the precious information provided by such kind of data. To know where a plant needs some practice is a priority for Australian farmers. Moreover, actually the spaceborne system can not provide such kind of data, with very high spatial resolution and hyper-spectral capabilities, not fulfilling the the wine market's needs.

1.5 A Wine Coming from the Far West

California, thanks to its geographical position and climate, became during the 90s'one of the most important wine producing area of the world. Nearly three-quarters the size of France, California accounts for nearly 90 percent of entire American wine production and the production in California alone is one third larger than that of Australia. From an historical point of view, the Californian wine is young: the state's viticultural history dates back to the 18^{th} century when Spanish missionaries planted the first vineyards to produce wine for Mass. California has over 1.730 km^2 planted under vines mostly located in a stretch of land covering over 1.100 km from Mendocino County to the southwestern tip of Riverside County. There are over 107 American Viticultural Areas (AVAs), including the well known Napa, Russian River Valley, Rutherford and Sonoma Valley AVAs. The Central Valley is California's largest wine region stretching for 480 km from the Sacramento Valley south to the San Joaquin Valley. This one region

Figure 1.13: View of wine producing area of Napa Valley, CA

produces nearly 75% of all California wine grapes and includes many of California's bulk, box and jug wine producers like Gallo, Franzia and Bronco Wine Company.

California is particularly sensible to new precision farming techniques, thanks to the presence of several Research Institutes and Universities (e.g. University of California at Davis, ...) with a lot of research topics about precision viticulture and satellite; moreover, the mean single vineyard property's area is large enough to enable a virtuous relationship between monitoring costs and profits.

The proposed method wants to assess the use of NDVI for obtaining absolute estimates of leaf area, as said in Chapter 1.3, one of the most important parameters, a variable of direct relevance to viticultural management. IKONOS data is the input dataset with acquisition starting at early June, persisting through harvest.

1.5.1 Leaf Area Calibration and Ground Campaign

Direct measurements of LAI were made at 16 sites all around in the Napa Valley, CA (Figure 1.13). Three to six sample vine replicates were measured per site, distributed over an area of 10 m x 10 m. All leaves were removed from each sample vine, placed in separate plastic bags and sealed. Total leaf weight was recorded per sample vine. A subsample area was extracted and weighed for each vine. Within 24 hours, subsample area was measured with a leaf area meter. Total area per sample vine was calculated as $LAv = LAs * (wt/ws)$, where LAv is leaf area per sample vine, LAs is leaf area per subsample, wt the total weight, and ws is subsample weight. Sample vine LAI was then $LAIv = LAv/VineArea$, where $VineArea$ is $VineSpacing * RowSpacing$. Site LAI was mean LAIv.

Measurements were made 22^{th} of September to 6^{th} of October, 2000, shortly after harvest. Indirect measurements of LAI were made at six additional sites based on shoot length observation. For each sample vine, the total number of shoots was recorded and mean length was calculated as the mean of five randomly selected shoots. Mean shoot length was then converted to shoot leaf area (based on an observed empirical relationship), and subsequently to LAv and site LAI. The location of each calibration site was mapped to sub-meter accuracy with differential GPS.

The input dataset consists into two IKONOS 4-meter multi-spectral satellite images, collected during the period of full canopy expansion: 21-AUG-2000 for Huchica Hills and 4-OCT-2000 for Tokalon. The images were calibrated to radiance units by applying radiometric calibration coefficients. The atmosphere was assumed uniform throughout each scene and no correction was applied. The images were then converted on a per pixel basis to NDVI. A relationship was established between NDVI and ground based LAI using a nearest neighbor approach, then LAI map have been produced (Johnson and Pierce, 2003).

The results suggested that NDVI provides a fairly robust basis for calculation of vineyard leaf area with respect to such potential confusion factors as trellis type (canopy architecture), planting density, variety, age, soil type, topography and image acquisition date. Leaf area is relevant to

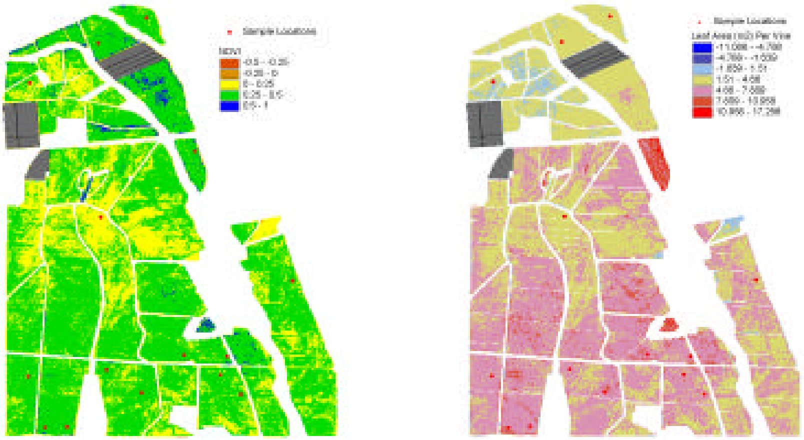

Figure 1.14: NDVI and LAI maps, (Johnson and Pierce, 2003).

canopy and irrigation management. Remote mapping of LAv and $LAmRow$ relates to canopy management, which is used to influence micro climate and assure adequate supply of photosynthate to fruit. Remotely sensed LAI can serve to parameterize irrigation management models for maintenance of vines at target levels of water stress.

1.5.2 New Chances from UAV

As shown in Chapter 1.4.9 and 1.5, the space-borne optical vineyard's remote sensing is not still ready for service providing in a precise and reliable way. On the other side, a competitive market pushes the research toward horizons with more competitive and low cost instruments: Unmaned Aerial Vehicle. Thanks to this quite recent airborne technology the vine precision farming is still growing and having a good success in California. During an other experiment held in Napa Valley, CA,(Johnson et al., 2003) a small UAV (RCATS/APV-3) was used to collect imagery over a large commercial vineyard. The aircraft, which is under development by RnR Products , MLB , and Lockheed-Martin is capable of remaining aloft for up to 8 hours, with an altitude ceiling of 3000 m. The UAV can support payload of approximately 5 kg and drawing 40 watts of power. The imaging payload for this flight was built around two charge coupled device (CCD) camera components acquired from Basler Vision Technologies (Germany) to provide complementary spatial and spectral information (Figure 1.15).

A Model A101fc 1280x1024 Bayer array RGB camera was used for high spatial resolution, geometrically coherent 2-d imaging. A Model A302fm monochromatic camera was fitted to a miniature imaging spectrograph and operated in push-broom (linear array) fashion to collect high spectral resolution (580 band) data of reduced spatial resolution and geometric quality. This small UAV can collect a total of 165 RGB images, at a spatial resolution of approximately 20 cm; the collected data can be downloaded directly via wireless into a GIS. An example of the output results is reported in (Figure 1.16), where a Vigor Index Map is produced.

The RCATS UAV works in association with a in-field sensor web network, to achieve a good data calibration level, providing high quality data in a

Figure 1.15: RCATS/APV-3 on vineyard imaging mission, (Johnson et al., 2003).

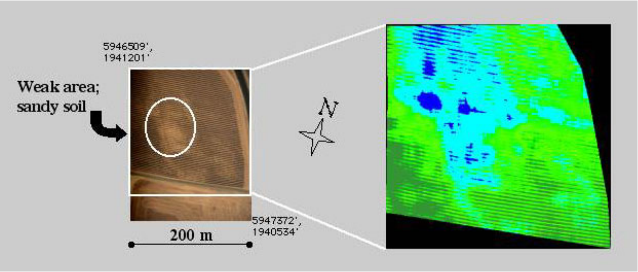

Figure 1.16: Left) RGB image of 4 ha vineyard. Right) Corresponding vigor map. Dark blue = 35-40% cover; light blue = 40-45%; light green = 45-50%, dark green > 50%, (Johnson et al., 2003).

near real-time way. This platform can cover quite large area, providing relevant information about the plant status, thanks to the very high spatial and spectral resolution of the cameras.

1.5.3 Analysis of the Californian case of study

The Californian Methodology has got several common points with the Australian (Chapter 1.4) and the Italian (Chapter 1.3) experience, the NDVI is the main input for the correlation with the ground measurement. The solution proposed is still at the research level and not product oriented. In literature, some small enterprises are providing precision farming services, having as a common reference high resolution optical data. During the last years, the Californian Wine Market is having a new technologic rise from the precision farming point of view: Networks of Wireless Nanosensors and UAV. The rise of such kind of precision viticulture is derived by the need of very precise in-field measurements, not easy achievable by spaceborne sensors. Indeed, when scattered on fields, networked sensors are expected to provide detailed data on crop and soil conditions and relay that information in real time to a remote location so that crop scouting will no longer require the farmer collecting measurements directly inside the field. Anyway, from the processing point of view, vine remote sensing is still optical based, using the NIR spectrum as the input dataset for any biological parameter estimation. The hyper-spectral sensors' development can provide better measurement but no improvement is present from the modeling and processing point of view.

1.6 Ground Radar measuring Soil Moisture

Coming directly from the Berkeley University (California), a new vineyard's monitoring instrument is suggested: the radar. The spaceborne radar's radar potential will be discussed in the next chapters, but it is interesting to analyze the use of a ground radar as an instrument for precision farming. As we said before (Chapter 1.2), soil moisture is one of the crucial parameter to be monitored to grow up the grape's and wine's quality, but accurately

Figure 1.17: Ground Penetrating Radar (GPR), (Rubin et al., 2002).

soil's water content monitoring is a difficult and expensive task; a solution is suggested by means of ground penetrating radar, or GPR, to map soil moisture in vineyards.

1.6.1 Introduction to GPR

Ground penetrating radar (GPR) is a geophysical method that can provide high resolution three-dimensional images of the subsurface of the earth. The environmental application in which the use of GPR is most likely to lead to significant improvements in the currently practiced methodologies is in the field of soil moisture estimation and contaminant hydrology (Huisman et al., 2003). GPR is an imaging method that utilizes the transmission and reflection of high frequency (1 MHz to 1GHz) electromagnetic (EM) waves within the earth. A standard GPR survey is conducted by moving a transmitter and receiver antenna, mounted on a small truck and separated by a fixed distance, along a survey line. The pair of antennas is moved to stations (measurement locations) with the spacing between stations determined by the survey objectives. At each station, a short pulse or *wavelet"* of EM energy is sent into the earth by the transmitter antenna. The GPR wavelet contains a number of frequencies, but is usually referred

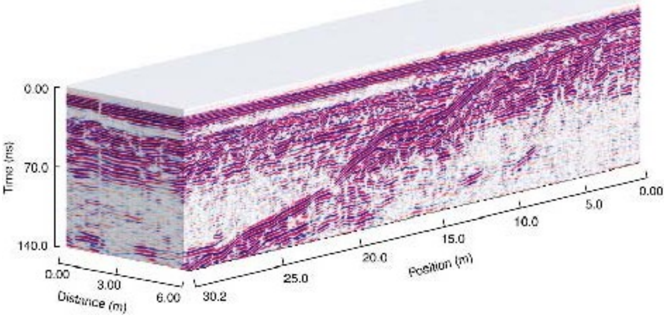

Figure 1.18: GPR image example, (Huisman et al., 2003).

to by the center frequency of the antennas, most typically 50, 100, 200, 400 or 900 MHz. The reflected energy returned to the earths surface is recorded at the receiver antenna. The GPR image (Figure 1.18) is produced from a compilation of the station recordings. The GPR image is a representation of the interaction between the transmitted EM energy and the spatial variation in the complex, frequency-dependent EM properties of the earth: the dielectric permittivity ϵ, the electrical conductivity σ, and the magnetic permeability μ.

For some applications (e.g. soil moisture's measurement), more quantitative information about the physical, chemical, and/or biological properties of regions of the subsurface is required. One way to approach this is to use the dielectric information contained in the radar image. This can be described as a two-step process, as is shown schematically in Figure 1.19. In step 1 a dielectric model is recovered by the radar image. In step 2 the relationships between the permittivity and the subsurface property of interest to obtain a model of the spatial variation in that property is used (in this example water content θ_w). The accuracy with which we can quantify subsurface properties is highly dependent upon our ability to obtain the dielectric model (Knight, 2001).

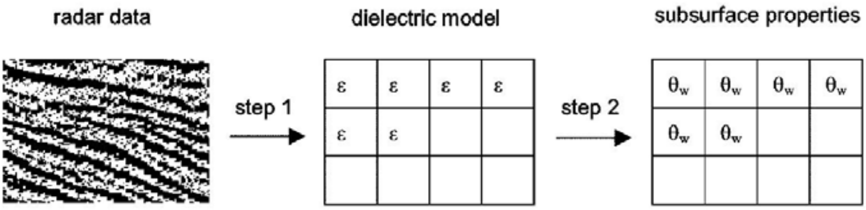

Figure 1.19: Schematic illustration of the methodology used for the quantitative interpretation of surface properties, (Huisman et al., 2003).

1.6.2 Hydrogeological Parameter Estimation using GPR

Geophysical data are being increasingly used in hydro-geological site characterization to obtain a better understanding of heterogeneity and its control on flow and transport. Such data can bridge the gap between the typically sparse conventional field characterization data and the need to realistically parameterize numerical transport models. It is clear that a complete vision of the soil condition can help farmers in agricultural practices' management.

Soil Moisture Content

Recent studies have shown that careful irrigation management can have beneficial effects on many crops, including almonds, citrus, prunes, pistachios and wine grapes. In particular, moderate water stress on grapevines early in the growing season can have a positive impact on grape quality. Thus, understanding when and how much irrigation (when allowed by D.O.C. rules) to apply is critical for optimized wine grape production. Natural geologic processes, however, can cause soil variations and associated water-holding capacity to vary significantly, even over distances of a few meters. Given that the "industry standard" to vineyard soil characterization is to collect soil or water content measurements on a 75 m grid, grape growers typically do not have enough information about water content variations to guide precision irrigation. By means of GPR, it is possible to estimate

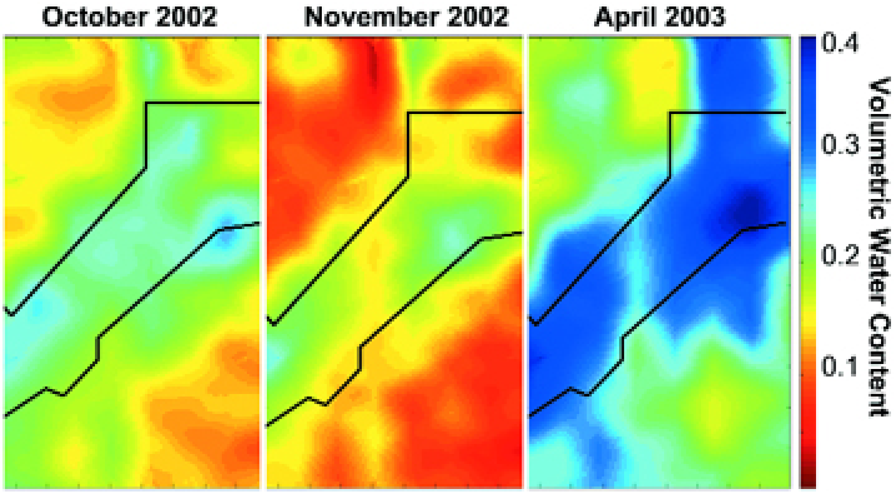

Figure 1.20: Average volumetric water content in the top 1.0-1.5m estimated over time using 100 MHz GPR reflection travel time data, (Rubin et al., 2002).

soil water content within agricultural sites in a non-invasive and manner and with high spatial resolution. Using 900 MHz GPR ground wave travel time data, soil water content distribution can be estimated in the top 15 cm of the soil layers at high spatial resolutions and as a function of time as reported in Rubin et al. (2002) during the experiment held at the Robert Mondavi Vineyard in California. Figure 1.20 suggests a correlation between water distribution and canopy density (as indicated by the low vigor outline drawn by the farmer). The experiment clearly showed that water content distribution is linked to soil textural and canopy vigor variations.

1.6.3 Analysis of GPR Methodology

GPR has the potential to help map soil properties such as soil texture and organic matter, thickness and depth of soil horizons and water tables, and differences in soil compaction due to plow pan development (Johnson et al., 1982) . Application of GPR traditionally requires visual inspection of the site and interpretation of the radargram regions into classes, followed by ground-truthing for verification, newer systems can perform some of these procedures automatically. If a quantitative procedure for systematic classification can be developed, GPR has the potential for broad use in precision agriculture as a non-invasive technique to delineate subsurface features. To accomplish on-the-go mapping, commercial GPR systems have been mounted on mobile platforms. Original studies were conducted using linear distance markers, which required substantial time. Freeland et al. (2002) linked geographic information system (GIS) and GPS packages with GPR to increase data collection and image post-processing efficiency and Huisman et al. (2003) has showed a GPR mounted on a mobile platform to provide on-the-go estimates of volumetric soil moisture content.

The experience reported in Rubin et al. (2005) suggests that surface geophysical methods may be very useful for accurately mapping soil variations in very high resolution. The soil-moisture patterns, often governed by soil texture, remain the same through time, even though the soil moisture content fluctuates with irrigation and season. Thus, once researchers and wine makers identify patterns in the soil properties, they can develop an efficient layout of the vineyards that allows for uniform farming that still renders high-quality wine grapes.

Even if this technique is at the research level, it seems to be a good precision farming instrument with high potential. The main problem is the cost of such instrument: if we imagine a large wine producing area to be monitored, it is clear that the time consumption in terms of data collecting, processing and map producing is large and hard to be handled. In the future, it is possible to imagine a GPR mounted on a tractor, measuring soil moisture in a fast way (after some sampling of the field), but this technique is still far away from the idea of a remote sensing system for vine precision farming when a large area is quickly monitored by different kind of sensors.

1.7 Automatic Vineyard Recognition

In order to complete the state of art about precision farming and remote sensing techniques applied to vineyards, it behooves to cite also an interesting processing technique proposed by CEMAGREF, a Research Institute in Montpellier. The proposed methodology (Delenne et al., 2008) is not strictly related to precision farming, because no biological parameter is extracted or calculated to provide information to farmers, but an automatic method for vine parcels detection and extraction is suggested. Anyway, if we consider a wine producing area inserted in its context, it can be easily understood **the importance of vine cadaster updating to have always a precise information of what is changing and how it is happening**. This topic is particularly hot for those wine producing are in the neighborhood of urban area, such as the Frascati D.O.C., where a lot of vineyards are rapidly disappearing. Vineyards' maps can be integrated within Geographical Information Systems (GIS) which can be used by winegrower cooperatives to improve the monitoring of quality compliance in areas registered in the list of Controlled Origin Denomination (D.O.C.).

The management of pollution, erosion and flood risks is another field that can take advantage of these maps. Indeed, these risks, depending on culture and soil surface condition, are worsened by mechanization and intensive cropping practices (Wassenaar et al., 2005) . User demand usually concerns:

- localization of vine plot
- detection of some characteristics that can be connected to cropping practices or crop quality (interrow width, orientation of rows, presence of grass between rows,. . .).

Most vineyard related studies using remote sensing data meet the second requirement by detecting vine rows (Bobillet et al., 2003), or by characterizing training mode (Wassenaar et al., 2002) or foliar density (Hall et al., 2003) for previously delimited plots. They emphasize the relevance of textural analysis applied to sub-metric spatial resolution images. Indeed, according to the Shannon- Nyquist theorem, periodic patterns resulting from the spatial arrangement of vine plants (often in lines or grid), become perceptible with a spatial resolution that is at least twice as small as the pattern period. In many wine-growing regions, the minimum distance between two vine rows, can be as small as 1 m; consequently, image spatial resolution should be lower than 0.5 m. Because of this periodic organization, a vine pattern can roughly be assimilated to a local planar wave of a given spatial frequency and orientation. Therefore, frequency analysis appears as a suitable approach for vine detection.

A Fourier Transform based analysis is straightforward and quite as effective since this tool is perfectly suited for oriented and periodic texture detection. Basically, the Fourier spectrum of a vine plot image contains two or four main amplitude peaks, the position of which being directly related to vine row orientation and inter-row width. Wassenaar (Wassenaar et al., 2002) successfully used it for vine/non-vine classification and characterization on 25 cm resolution images. This method also gave a very precise estimation of inter row width and row orientation. In Chanussot et al. (2005), a Radon transform is applied to the Fourier spectrum of a 2 cm resolution image which allows a more precise evaluation of row orientation, used in a further algorithm of missing trees detection. However, in this case, a preliminary delineation of the vine plots is required. The problem of vineyard detection, segmentation and characterization in VHR[4] aerial images, is addressed without any parcel plan availability and an original recursive scheme is proposed to meet this need. The main idea of the proposed technique is to isolate each individual plot by selecting the corresponding frequencies in the Fourier spectrum, using a specific Gabor filter. This algorithm has been developed in the framework of *Bacchus Project*.

1.7.1 The test site: the Languedoc region

In the study area, like in most of vine-growing regions, two main patterns can be observed on aerial images according to vine training mode:

---

[4] Very High Resolution

- **Grid pattern**: about a quarter of the vineyards considered in this study is trained in *"goblet"*. This old method of vine training involves no wire or other system of support: vine stocks are planted according to a grid pattern, often square, with approximately 1.5 m 1.5 m spacing in the study area but sometime up to 3 m spacing in dry regions.
- **Line pattern**: most of the recent vineyards are trained using horizontal wires to which the fruiting shoots are tied. Spacing separating two wires is higher than spacing between vine stocks guided by the same wire (often 1 m 2.5 m spacing in the study area), which leads to row patterns. More adapted to mechanization, this training mode named trellis, is mainly used.

For tests and validation, data acquisition was made on a 200 ha study area (Figure 1.21), during the first week of July 2005, when foliar development was such that both vine and soil were visible on aerial images. The images, acquired by an optical sensor mounted on a small aircraft, were geometrically corrected, mosaicked and re-sampled for a 50 cm resolution. However, the original image required for FFT computation must be in gray levels and only the red one is used thereafter, since it provides higher contrast between vine and soil even covered by grass. Ground-truth information was collected at the same time as image acquisition, especially concerning land use and vine pattern (grid or line). Inter-row width (pattern period) and orientation were obtained by precise on-screen measurements.

1.7.2 Fourier Transform of a vine plot image

Fourier theory states that almost any signal, including images, can be expressed as a sum of sinusoidal waves oscillating at different frequencies. The Fourier Transform amplitude (or Fourier spectrum) of an image I, can be represented in the frequency domain as another image FI. In the conventional representation, this image is symmetric with respect to its center, which contains the average of I, (i.e. the amplitude of the null frequency F_0). Each position of pixel corresponds to a particular spatial

Figure 1.21: View of the test site in the Languedoc region, (Chanussot et al., 2005).

frequency f increasing the further it is from center from $f = 0$ to $f = \pm 0.5$. Its value codes the amplitude of Fourier spectrum, which depends on the presence of the corresponding frequency in the original image I. Since vineyard patterns on aerial images are periodical and oriented, they induce very located peaks of amplitude in Fourier spectrum.

Three characteristics can be deduced from the value and positions of these peaks:

1. peak value can be seen as an estimation of the vine presence in the original image.
2. The angle formed by vector (center, peak) with the horizontal line, determines the wave direction in a polar coordinate system, which is perpendicular to the pattern direction, i.e. the vine row orientation θ.
3. The distance r between one peak and the center, is the frequency f of the corresponding wave ($f \in [0, 0.5]$). This value is directly linked to the pattern period T in pixel i.e.the vine inter-row width, by $f = 1/T$.

The horizontal and vertical lines intersecting at the spectrum center are due to the non-periodicity of the original image: they represent the frequency components of the image edge discontinuities. These edge-effect peaks, which could mask plot peak detection, can be avoided by applying a Hanning window to the original image before Fourier transform computation (Figure 1.22). Note that, due to the gray-level attenuation, the modified image is used only for peak detection, the original one being taken again for the filtering process itself.

1.7.3 Gabor Filters

In the spatial domain, a Gabor filter is defined by an impulse response, which is a complex sinusoid with frequency (u_0, v_0), modulated by a Gaussian envelop $g(x, y)$:

$$h(x, y) = g(x, y)\, e^{-2\pi j(u_0 x + v_0 y)} \tag{1.3}$$

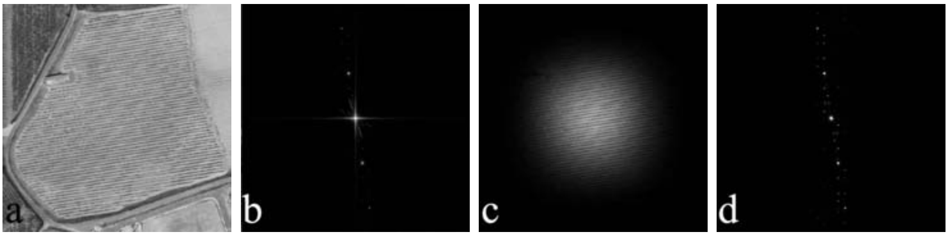

Figure 1.22: Hanning window effect: a) original image, b) FFT calculation without Hanning window, c) original image multiplied by the Hanning window, d) FFT calculation with Hanning window,(Chanussot et al., 2005).

where

$$g(x, y) = \frac{1}{2\pi\sigma^2}\, e^{\frac{x^2+y^2}{2\sigma^2}} \tag{1.4}$$

Going into the frequency domain, the Fourier transform of $h(x, y)$ is a Gausssian function centered on the frequency (u_0, v_0):

$$FT(h(x, y)) = H(u, v) = G(u - u_0, v - v_0) \tag{1.5}$$

where

$$G(u, v) = e^{-2\pi^2\sigma^2(u^2+v^2)} \tag{1.6}$$

Therefore, the Gabor filter acts as a Gaussian band-pass filter, which can be used to select a given range of frequencies around a particular amplitude peak centered on (u_0, v_0) in the Fourier spectrum. The parameter σ is the filter width. A large value of σ will decrease the accuracy of plot edge location while a too small value, which corresponds to a large filter radius in the spectral domain, will decrease the filter selectivity. A value of about eight pixels, leading to a filter support width of about 2% of the total frequency range in the spectral domain, appears to be a good trade-off. It corresponds to a plot edge location inaccuracy of a few meters. The filtering process can be applied directly in the Fourier domain:

$$TF(O(u,v)) = TF(I(u,v)) \cdot H(u,v) \tag{1.7}$$

where $TF(I(u,v))$ is the Fourier transform of $I(x,y)$. The final result image $O(x,y)$ is then obtained as the inverse Fourier transform of $TF(O(u,v))$.

Figure 1.23 shows two examples of Gabor filtered outputs corresponding to two different amplitude peaks in the Fourier spectrum of the original image. As we can see, this filtering process appears to be very efficient for vine plot segmentation, provided that it is followed by a thresholding step and a binary object enumeration.

The Gabor filtering process described above must be applied on limited size images (typically 500 500 pixels) both for computational reasons and to get exploitable Fourier spectra. When dealing with large aerial images (typically 5000 5000 pixels), an image partitioning is used. As a result, a set of adjacent sub-images is obtained which will be processed successively. Moreover, as the Hanning window tends to decrease image contrast near its edges, adjacent sub-images issued from the initial partitioning step must present a significant overlap to ensure that every portion of the original image is examined under its optimal contrast.

1.7.4 On overview of the Algorithm

The iterative algorithm can be easily summarized as follow:

1. The original image Fourier spectrum is computed, and only the highest peak is searched for within potential frequencies of vineyard (given by minimum and maximum inter-row width encountered).

2. A Gabor filter, centered on this peak is processed, followed by Fourier inversion and binary thresholding. For each plot found at this step:

    - a new sub-image is created where all pixels but those of the candidate plot are painted in black, so that only its corresponding amplitude peak will appear in the Fourier spectrum. A new Gabor

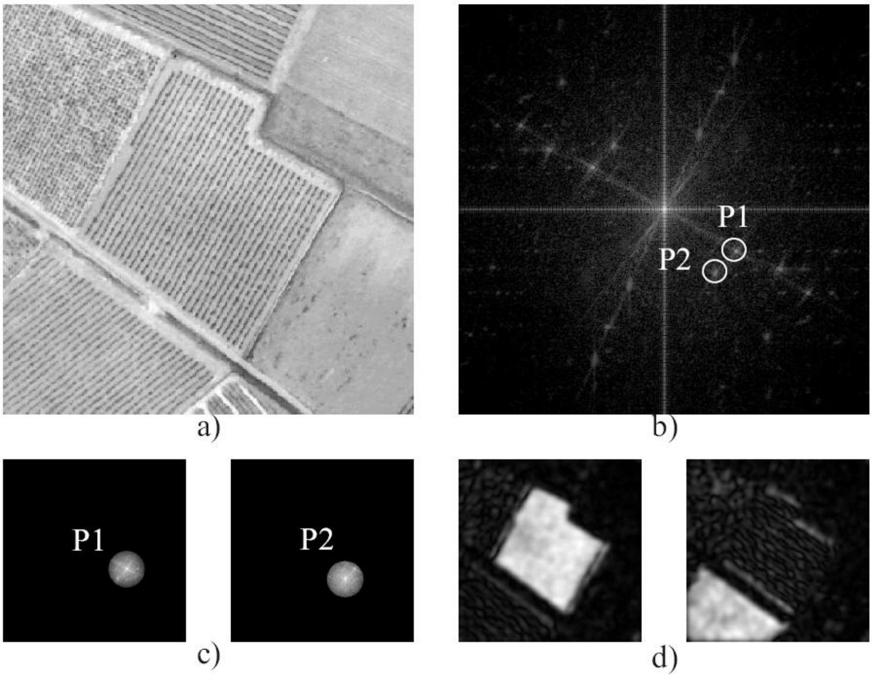

Figure 1.23: Gabor filtering. a) Original image, b) its Fourier transform, c) Peak selection using Gabor filters, d) modulus of the output complex image for both peaks, (Chanussot et al., 2005).

  filtering is then applied around this unique peak and the FFT inversion is carried out on the original image to obtain a possibly more closely matching vine plot

  - if the resulting binary object touches a sub-image edge, a new sub-image is built around it with extended margins, and the whole process is reiterated. By this way, we are guaranteed to recover the complete plot in one or several iterations.

3. when the corresponding plots have been completely recovered, they are listed and erased from the original image by painting them in black.

4. The process is reiterated from 1.

A schema of the algorithm can be found in the Figure 1.24.

1.7.5 Automatic Vine Detection Algorithm Analysis

The proposed vine plot detection algorithm proved its efficiency, extracting several parcels by high resolution images. While most of detection studies - not only concerning vineyards - provide a pixel classification, the main originality of this method is that results are directly available in a polygonal form, thanks to the automatic segmentation process. Another significant advantage is that largely available data can be used. Indeed, the method does not requires any multi-spectral information, and can be successfully applied on the red channel of an aerial image. Moreover, since the appropriate spatial resolution is linked to the researched pattern period, a poorer resolution could be used in many other vine-growing regions, especially dry regions such as in Spain where inter-row widths are up to 3 m. Then, satellite images, such as those provided by IKONOS or Quickbird, could be used. Using frequency analysis, very precise information of row orientation and inter-row width can be deduced from the peak position in the Fourier spectrum. Moreover, this algorithm can be used as a first step for a more complex system with value-added products, e.g. detection of dead vine trees.

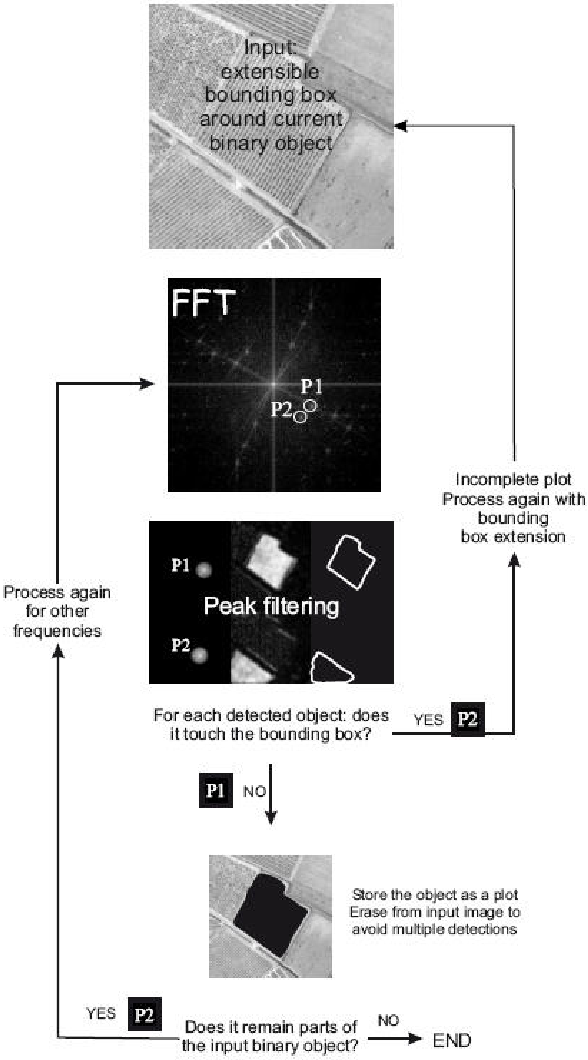

Figure 1.24: Schema of the vine plot detection algorithm, (Chanussot et al., 2005).

Figure 1.25: Example of Dead Tree Detection, (Chanussot et al., 2005).

1.7.6 Detection of dead vine trees

Also for the detection of the dead vine trees (Chanussot et al., 2005), the geometrical properties of a vine parcel is used. To automatically estimate the orientation α of the selected vineyard, the Radon transform of the Fourier spectrum is computed. Each line of the Fourier transformed image, even discontinuous, gives a peak positioned at the corresponding line parameter in the Radon domain. From the spectrum, it is possible to derive the inter-tree space d. Starting from the origin of the Fourier spectrum, the first peak along the direction estimated thanks to the Radon transform is sought. The distance between the origin and this peak is inversely proportional to the periodicity of the features along one vine row, i.e. inversely proportional to the typical inter-tree space. After a calibration, the coefficient of proportionality is estimated leading to the knowledge of the inter-tree space. After the estimation of parameters α and d, the detection of missing trees can be achieved, based on the use of classical morphological operators. The result of this technique can be seen in Figure 1.25.

1.8 Thesis Objective and Outline

General Aims

The Thesis illustrates the following main points:

- SAR in vine precision farming: evaluation of potential, processing techniques and investigation about the backscattering sensitivity to agricultural practices, in particular during the harvest period. Three main platforms have been analyzed, by means of multi-temporal analysis:

    - Airborne very high resolution ESAR fully polarimetric both L and C Band Data
    - High resolution fully and dual polarimetric ALOS PALSAR L Band Data
    - High resolution fully polarimetric RADARSAT-2 C Band Data

  The different behavior of radar data at different polarizations, incidence angles and frequencies has been analyzed; the potential of high resolution SAR for crop monitoring purposes is also discussed.

- High resolution optical data in vine precision farming: Vigor Index and LAI estimation by means of an empirical model

- Fusion of Optical and Radar data for classification of vineyards.

- Design and implementation of an open source precision farming platform and its integration in a collaborative environment: Geovine and Frascati Living Lab experiences.

Outline

- Chapter 1 draws an outline of the state of the art of vineyard precision farming supported by remote sensing techniques. Several case studies are presented and critically discussed, focusing on results, efforts and costs of the proposed techniques.

- Chapter 2 analyzes the classification potential of high resolution SAR data by means of Neural Networks. A comparison between optical data and radar data classification capability is presented.

- Chapter 3 analyzes the sensitivity of backscattering to vigor index and to LAI. The retrieval of such indexes by means of SAR data is presented and discussed.
- Chapter 4 analyzes the sensitivity of backscattering to grapes by means of different SAR Platform (airborne and spaceborne), at different spatial resolutions (high and very high resolution), at different frequencies (L and C Band) and at different polarization (Dual and Fully Polarimetric Mode). The analyzed data are from BACCHUS-Doc mission, ALOS and RADARSAT-2 Space Mission.
- Chapter 6 shows the design and implementation of an open source web service for precision farming and the value added map integration.
- Chapter 7 summarizes the conclusions for each topic.

Chapter 2

Classification of vineyards by means of HR SAR

In this chapter the potential of high resolution polarimetric radar for classification purposes will be analyzed and discussed; in particular, the radar capability in vineyard detection will be discussed and related with the classical vine cadastre updating procedures as a new support layer; the vine cadastre, as reported in the Chapter 1, is an important common layer in a precision farming system and its update and accuracy is crucial.

2.1 The Radar as an instrument for cadastre updating

As reported in Srinivasan (2006), the management and monitoring of territory play a key role for a precision farming system's definition: each instrument or techniques that can provide reliable informations about the land use (in perspective also the changes in land-use) or about plants'status has to be provided as an input information layer to the main system (Chapter 1.1.1, Figure 1.2). The aim of this chapter is to evaluate the potential of polarimetric radar as an instrument for classification purposes and for cadastral data updating. The preliminary strategy aimed at precisely define the actual borders of the parcels (vineyards and olive groves) in the area and at identifying man made structures, roads and bare soil. The mapping is based on a supervised neural network algorithm fed either by radar polarimetric, or by multi-spectral optical data. Co-registered radar and optical data are then fused in a higher-dimensional input to feed the neural network classifier. The performances of each algorithm is evaluated by means of confusion matrix. An outline of the main algorithm is showed in Figure 2.1

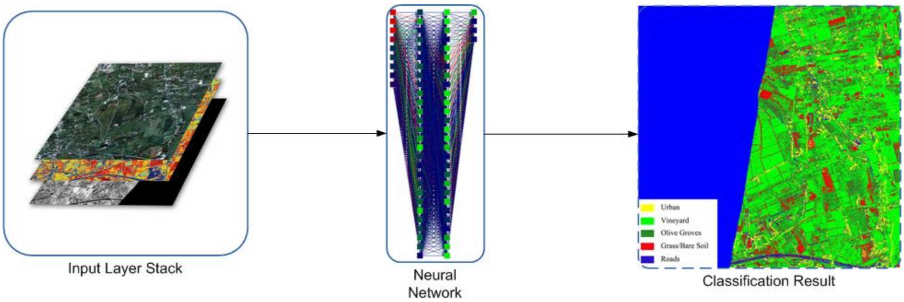

Figure 2.1: Outline of the classification algorithm

The analysis has been carried out by considering the same training pixels for all the data-sets and the same neural network topology (2 hidden layers with 28 neurons each) in order to have the same conditions for all the scenarios. A fixed topology with a so large number of hidden neurons has been selected to better manage the number of input layer, up to 7 inputs when Radar/Optical data feeds the system; growing with the input dataset's complexity, the system is fed by L Band data, C band data and then with the fused dataset Optical/Radar. The reference ground truth map is reported in Figure 2.2

2.1.1 L Band data at 25 degrees incidence angle

L Band dataset, in the near range zone, is considered. Results are reported in Figure 2.3 and the confusion matrix in Table 2.1. A confusion between Olive Groves and Vineyard class has been noticed all over the vineyards

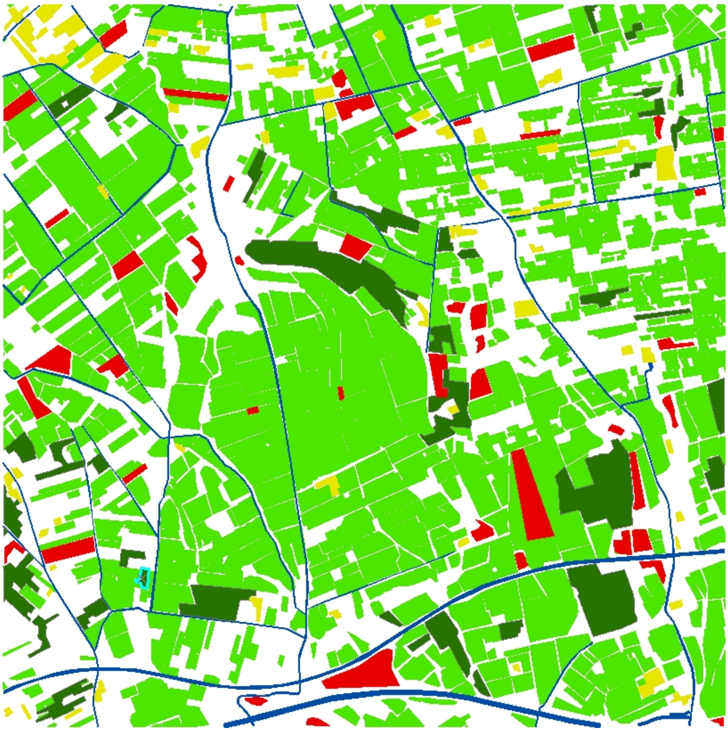

Figure 2.2: The Ground Truth map used as a reference

with a row perpendicular orientation to the flight direction, while a good correspondence has been reported for the other classes, especially for the Grass/Bare Soil.

	Urban	Vineyards	Olive	Roads	Grass	
Urban	25032	20	60	326	79	25517
Vineyard	1458	20225	3465	12	188	25348
Olive	756	2456	18326	82	138	21758
Roads	265	154	54	22982	5460	28951
Grass	489	145	95	598	17235	18562
	28000	23000	22000	24000	23100	103800

Accuracy = 86.43%

Table 2.1: Confusion Matrix for L Band data, near range area

2.1.2 L Band data at 45 degrees incidence angle

L Band dataset, in the far range zone, is considered. Results are reported in Figure 2.4 and the confusion matrix in Table 2.2. the confusion between Olive Groves and Vineyard is sensibly reduced; an over-estimation of Roads all over the shadow areas can be easily noticed with a decrease of the accuracy over the Urban class. The detection of Grass/Bare Soil is still good, with an increase of the accuracy over the small paths used by tractors to access the fields.

2.1.3 Multi Angle L Band Data Classification

Thanks to the acquisition geometry (Horn, 2005b), for a 500 m wide stripe, a multi angle configuration has been used to feed the neural network. The classification result is reported in Figure 2.5. To correct overlay the two different data, a DEM[1] has been used to horto-rectify the dataset and to

---

[1] Digital Elevation Model

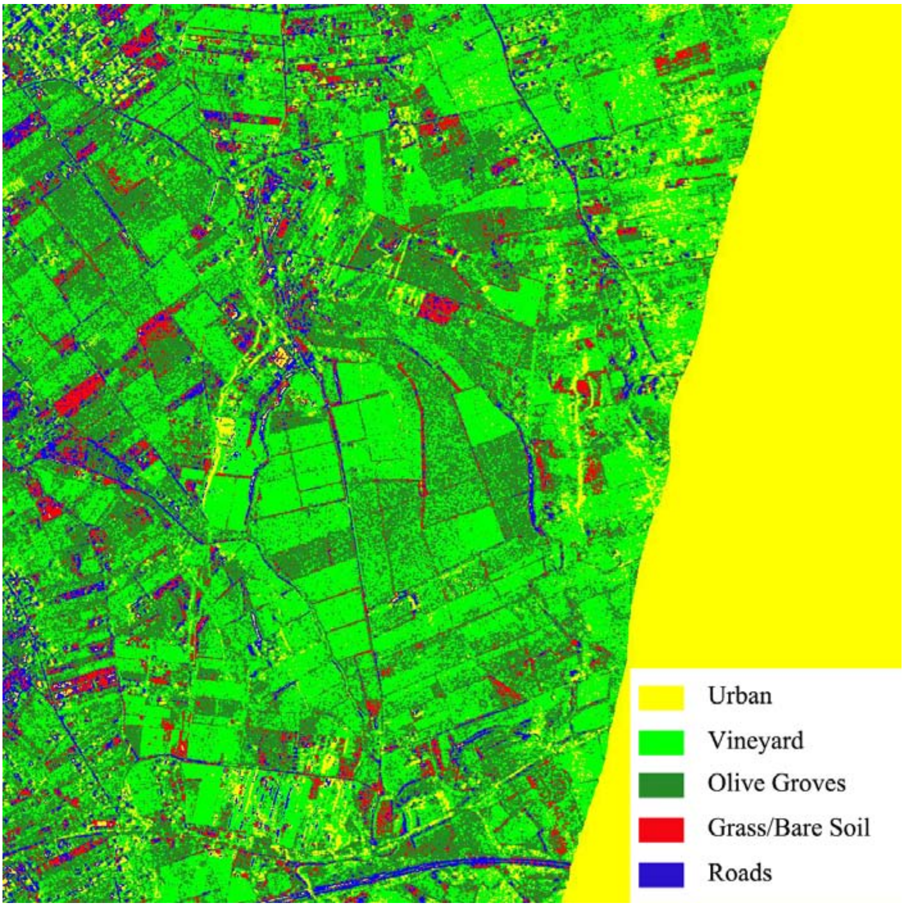

Figure 2.3: Test Site classification by means of L Band Polarimetric data @ 25° incidence angle

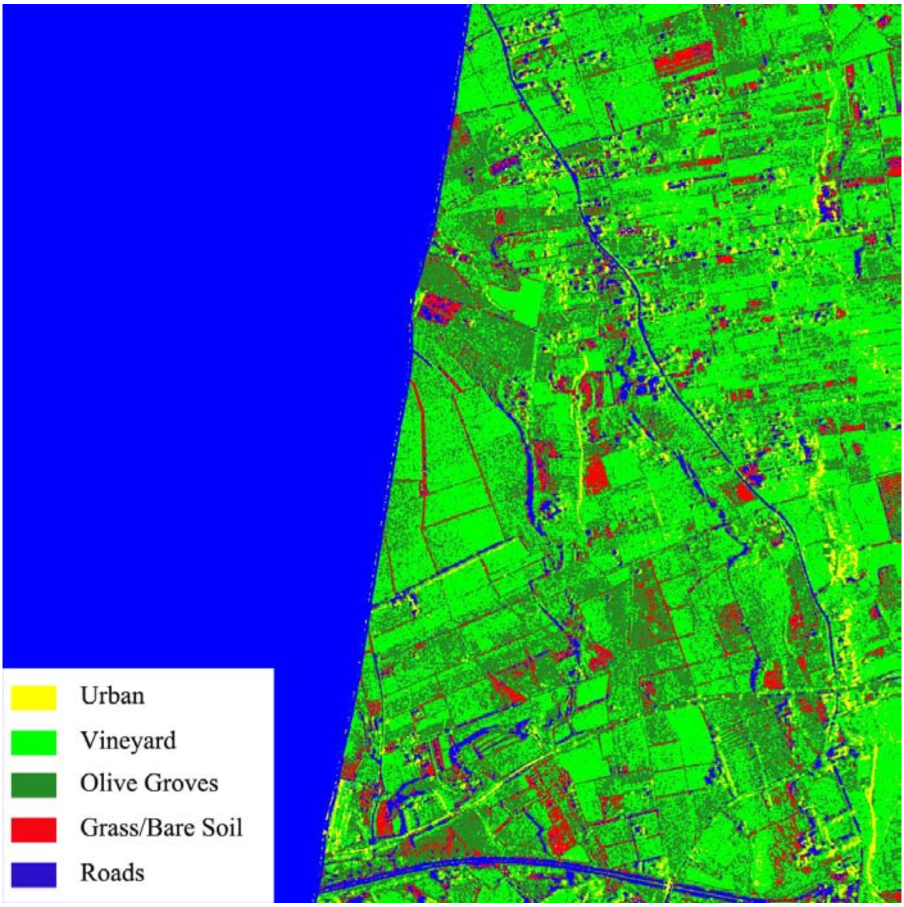

Figure 2.4: Test Site classification by means of L Band Polarimetric data @ 45° incidence angle

	Urban	Vineyards	Olive	Roads	Grass	
Urban	10326	126	160	53	298	10963
Vineyard	1852	17436	921	41	278	20528
Olive	495	2202	17562	178	265	21702
Roads	568	126	123	9253	358	10428
Grass	759	110	234	475	13801	15379
	15000	20000	19000	10000	15000	68378

Accuracy = 86.55%

Table 2.2: Confusion Matrix for L Band data, far range area

better correct the incidence angle effect. No significant improvement has been noticed.

2.1.4 L and C band data at 25 degrees incidence angle

L-Band Polarimetric and C-Band Dual - Pol Data are now used, with the aim of evaluating the joint potential of a multi-frequency dataset. The results for each incidence angle is reported into the Figure 2.6 and the confusion matrix in Table 2.3. The overall accuracy increases; confusion between the road and bare soil class is present, but the accuracy of vineyards/grassland recognition increases.

	Urban	Vineyards	Olive	Roads	Grass	
Urban	25619	45	72	326	124	26186
Vineyard	1106	21305	2366	12	189	24978
Olive	743	1469	19253	82	256	21803
Roads	163	98	67	22982	5178	28488
Grass	369	83	242	598	18253	19545
	28000	23000	22000	24000	24000	107412

Accuracy = 88.77%

Table 2.3: Confusion Matrix for L and C Band data, near range area

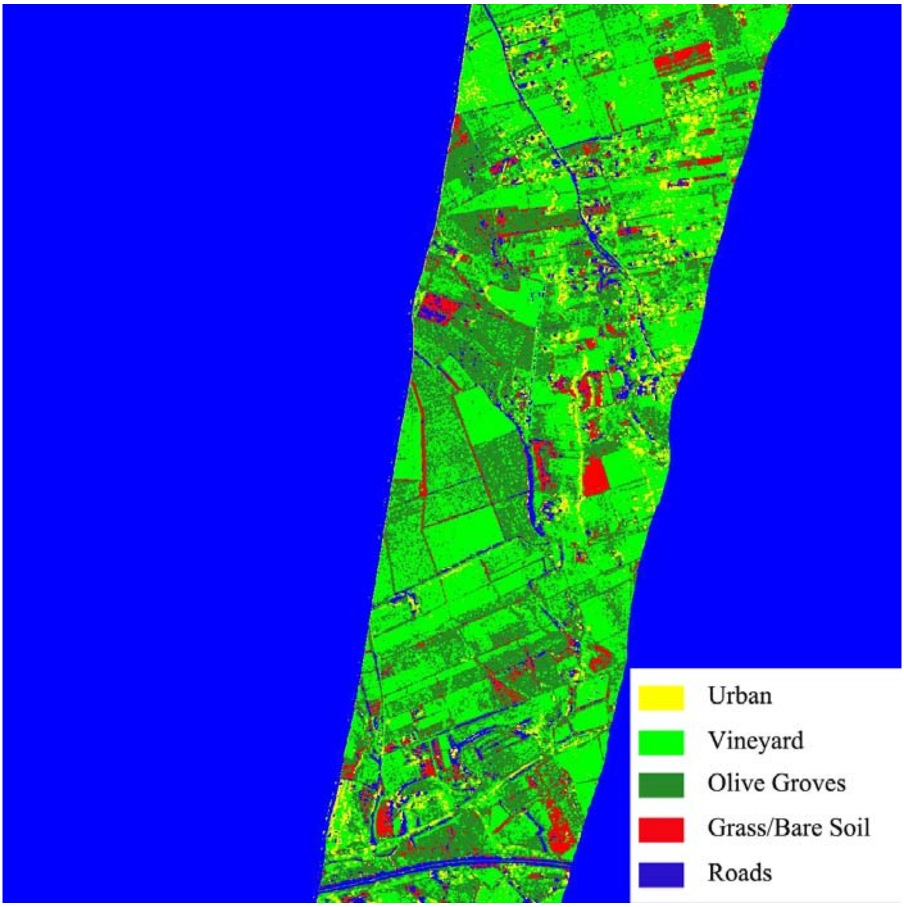

Figure 2.5: Multi angle classification at L band (Overlapping area, with 25° and 45° incidence angle)

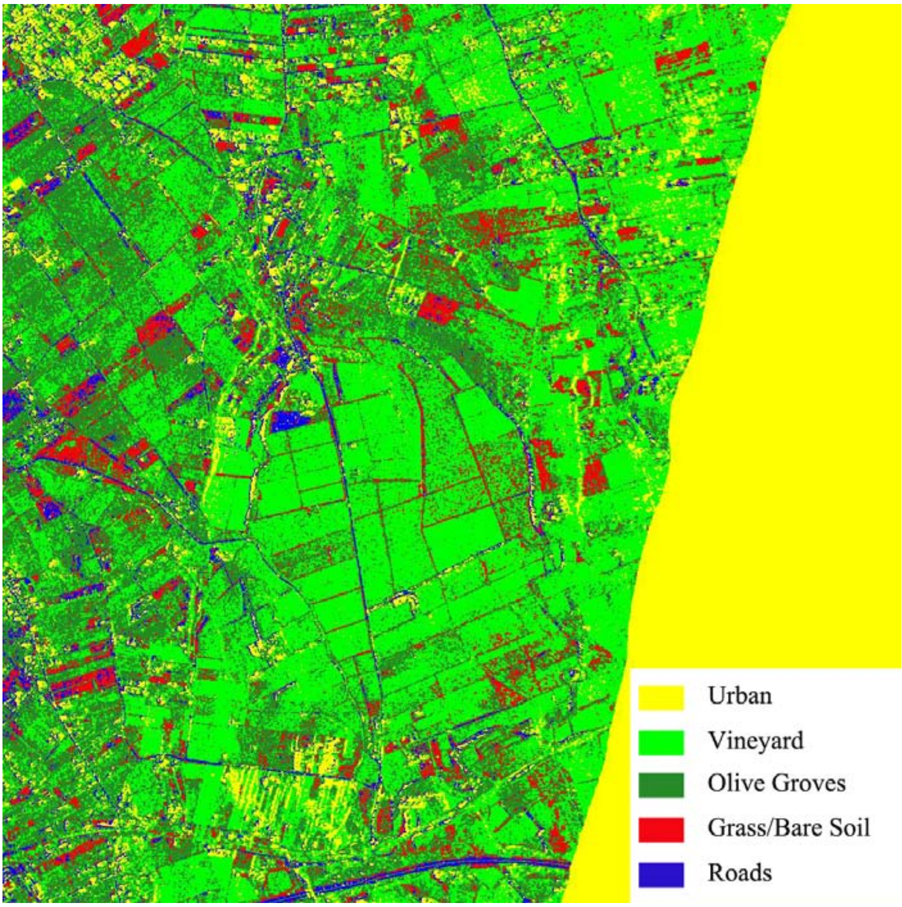

Figure 2.6: Test Site classification by means of L Band Polarimetric and C Band Dual-Pol data @ 25° incidence angle

2.1.5 L and C band data at 45 degrees incidence angle

L-Band Polarimetric and C-Band Dual - Pol Data feed the network. The results for each incidence angle is reported into the Figure 2.7 and the confusion matrix in Table 2.4. The overall accuracy is sensibly increased with an improvement in all classes; In particular this configuration showed great capability in wasted vineyard recognition and detection.

	Urban	Vineyards	Olive	Roads	Grass	
Urban	12684	35	65	12	94	12890
Vineyard	468	18580	1021	53	144	20266
Olive	1562	1253	17857	82	183	20937
Roads	134	78	23	9623	254	10112
Grass	152	54	34	230	14325	14795
	15000	20000	19000	10000	15000	73069

Accuracy = 92.49%

Table 2.4: Confusion Matrix for L and C Band data, far range area

2.2 On the Radar classification potentiality

The potential of SAR for agricultural landscape classification purposes has been already discussed in literature (Del Frate et al., 2003) and several experiments demonstrated its capability in several cultures's discrimination (Ferrazzoli et al., 1999), but no study is present dealing with the vineyard identification and status classification. The SAR showed a good classification capability also at pixel level, with some unexpected results over particular fields, with the discrimination of productive vines from young and small vineyard. It has been noticed that by means of a more complex input dataset (multi-frequency analysis) the achieved results improves the classification's quality. It is very interesting the analysis of a vineyard where a fist half of the field is covered by stable and productive vines and the second half covered by small, young and still unproductive vines (Figure 2.8). None

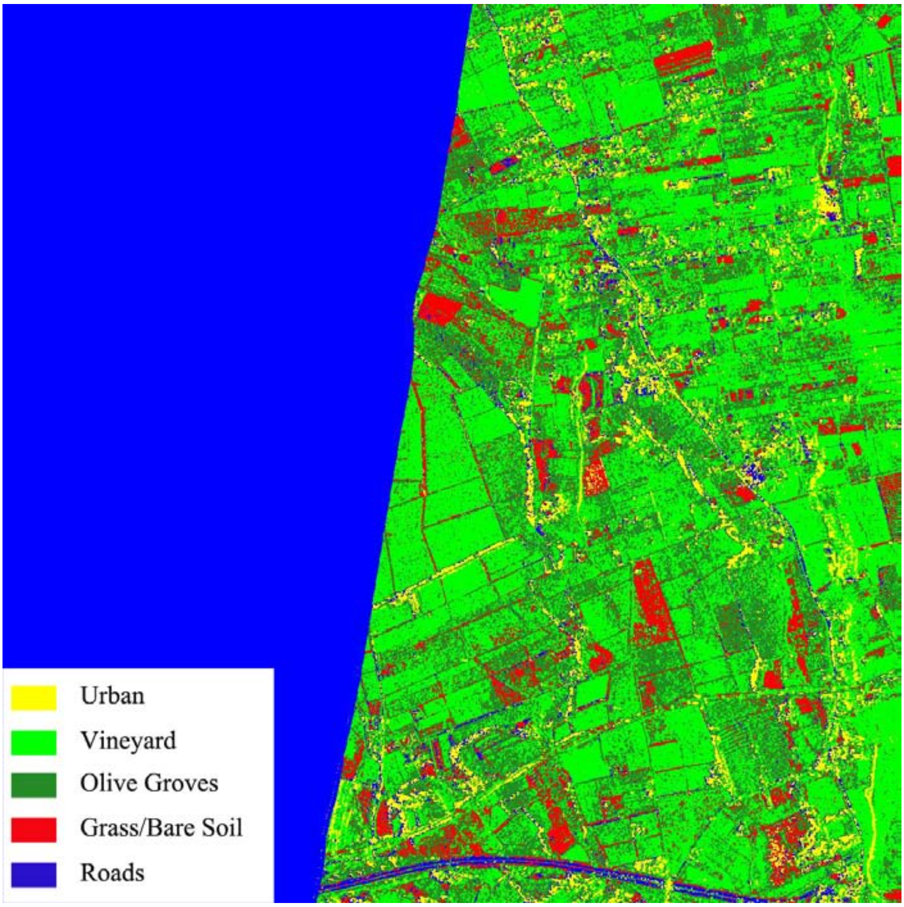

Figure 2.7: Test Site classification by means of L Band Polarimetric and C Band Dual-Pol data @ 45° incidence angle

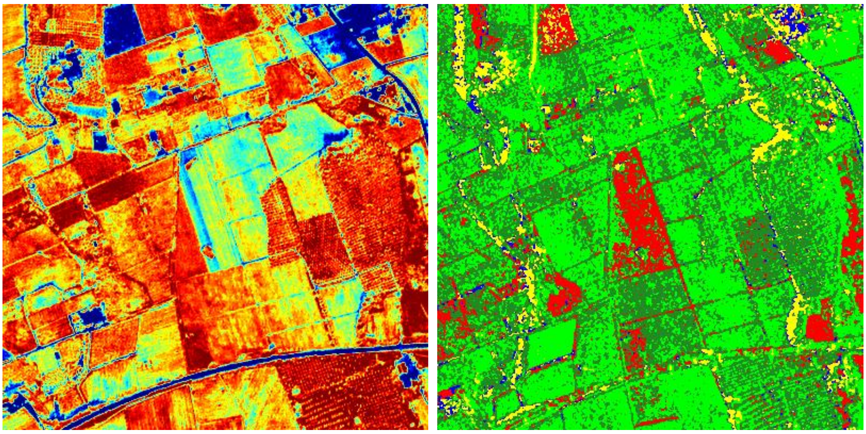

Figure 2.8: The Vigour Index map (left) is compared to the C and L Band (40°) classification(right): Radar provides the correct interpretation of the field status.

of the previous input dataset configuration (L Band or C band processed separately) and also the use of optical data provided such good results. The Vigor Index Map shows a low vigor area, where also the neighbor parcels are affected by this condition and no information, also by means the Quickbird data's spectral information it is possible to discriminate a productive vineyard from an unproductive one. Moreover, the grass covering the parcel can mask the vigor signal and optical data does not provide any information about the structure of the parcels. Indeed, also by means of panchromatic channel at 60 cm of resolution, the *"row texture"* was present, providing all the information to classify this parcel as a productive one or at least as a permanent crop. After the dataset processing, this Optical/Radar contradictory result suggested an in-field visual inspection: the vine parcel was covered by grass and small vines, with few leaves and without the complete supporting stable structure as in a productive parcel's case. Asking directly to the farmer about the parcel status, he reported that the vineyard was very old and became unproductive; hence, the old vines were rooted out and new ones were planted. The parcel was reported to be in a very young phase, with still about 5 years before of the productive phase. Moreover, in the near range domain, the classification exercise showed a mixed vineyards'behavior, with not negligible number of bare soil pixels, specially for orthogonal row orientation respect to flight's direction. This effect can be explained with the geometric schema of the vineyard and the effect of incidence angle, as reported in Chapter 3.2. Indeed, this effect disappears at higher incidence angle.

Chapter 3

Backscattering Sensitivity to Vigor Index

In this chapter the choice of using radar as a new instrument for precision farming, its main capabilities and limitations, will be shortly introduced . Then, the BACCHUS-DOC mission is presented and analyzed, focusing the research on the sensitivity of backscattering to Vigor Index. The integration between High Resolution Polarimetric SAR and Optical Data (QuickBird) will be discussed.

3.1 The Baccus-DOC mission

A first study on the sensitivity to vine phenology was carried out using the C-Band SAR mounted on ERS-2 (Burini et al., 2005), analyzing the Frascati agricultural zone because of the dense cultivation of vines and olives and the presence of a large radar and optical data set. The study demonstrated the capability of SAR in monitoring task also for complex agricultural land scape, such as the Frascati zone, made by small fields rarely situated in a flat area; the multi temporal approach, underlined a clear backscattering signature during the principal agricultural practices (harrowing) and some interesting result during the fruit maturation period.

This unexpected result suggested new researches with more powerful sensors than the ERS's SAR, to better understand the complex electromagnetic environment of a vineyard: a mix of stable woods, metallic wires and grapes.

In the fall of 2005, in collaboration with DLR and ESA, two polarimetric SAR acquisition were planned in order to verify the sensitivity of backscattering to grapes variations: the *Bacchus DOC* campaign (ESRIN/Contract No. 19188/05/I-LG), in which two polarimetric very-high resolution SAR data acquisitions have been carried out to investigate the backscattering behavior during the harvest period (Burini et al., 2006). The "Bacchus - DOC" campaign was made of multi-temporal observations by the polarimetric high resolution SAR, from one side contributed to enhance the database by adding the polarimetric microwave backscattering data and, on the other, provided some further insight into the backscattering behavior of grapes. The main scientific objectives of the campaign can be summarized as follow:

- Investigation on the potential of polarimetric radar in vineyards inventory and characterization
- Assessment of the potential of polarimetric radar in monitoring bio geo physical parameters, like soil moisture and grape biomass, which can be useful in farming practices

The experiment took place in the fall of 2005; the DLR E-SAR system on board a Dornier DO 228 aircraft (Figure 3.1) flew over part of the Frascati wine producing area on 5 October, when a large part of grapes were still present, and on 25 October, after vintage. The study area was imaged at high spatial resolution (≈ 2 m) at C-band at VV and VH polarizations and at L-Band in a fully polarimetric mode. The area of interest was covered by two strips of size 3 km x 7 km each, overlapping each other by about 500 m, with corner reflectors placed as ground control points for georeferencing and calibrating purposes (Figure 3.2).

During each SAR acquisition, contemporary intensive and extensive measurements were carried out to implement a georeferenced ground truth database: extensive measurements aimed at collecting information on the general condition of the terrain and the state of some test fields in a wide

Figure 3.1: The Dornier DO-228 re-fueling just after the second flight on the Ciampino Taxi Way

area of the Frascati wine production area; intensive measurement were performed in a selected estate to gather detailed data about geometrical features of the vineyard, such as row orientation and vine spacing, and plant parameters as leaf density distribution and dimension and mass of grapes (Horn, 2005a). For the support of the SAR operation one set of two 90 cm radar reflectors and a GPS monitoring receiver (equipment) were required on ground. 2 trihedral corner reflectors (size: 90 cm) have been deployed in the field in order to provide good radiometric calibration and stable GPS measurements (Figure 3.3).

The IGS station INGR located in Rome and operated by the Agenzia Spaziale Italiana was selected as the geographical reference. The data of this station were used for all static DGPS survey work, i.e. the positioning of the radar reflectors and the GPS monitoring receiver at Ciampino airport. The INGR stations position was cross-checked with data of the EUREF station AQUI which is located in L'Aquila. All the data collected has been integrated into a G.I.S.

3.1.1 The Bacchus DOC Data Set

The Bacchus DOC campaign consisted into two SAR surveys over a part of the Frascati Wine Producing Area. Each acquisition was made by sub-swath

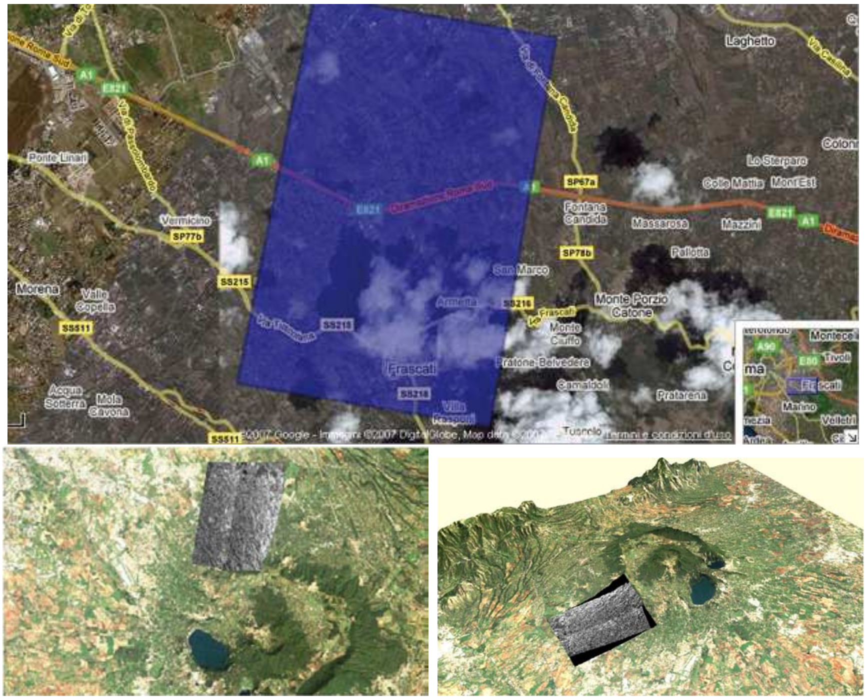

Figure 3.2: View of the Bacchus-Doc Test Site. On the top, view of the test site. On the left, the two radar stripes overlaid on Landsat Image. On the right, 3D rendering of the imaged area.

Figure 3.3: The corner reflector for radiometric calibration. It is possible to notice also the GPS equipment for the gecoding operation.

of about 3 km x 7 km , with an overlapping zone of about 500 m. The SAR imaged the area using 2 polarizations, L band, in a fully polarimetric mode and C band, in a dual polarization mode. Data were delivered by DVD into several format:

- Single Look Complex - Each polarimetric channel is coded into an image with a pixel spacing of 0.49 m x 1,49 m. Complex Format
- Single Look Complex Geocoded - Each polarimetric channel is coded into a geocoded image. Complex Format
- Precision Image - Each polarimetric channel is coded into an integer image with a pixel spacing of 1 m x 1 m. The speckle is reduced by multi look technique (3 looks)
- Geocoded Precision Image - Each polarimetric channel is coded into a geocoded DEM corrected image.

3.1.2 ESAR system

The E-SAR is a multi-frequency SAR system mounted on board a Dornier DO 228 aircraft, which is owned and operated by DLR. At present the

	SLC	**SLC Geo**	**PRI**	**PRI GEO**
L-Band Full Pol.	16 images (complex data format)	16 images (SLC format emulation)	16 images (Long Integer)	16 images (Long Integer)
C-Band Dual Pol.	8 images (complex data format)	8 images (SLC format emulation)	8 images (Long Integer)	8 images (Long Integer)

Table 3.1: Baccus Doc Image Data Set

radar is operational in P-, L-, C- and X-Bands with selectable vertical or horizontal antenna polarizations. System extension to P-Band (450 MHz centre frequency) operation was completed in 1994. A L-Band multi polarization capability was realized in 1995. SAR interferometry and SAR polarimetry are new functional modes of the radar, which are on their way to be integrated during 1996.

The Figure 3.1 shows a DLR research aircraft of type Dornier DO 228 with the E-SAR radar installed on-board. Antenna installations are visible under the nose and in the back of the aircraft. The cigar-like pod under the nose contains the P-Band antenna. Beneath the cargo door in the back a radome covers both the C- and X-Band antennas. The L-Band antenna, splitted into two individual arrays, one for each polarization, is attached to the tail of the aircraft and carries the aircraft's ID.

A special feature of the system are small, fixed mounted antennas. The associated wide azimuth beam avoids having to steer the antenna to compensate for yawing of the platform. A small antenna also permits very high azimuth resolution ($<$ 100 cm) to be achieved under favorable flight conditions. Depending on the Doppler offset used during processing of the SAR data, scenes can be imaged under different azimuth viewing angles (squint mode, spotlight mode). These characteristics consequently lead to a very high data amount to be recorded at high data rate.

The E-SAR is able to collect raw data in three different swath modes, narrow (3 km), wide (5 km) and super wide swath (15 km), with accordingly reduced slant range resolution. One range line consists of 2k complex samples, which is fixed by the present on-board data recording system. Thus, a larger coverage in range can only be obtained by increasing the slant range sample spacing, narrow swath (1.5 m), wide swath (2.5 m) and super wide swath (7.5 m).

E-SAR's imaging geometry is ruled by flight altitude, swath width and antenna footprint. Flight operations, which require maximum endurance of the platform, can only be performed at altitudes up to 3600 m above mean sea level (flight level FL 120). The off-nadir angle ranges from 25 to 60 degrees (narrow swath) or 70 degrees (wide swath). At an altitude of 5700 m (FL 190) the off-nadir angle in far range is reduced to 55 (narrow swath) and 65 degrees (wide swath). The endurance, however, is reduced by approx. 20 %, because additional equipment providing oxygen has to be installed in the aircraft.

Narrow and wide swath imagery of land surface can be obtained in all spectral bands with a ground range coverage of 3.5 to 4 km and 5.5 to 6 km, respectively. Sea surface must be imaged in narrow swath mode only, due to limited available signal power, especially at low sea state. The off-nadir angle range in this case is reduced to 25 to 55 degrees.

3.2 Backscattering Interaction with Vines

The vineyard, from an electromagnetic point of view, is a very complex system; metallic wires, stems, time-variable soil roughness and moisture, biomass's variations and many other characteristics make the problem of vineyard's electromagnetic interaction very arduous. While several studies are present in literature about backscattering modeling of corn or rice fields, for vineyards no model is present. In addition, the vineyard has got a clear periodic geometry and also its row orientation respect to flight direction can affect the radar response. This section wants to qualitatively analyze the vineyard geometric structure and its interaction with SAR signal to better understand which strategy has to be adopted to perform our task.

Referring to Ferrazzoli et al. (1997) and to the model proposed by

Bracaglia et al. (1995), in an agricultural scenario, such as the Frascati area, the following main scattering sources may be identificated:

- Surfaces (soils)
- Near Vertical Cylinders (Vineyard Stakes and Shoot)
- Cylinder with various dimension and orientation (leaf ribs, ...)
- Leaves

According to well established theories (Ulaby and Elachi, 1990), *rough surfaces* produce weakly cross-polarized backscatter. For soils, σ^0_{HV}, σ^0_{RR} (Circular Co-Polar) and σ^0_{45X} (Linear 45° Cross-Polar) are much lower than σ^0_{VV}, σ^0_{HH}, σ^0_{RL} (Circular Cross-Polar) and σ^0_{45C} (Linear 45° Co-Polar), and the latter are heavily influenced by soil moisture and soil roughness.

Near Vertical Cylinders generate a soil-cylinder double bounce effect which can be high. For dihedral plane corner reflector, the electromagnetic theory indicates that the backscattering cross section σ^0_{RL} and σ^0_{45C} should be null, while σ^0_{RR} and σ^0_{45X} should be as high as σ^0_{HH} and σ^0_{VV}, (Ulaby and Elachi, 1990). In reality, the situation is quite different and the electromagnetic theory can be better calibrated by means the model proposed by Bracaglia et al. (1995).

Vineyards stakes, which are made of artificial materials, could generate high double bounce effect, particularly at L Band and when the azimuth direction of the incoming wave is perpendicular to the stakes alignment, so that single contribution add up coherently.

Inclined Cylinder produce a much more depolarized backscatter than that of the soil. HV, RR and 45X give the maximum contrast between bare and vegetated soils.

Leaf Contribution is negligible at L-Band for both forest and most crop types (Ferrazzoli and Guerriero, 1994), but it shows a rapid increase for wide leafs crops at C-Band, where it is comparable, and even higher, than stem backscatter.

Focusing on the vineyard's structure, it is possible to hypothesize that backscattering is effected also by the regular periodic poles' structure and its orientation.

Let's try to individuate the backscattering contribution in a typical vineyard. First of all, it is necessary to separate to different case: a vineyard imaged in the near range area (incidence angle of ≈30°) by a vineyard imaged in the far range area (incidence angle of ≈ 45°), because the incidence angle strongly affect the contribution of each single scattering mechanism (Ferrazzoli et al., 1997). Thanks to the mission design, the two swaths were overlapping for an area 500 m wide, where several vineyards have been acquired under two different viewing angle. Moreover, precise ground measurements of the vineyards'structure, as inter-row distance, pole dimensions and orientations, have been collected.

Assuming the approximation of ray-propagation and not considering the second order reflection and diffusion of the scattered wave, the scattering mechanisms involved at 30° can be schematized as reported in the Figure 3.4. Considering the resolution of the ESAR (2 m), each resolution cell is dominated by the following main scattering mechanism:

- Green Line - Structure Double Bounce and Direct Metallic Wire Scattering. The incident wave interacts with the horizontal section of the vertical poles ($\delta x \approx \lambda/2$) and with the inter plant's metallic wire. As said before, σ^0_{VV} should be sensible to vertical poles, while σ^0_{HH} should be also influenced by horizontal metallic wire.

- Red Line - Surface Single Bounce Scattering. The incident wave interacts directly with the surface and it is mostly influenced by the soil roughness and soil moisture. Moreover, because of the viewing geometry, at 30°, the soil contribution has got a relevant effect on the backscattered wave.

- Blue Line - Volume Scattering. This is the contribution of the parcel's vegetation, such as the grass (when present) and the leaves. σ^0_{HV} can take into account the biomass signal.

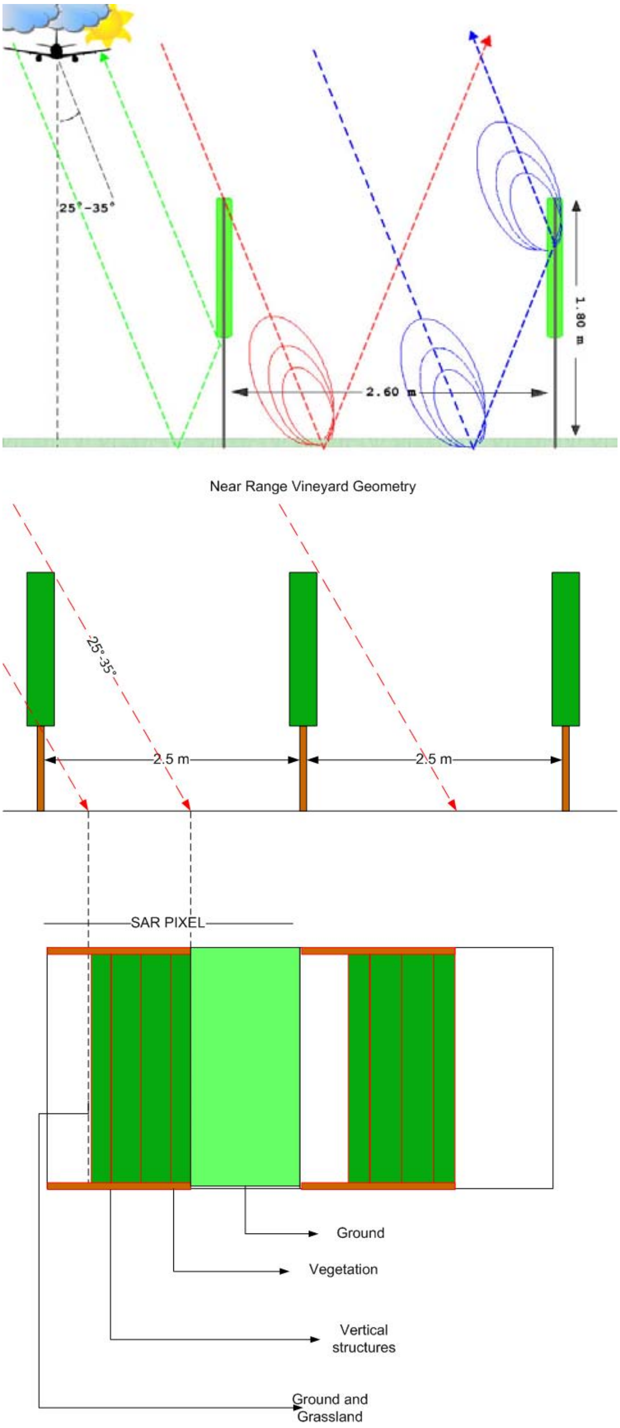

Figure 3.4: Vineyard schema at 25° incidence angle

In the near range field (25-35°), because of the canopy's geometry and height, the radar response is affected by the effect of soil moisture and roughness and no information about the geometric structure is directly visible. Specially at this incidence angle range, it is important to reduce the terrain clutter to better emphasize the biomass'signal (Figure 3.4).

In the far range field (45-55°), it has been noticed a very particular behavior of the radar signal: the geometric structure of the vineyards, in therms of number and orientation of row, becomes clearly visible in the parcel's texture, verifying the hypothesis of an interaction of the wave and the periodic structure.

Going deeper this argument, we can refer to Whitt and Ulaby (1994) for a periodic canopy structure. The periodic canopy model is obtained by placing the stalks on a two dimensional grid of fixed spacing δx and δy in the x and y directions respectively. A top view of the canopy is depicted in Figure 3.5.

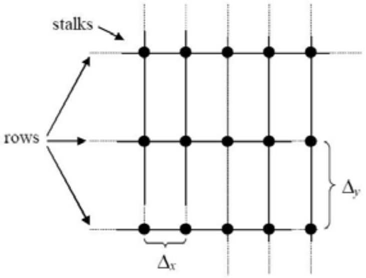

Figure 3.5: Top view of periodic canopy

According to Bloch-Floquet theorem the incident wave on such a canopy is diffracted in discrete directions. In the principal plane, the angles associated with these directions are given by:

$$\cos\theta_{mn} = \left[1 - \left(\sin\theta_i + \frac{2\pi m}{k_0\delta_x}\right)^2\right]^{1/2} \tag{3.1}$$

where m , $n \in$, $-1, 0, 1,$. In 3.1 only a few of these angles are real and actually contribute to the far field scattering. Many techniques are available to predict the amplitudes of the diffracted waves. These however will not be addressed here. For a periodic canopy of finite extent one can use the Bloch-Floquet theorem as a good approximation and obtain a far field scattering pattern for the canopy with sharp peaks at the angles given by 3.1.

Let's now consider the radar response from a periodic structure, as reported in Ulander and Le Toan (1999), where a set of regularly spaced point scatterers is separated at a distance d. The radar system is characterized by an impulse response $h(t)$ in time domain, after the pulse compression. Let $h(t)$ denote the band-pass response including carrier frequency. The response from N point scatterers of equal-cross section is thus given by

$$g(t) = \sum_{i=0}^{N-1} h(t - 2R_i/c) \tag{3.2}$$

where R_i is the range to scatterer number i. Fourier transform of (3.2) results in the spectral response according to

$$G(f) = H(f) \sum_{i=0}^{N-1} \exp\left(-j\frac{4\pi f}{c}R_i\right) \tag{3.3}$$

This is a general expression pf the spectral response from N equal point scatterers. Let's now introduce a periodic structure by setting

$$R_i = R_c + \left(i - \frac{N-1}{2}\right) d \tag{3.4}$$

which together with (3.3) results in

$$G(f) = H(f) \frac{\sin\left(N\frac{2\pi f}{c}d\right)}{\sin\left(\frac{2\pi f}{c}d\right)} \exp\left(-j\frac{4\pi f}{c}R_c\right) \tag{3.5}$$

The interpretation of (3.5) is the following: The frequency response of a periodic structure is the product of three factors:

1. the system transfer function $H(f)$
2. the resonance response from the periodic structure
3. a linear phase factor which determines the position of the structure.

The *resonance* factor is the most interesting, and is identical to the response from a diffraction grating. It is a function which has a narrow peaks at a discrete set of resonance frequencies. the function becomes more strongly peaked as N increases the corresponds to Bragg resonance. The role of the system transfer function is to window out a portion of the resonance. The Bragg resonance frequencies occur at the following frequencies:

$$f_p = n \cdot \frac{c}{2d} = n \cdot \frac{c}{2d_g \sin\theta} \tag{3.6}$$

where n is the order of the Bragg resonance, θ is the local incidence angle and d_g is the ground separation of scatterers. The resonance frequency increases as the incidence angle decreases, since the ground to slant projection increasingly compresses a ground structure and thus results in a higher resonance frequency. Let's now consider the case when one resonance line dominates within the system bandwidth. Only one peak of the resonance response will therefore contribute significantly to the result. Due to the periodic nature of the response factor, we can approximate (3.5) close to the resonance frequency f_s according to

$$G(f) \approx NH(f) sinc\left(N\frac{s\pi(f-f_s)}{c}d\right)\exp\left(-j\frac{4\pi f}{c}R_c\right) \tag{3.7}$$

The results reported in Ulander and Le Toan (1999) showed a *"wave"* modulation of the simulated and measured amplitude of the radar response to a periodic structured forest, with the inter-row distance and frequency in a Bragg interacting mechanism. Because the same behavior has been noticed in the vineyard's analysis, the ground measurements, collected during the two ESAR flights, have been used to verify the Bragg resonance conditions. It has been noticed that the periodic structure influences particularly the HH polarization at L-Band, while other polarization and C-Band seems not to be affected by this effect. Considering the Bragg equation, expressed in (3.6), the ESAR frequency carrier at L Band (1.3 GHz), an incidence angle of 45° and an inter-row spacing of 2.6 m, it has been verified the presence of a Bragg resonance frequency. This could explain the vineyard behavior in the far range area. Bragg scattering has been also observed for a vineyard parcel in Lewis et al. (1999).

Let's now consider the same vineyard, acquired at 45° of incidence angle, as represented in Figure 3.6.

It is possible to identify the following mechanisms:

- Blue Line - Volume Scattering, taking into account the vegetation's contribution from the leaves, woody stems, ... The soil contribution (soil roughness and moisture, the grass's backscattering, ...) is mitigated by the vine's canopy, but still present. Also the contribution of vertical poles is still present.

- Red Line - Bragg Scattering, considering the viewing angle, this effect is clearly visible as showed in Figure 3.10.

In Figure 3.7, 3.8, 3.9, the test site area at different viewing angles at L Band is reported; the images show a clear difference in the backscattered power at different angles and the particular vineyard "*row*" texture, present only in the far range area. In 3.10 it is possible to appreciate the effect of the regular structure on the radar image. Moreover, the Fourier transform has been applied to better understand the effect in the frequency domain. A secondary peak is visible (in red circle) in both transformed images, corresponding to spatial frequency and orientation of the row structure. Even if, the spatial resolution of the radar is as great as the row spacing, thanks to the Bragg's scattering mechanism, some information about the parcel's stable structure can be retrieved.

It is possible to summarize as follow the first simple considerations about the vineyard:

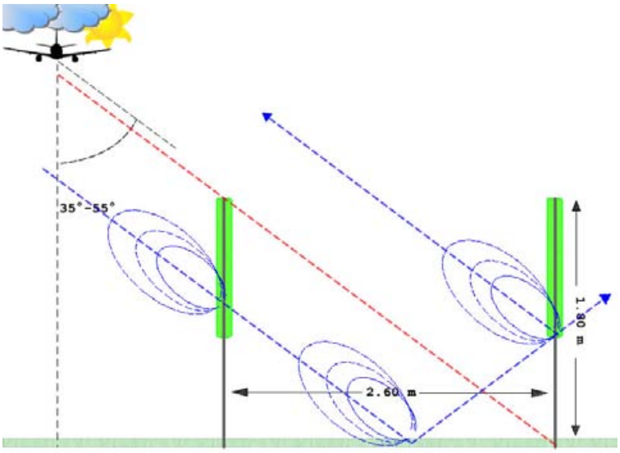

Far Range Vineyard Geometry

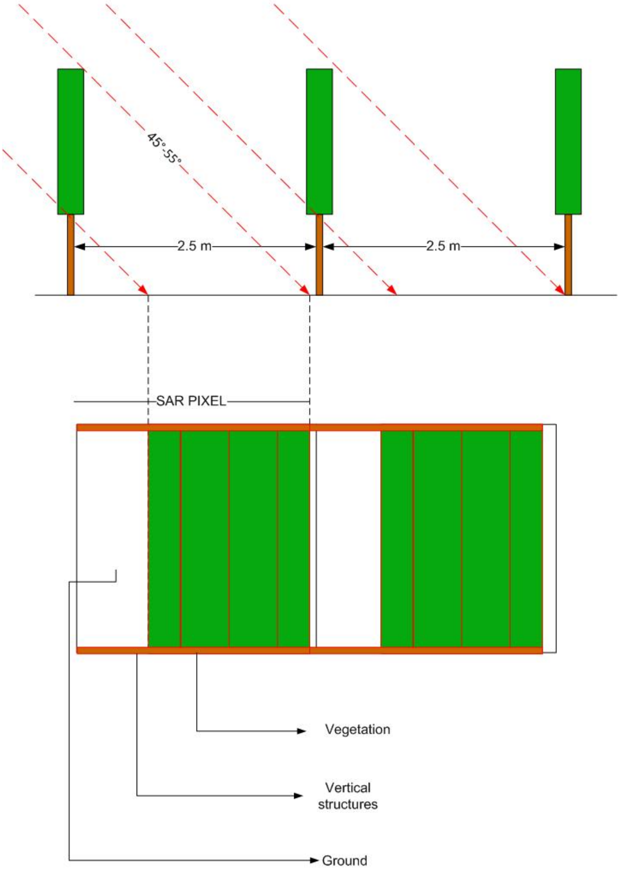

Figure 3.6: Vineyard schema at 45° incidence angle

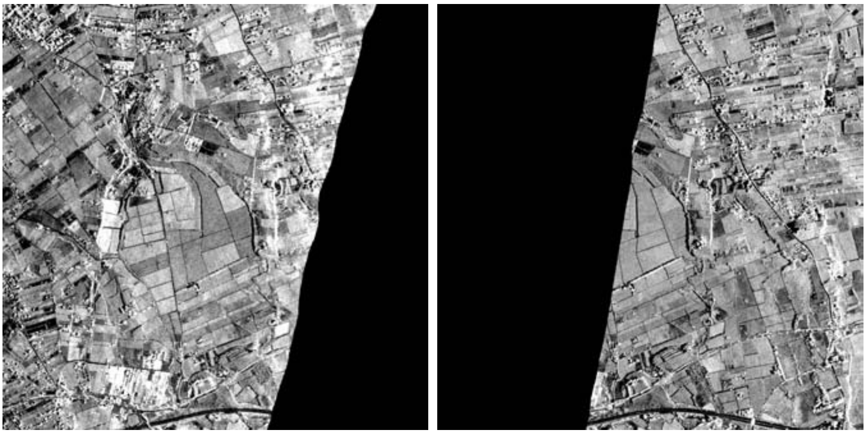

Figure 3.7: The Prataporci Area as viewed at L Band, Power Image (25 deg on the left and 45 deg on the right)

1. At L Band the stable structure is clearly visible at high incidence angle and it decreases for steeper angles. An important contribution is the periodic poles' structure, their horizontal section ($\approx \lambda/2$) and their double bounce scattering mechanism.
2. The row orientation and incidence angle have to be considered for test parcels'selection. The soil's effect decreases as the incidence angle increases.
3. At C Band no structure is visible because of the smaller penetration depth of the working frequency, the soil contribution is negligible while the leaves effect is predominant.

In the vineyard's case of study, fruit or biomass monitoring by means of radar observations is made difficult by the small variations of backscattering with respect to a strong background, which tends to saturation. The presence of metallic wires and vertical poles complicates the problem. The signal estimated was not clearly linked to the grapes biomass variation and also for adjacent parcels the *biomass signal* was not clear, often with a random

Figure 3.8: Zoomed area for wine producing area at 25° of incidence angle

Figure 3.9: Zoomed area for wine producing area at 45° of incidence angle

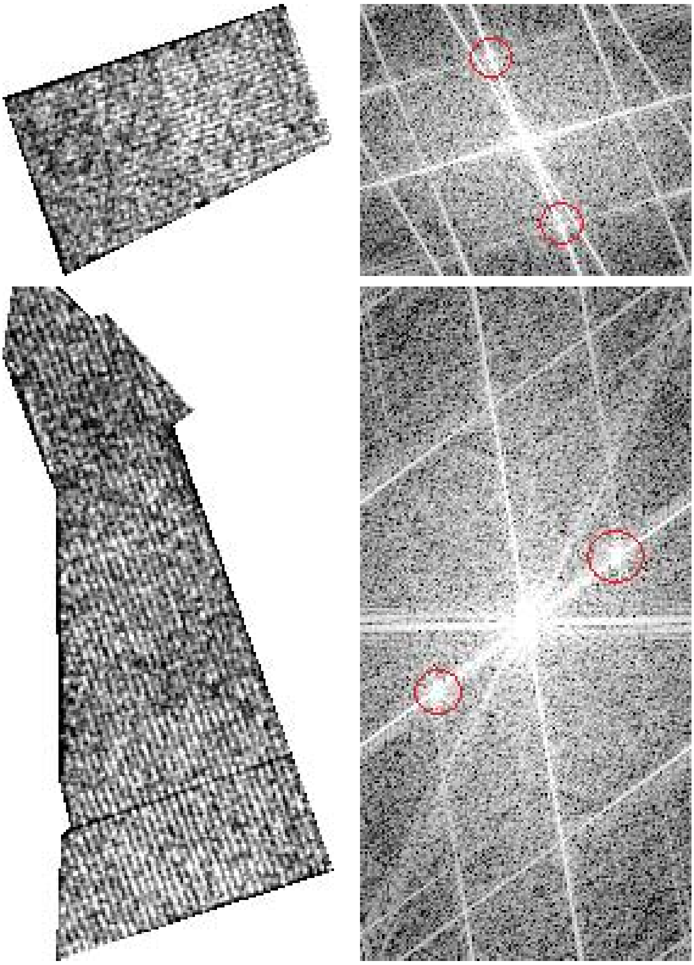

Figure 3.10: Subset of two parcels of Prataporci Area at 45°(on the left) and their Fourier Transform (on the right). Row Texture are clearly visible. In the red circles, the peaks of the periodic structure of the vineyard are visible.

behavior. Further noise could also be contributed by some calibration problems noted in the Geocoded Data (σ_0 was not stable on the pixel related to corner reflectors). Hence, a different approach has been followed, by using SCL data and better exploiting their polarimetric information. In the next paragraph. the processing chain for ESAR Detected product will be shortly explained and results will be reported.

3.3 Integration of Ground Measurements

During each flight, ground measurements have been collected, two teams were contemporaneously working, the main team, made by 15 people, precisely measuring several parameters in 2 selected parcels, and the other team, made by 3 people, collecting large scale information about the general condition of the area. The first team sampled 2 parcels of the farm *Tenuta di Pietra Porzia* located in the middle of the two sub-swath overlapping area, in an ancient drained volcanic lake, the *Lago Regillo* area (Figure 3.14). The sampled parameters were annotated on geocoded grid, measuring:

- Vine Spacing
- Row Spacing
- Grapes' Biomass
- Leaves's dimensions and number
- Poles'geometry and dimensions
- Soil Moisture and Roughness

The main team was collecting measurements in the parcels reported in Figure 3.13, while the second team provided large scale vintage status map. All the collected measurements have been processed to produce new information layers easy to be integrated. In particular, while the geometric information have no spatial variability and can be assumed as a constant (the standard deviation on inter-row spacing is lower than 2%, while for poles dimension is lower than 1% for width and about 5% for height), the leaves' and grapes' spatial variability has to be carefully processed.

3.3.1 LAI estimantion by means of Ground Measurements

Each operator annotated the leaves'dimensions (in term of width and eight, with a rhomboidal shape model to fit the real vine leaf's shape) and the leaves'number per sampling cell. We assumed as a first approximation, that the LAI[1] is mainly affected by number of leaves per sampling cell and that the leaves'dimensions variability is negligible. So the LAI can easily derived by:

$$LAI = Area_{leaf} \cdot NLeaves \tag{3.8}$$

Anyway, because of the large number of leaves per sampling cell, the estimation of $Area_{leaf}$ has got a strategic importance to better retrieve LAI. Considering all the measurements of leaves'dimensions collected during the ground campaign, it is possible to estimate the mean and standard variation for height and width, considering these variables statistically independents and gaussian distributed, by means of:

$$\begin{aligned} \overline{x} &= \frac{1}{N}\sum_{i=1}^{N} x_i \\ \sigma_x &= \sqrt{\frac{1}{N}\sum_{i=1}^{N}(\overline{x} - x_i)} \end{aligned} \tag{3.9}$$

where $\overline{x}$ is the mean and σ_x is the standard deviation of the measured data. Assuming a gaussian density function for height and width, the leaf area as reported in Persaud et al. (1993), is statistically distributed as modified Bessel function of the second kind (Springer and Thompson, 1970).

---

[1] Leaf Area Index

Due to the difficulty of working with such functions, a numeric statistical tool has been implemented.

Considering a single leaf area, it can be easily expressed by:

$$Area_{leaf} = k\ h \cdot w \tag{3.10}$$

where k is a corrective factor, h the height and w the width (Figure 3.11).

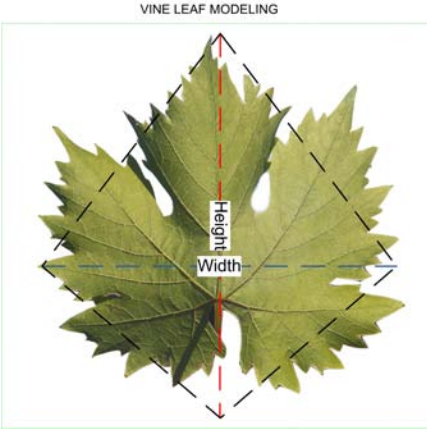

Figure 3.11: Vine Leaf Modeling

A gaussian random number generator has been coded in IDL environment and calibrated by the statistical parameters derived by the (3.9) and by the ground measurements. Each single modeled leaf is randomly produced according to (3.10) and summed to the other *randomly generated leaves* according to the number of measured leaves per cell. After this process the LAI estimation per cell is produced. To have a stable and reliable LAI estimation, this process is iterated at least 10000 times and the mean LAI is used. Due to the performances of the modern processors, the LAI estimation per cell takes few minutes of processing time ($\approx$ 3 min). This process is then extended to the other sampling cell, until all the cells are covered. The block diagram of the LAI estimator can be seen in Figure 3.12. Each sampling cell provides also the geographic coordinates, hence a LAI ground truth map is produced.

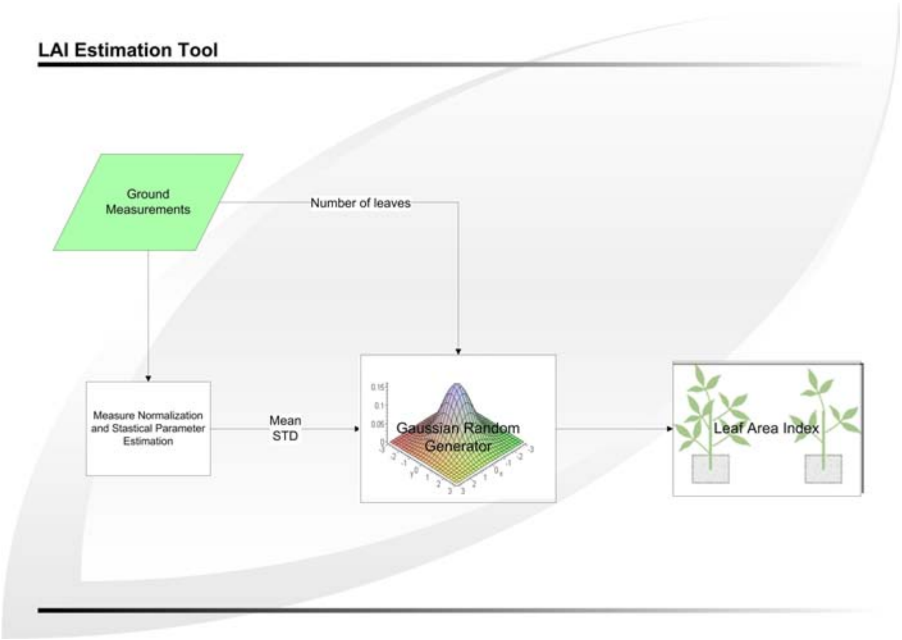

Figure 3.12: Schema of the Statistical LAI Estimator

Figure 3.13: View of the Ground Sampling Points

Figure 3.14: View of the Pietra Porzia Farm

3.3.2 Quickbird Data Measuring LAI

During the 2^{nd} flight, on 25^{th} of October, a QuickBird image has been acquired, providing a unique optical/radar dataset. A second image was present in the archive, acquired 6^{th} of August. According to the techniques presented in Chapter 1, optical data have been radiometrically calibrated and processed to obtain the vigor index. The images have been integrated into a GIS and by means of cadastral information (number of plants per parcel), a vine density map has been plotted for each parcel. After a precise location of sampling cell on the map (Figure 3.13), by means of GPS measurements of the reference poles in the test site, the Vigor Index and Measured LAI have been correlated. Results are reported in Figure 3.15. According to the results presented in literature (Johnson et al. (2004), Baret and Guyot (1991)), the Vigor Index is linked by an exponential function to the Measured LAI. The non-linear regression function and its parameters have been calculated according to the routines proposed by More et al.

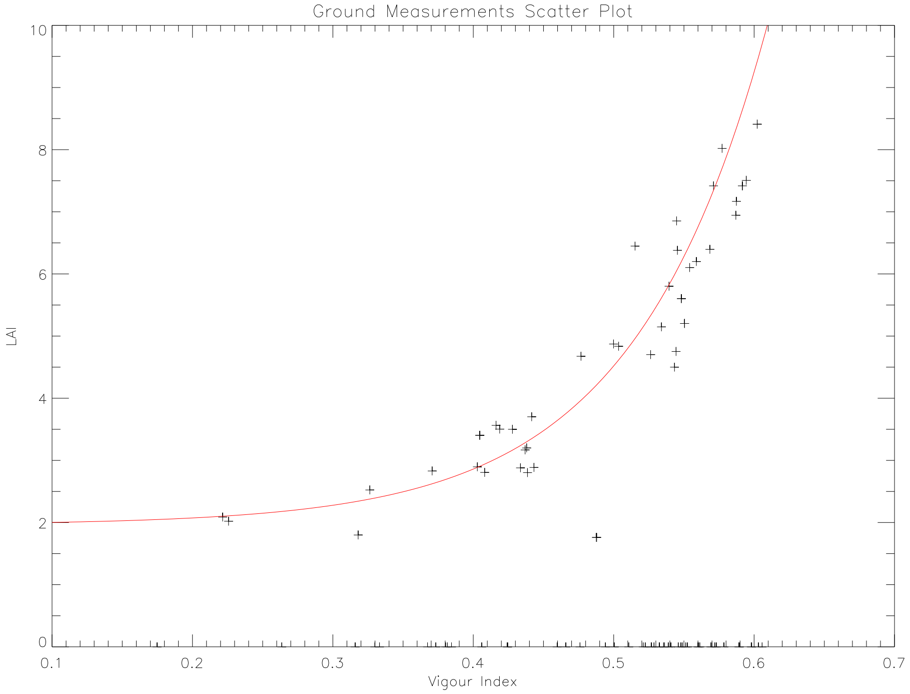

Figure 3.15: Vigor Index and Measured LAI. The red line fits the points. The LAI is expressed in terms of $m^2/pixel$; considering a square pixel of about 2.4 m, each sampling cell has got an area of about 5 m^2. The dinamic range of the measured LAI is below 1.6 m^2/m^2

(1980).

The empirical model is then used to process the vigor index and to produce a LAI map of the Test Site (Figure 3.16). Some farmers of the zone, quickly analyzing the map, showed them during a meeting, recognized some low producing or problematic areas of their own parcels.

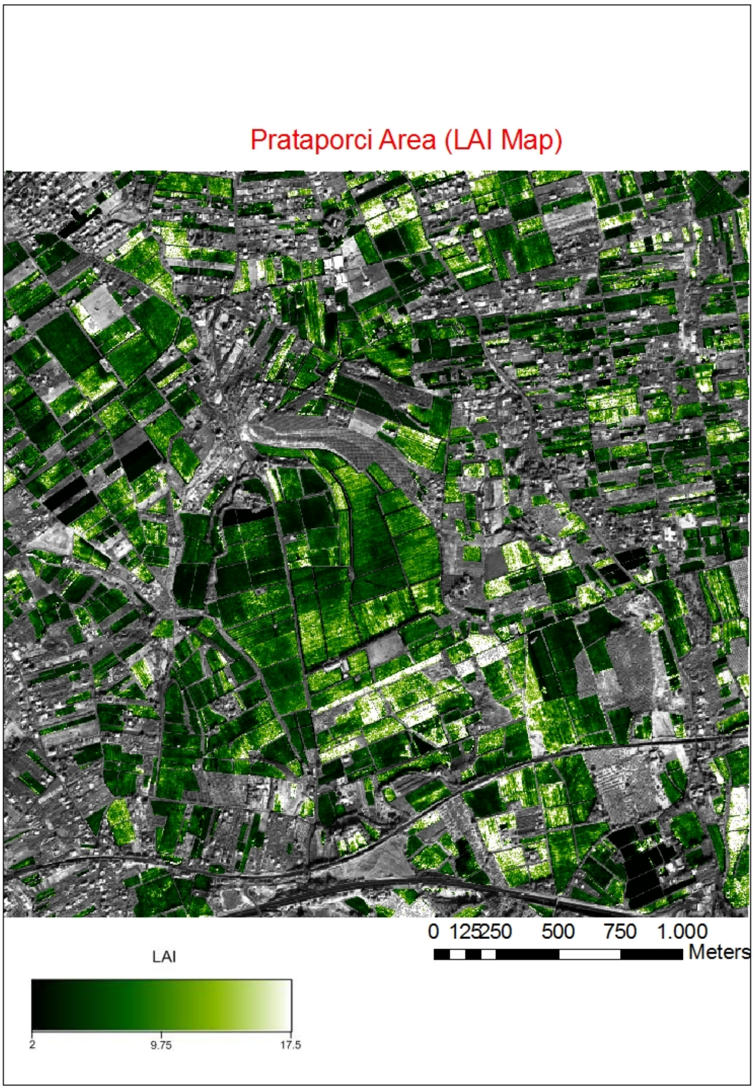

Figure 3.16: LAI Map of the Prataporci Area

3.3.3 Correlating Radar and Ground Measurements

The radar capability in biomass and LAI retrieving has been largely demonstrated in several works (Del Frate and Solimini (2004), Ferrazzoli et al. (1997)), but high resolution radar for agricultural purposes is still a challenge. A systematic polarimetric SAR observations have been carried out during the whole 2006 to assess the high resolution radar's behavior in farming practices techniques. In this section will be analyzed the correlation between the LAI measurements and Radar data and results and issues will be discussed.

Considering the LAI's non-linear link to the Vigor Index, as shown in Chapter 3.3.2, the L - C Band dataset has been related to the Vigor Index at pixel level. The aim of this study was to evaluate the radar's capability in in-field vigor's variation detection. Considering the QuickBird data's pixel size (2.4 m), the radar data have been processed using the same pixel dimensions but very noisy results were reported. The strong dispersion of radar measurements can be related to

- Speckle Noise
- Mis-registration Errors

The first is a well known problem of radar processing, due to the presence of multiple scatterers per resolution cell, and the second is a new effect, occurring when an high resolution radar image is processed. The radar geometric distortion, typical of its acquisition geometry, is well known and several methods are available to easy correct this effect, but if a a very high resolution DEM is not provided, residual geometric distortions and pixels's misplacement are present. This effect is clearly visible on buildings, forest and on terrain's rapid height variation, not sampled by the DEM. Also for a vineyard, were the maximum height can be 1.80 m, the mis-registration error between Radar and Optical data can have the dimension of 1 pixel (Figure 3.17).

In order to reduce the speckle noise's effects, the resolution is degraded, averaging the neighbor pixels and reducing the pixel size up to 5 m . By this

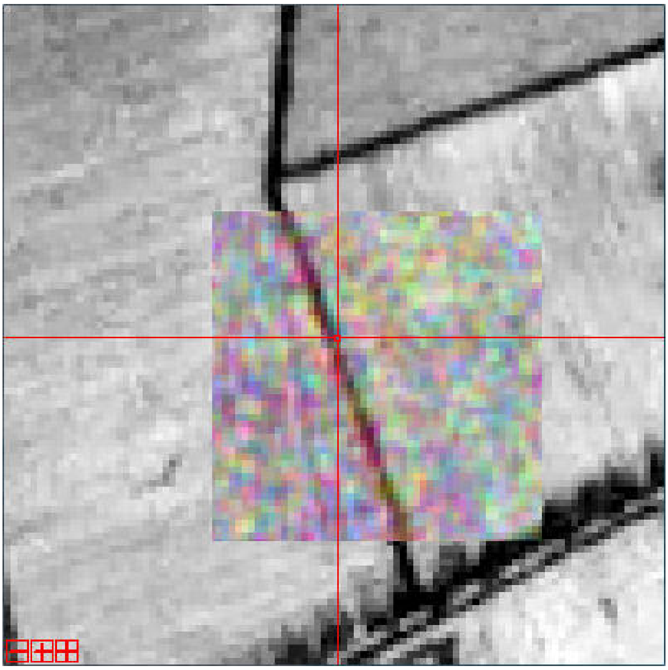

Figure 3.17: Example of mis-registration error on the Radar/Optical Dataset

operation, the noise is lowered and the mis-placement errors are not more present. After this operation, some test parcels have been selected, also considering the local incidence angle by means of the orographic information provided by DEM. The local incidence angle map are reported in Figure 3.18. It is possible to conclude that a better resolution is not directly linked to a better performance in parameters retrieval; the speckle noise masks each in-field variation and SAR can not be used directly as a precision farming instrument and a model that takes into account each noisy contribution is needed.

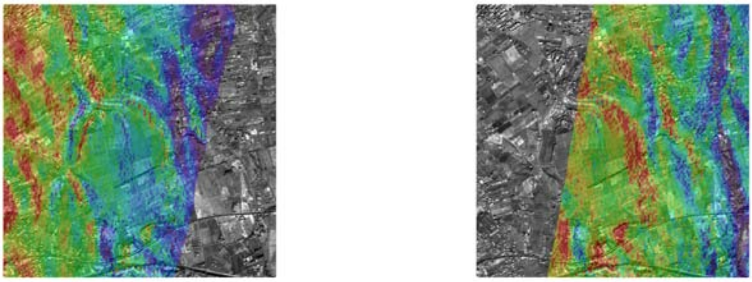

Figure 3.18: Local Incidence Angle Map: (left) Near Range Area. (right) Far Range Area.

Once selected the test parcels, taking into account their mean local incidence angle (Figure 3.18), radar pixels have been plotted together with Vigor Index data. The results are still noisy, but a correlation can be noticed (Figure 3.19).

The results shown in Figure 3.19 suggest that, without an accurate model that takes into account all the noisy effect for high resolution data, the radar does not show sensibility for full resolution data, but a resolution's degradation is needed. This first conclusion clearly shows that radar is not still ready in in-field variation detection, considering the small parcels of the Frascati Area. The idea of providing accurate spatial informations about the plant status actually is not technically possible, particularly for a fragmented area as the examined one.

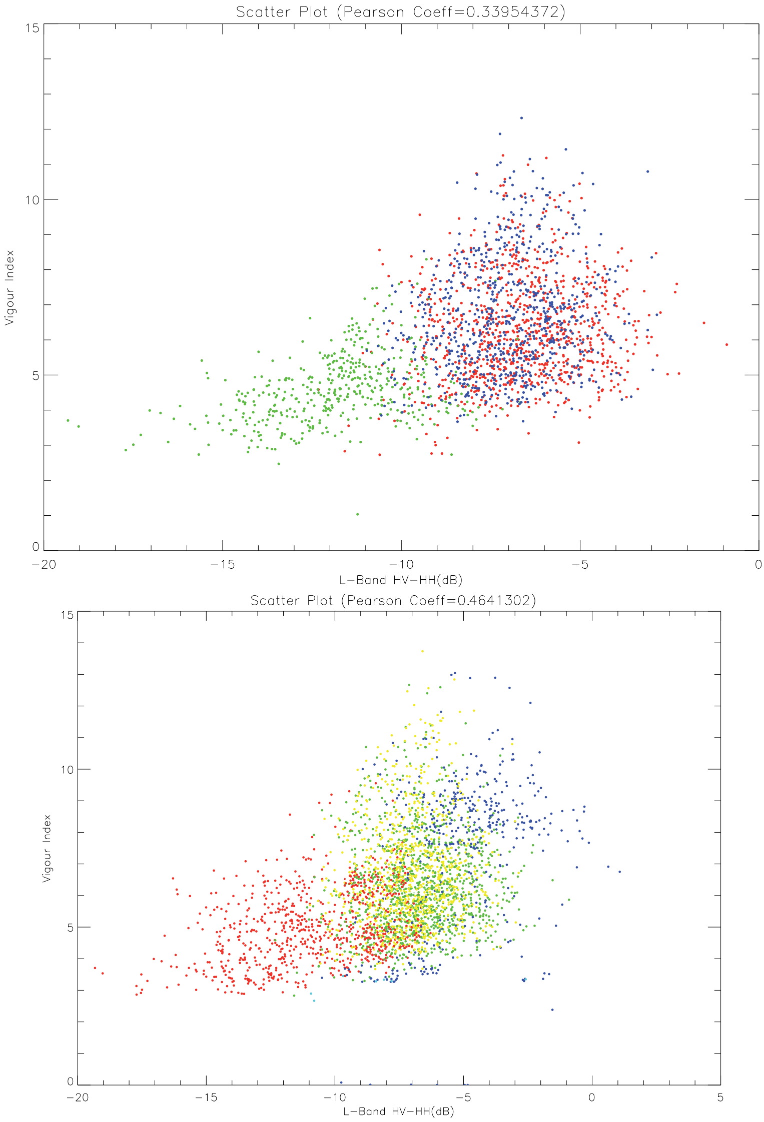

Figure 3.19: Scatter Plot of Radar Data (HV-HH) and Vigor Index for parcels in the Near Range Area (top) and Far Range Area (below)

The same dataset is then processed with the aim of reducing all the noisy effect. The speckle noise suppression is performed by computing backscattering at parcel level, averaging all the pixels contained into the field; the measurements' variability is reduced to the instrument precision (0.5 dB). At field level, considering only parcels with area greater than 0.5 Ha, the backscattering is again correlated to Vigor Index. The position of selected parcels in the local incidence angle map (Figure 3.18) is considered again.

It is known that the relation between scattering and biomass (LAI) is strongly influenced by soil moisture, soil roughness and plant type (Ulaby et al., 1984). Dealing with a vineyard, the problem is made more difficult because of other interfering structures, such as row orientation, vertical poles or metallic wires. Backscattering is strongly influenced by the geometric structure of the target and in a vineyard the geometric scenario is particularly complex. Referring to a North-South orientation, different incidence angles, L and C Band have been considered and the results are reported in Figure 3.21 for the Near Range Area (25°–35°) and in Figure 3.22 for the Far Range Area (45°–55°). The considered parcels have got a quasi-parallel orientation (North-South Orientation), respect to the flight heading, because it showed better results than the perpendicular one (East-West Orientation); while the "North-South" parcels, also at pixel level, showed some link to the Vigor Index, the "East-West" parcels were completely uncorrelated and it has been decided to stop the investigation with such kind of fields. This can be explained considering the geometric structure of the vineyard and the acquisition geometry. Referring to the (Figure 3.20), the red parcel (a) has got an "East-West" orientation, while the blue parcel (b) a "North-South" orientation; it is clear the different presence of the soil signal and canopy signal in the two analyzed case. The red parcel is dominated by soil clutter and offer a small canopy profile to the sensor, while the blue parcel offer the full canopy profile while the soil effect is incidence angle dependent.

At field level and at L Band, the correlation is clear also for different incidence angles. The combination HV-HH seems to better emphasize the biomass presence, reducing the soil effect, but also the HV-VV shows a clear link with the Vigor Index. The parcels have got a backscattering range

Figure 3.20: View of the Pietraporzia Area simulating the angular view of the acquisition geometry

of 4–5 dB and some uncorrelated measurements are present. Referring to the graph reported in Figure 3.21, one of these uncorrelated field has been visual inspected, the ID10 parcel because of its unusual behavior at L and C Band. The ID10 parcel was in a deep valley, half imaged in the shadow area (referring to the acquisition geometry) and with an uncorrected incidence angle, if we consider the DEM as a reference.

C Band does not show any clear sensitivity, the signal seems to be saturated and no retrieval can be expected (signal range lower than 1 dB).

3.3.4 Neural Retrival of Vigor Index

The correlation shown at L-Band between Vigor Index and backscattering (Figure 3.21 and 3.22) suggested the use of neural networks to retrieve information about the vigor index by means of radar data. The use of Neural Networks for retrieval purposes is a well established technology (Krasnopolsky and Schiller, 2003), providing fast data processing and reliable retrieved data. Neural Networks need a “training” phase, where the perceptrons are trained by a well established dataset; this is one of the most important phase during the designing process of a network. Focusing on the ESAR

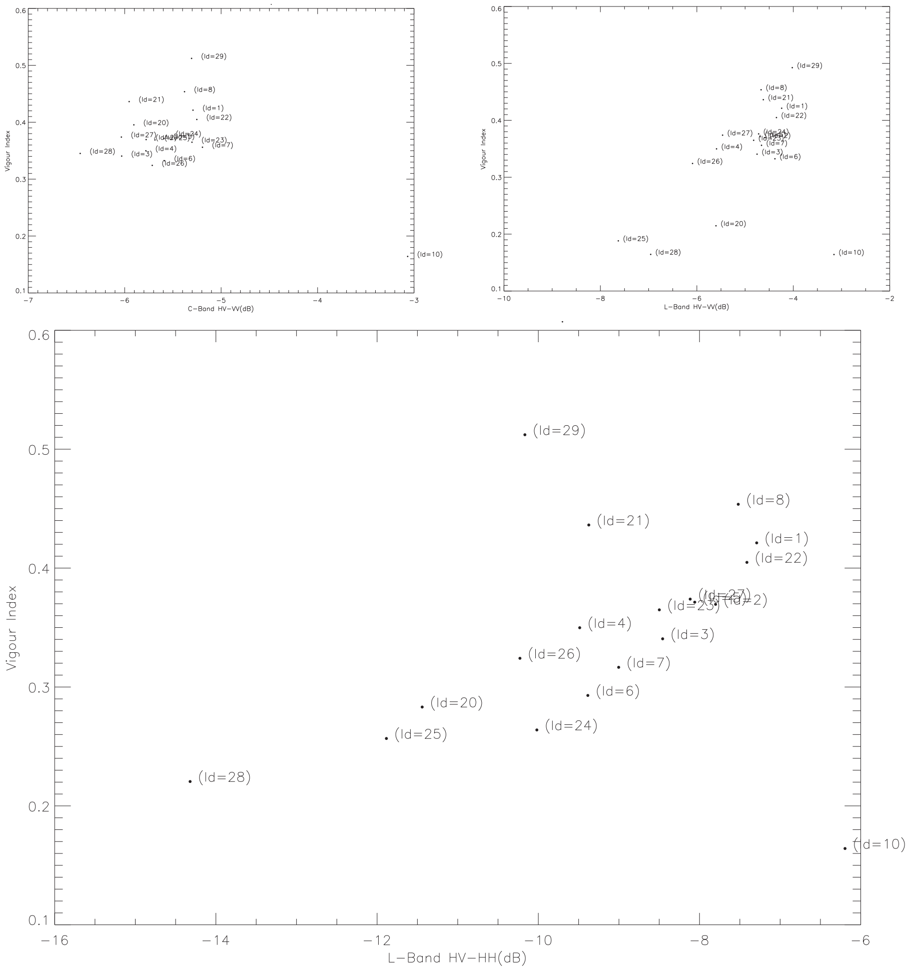

Figure 3.21: Backscattering at Field Level in the Near Range Area. (Top Left): C Band Data in HV-VV configuration. (Top Right): L Band Data in HV-VV configuration. (Below): L Band Data in HV-HH configuration

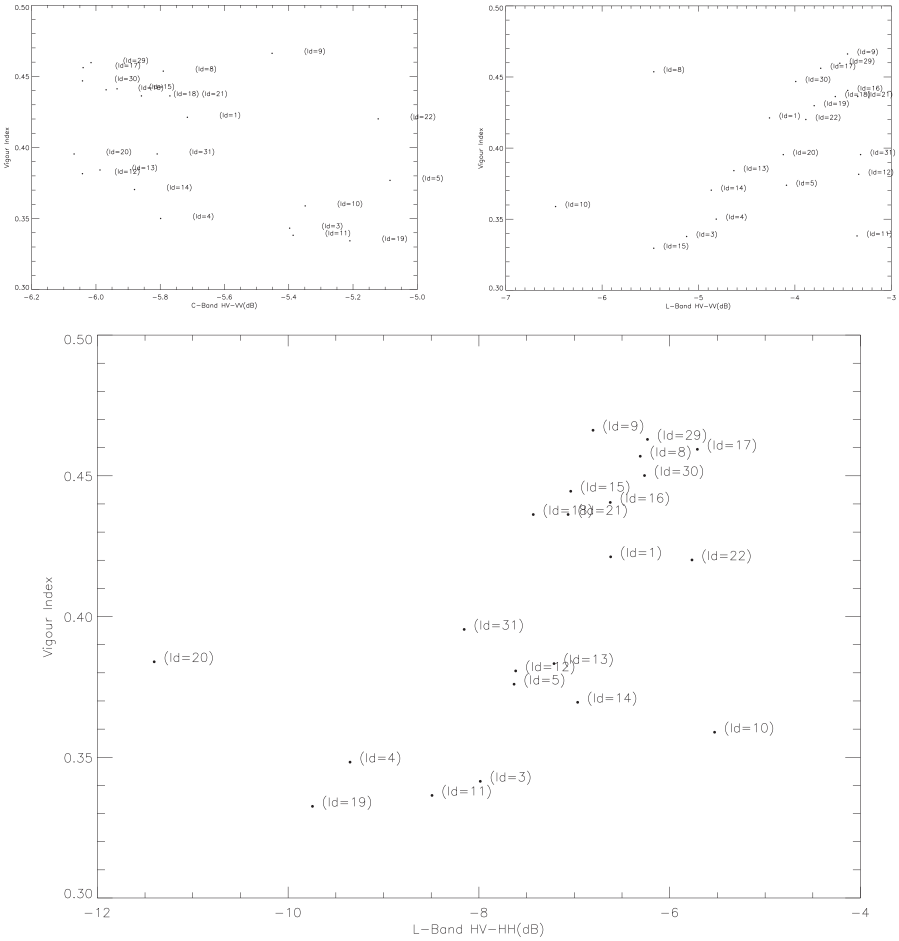

Figure 3.22: Backscattering at Field Level in the Far Range Area. (Top Left): C Band Data in HV-VV configuration. (Top Right): L Band Data in HV-VV configuration. (Below): (Top Right): L Band Data in HV-HH configuration

case of study, the ground truth dataset (containing LAI measurements) has not so many samples as needed by the training algorithm; a second training dataset has been produced by means of Vigor Index calculated by QuickBird data, remembering the empirical relation between LAI and Quickbird data (Figure 3.15); this new dataset is then used to train a single hidden-layer neural network fed by backscattering matrix's coefficients.

In order to reduce the speckle noise, the resolution has been reduced to 10 meters and Vigor Index sampling cells have been selected all over the observed area. Once trained, the neural network has been used to retrieve the vigor index; the algorithm's performance is reported in Figure 3.23. The algorithm showed good results; the spread of the retrieved Vigor is again linked to the speckle noise of radar data and to the complex scattering mechanism involved during the interaction with the vineyard structure, not directly linked to the plants' vigor and strongly influenced by the geometrical structure.

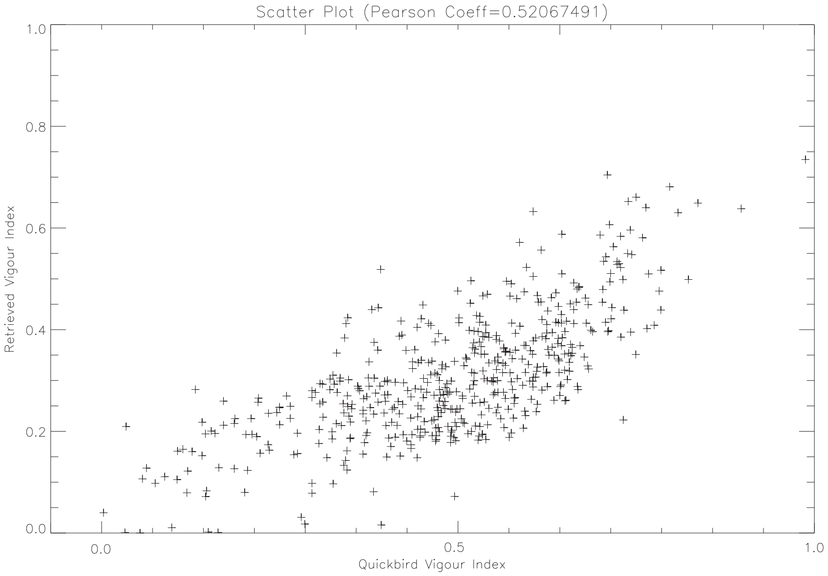

Figure 3.23: Vigour Index (VI) retrieved from HV-HH L Band SAR Data vs VI retrieved from QuickBird Image

Chapter 4

Backscattering Sensitivity to Grape Biomass

In this chapter the backscattering sensitivity to biomass variations during the farming practices will be investigated and analyzed, focusing on the harvest period. Data, coming from different missions, covering the L and C Band for a period going from 2005 to 2008, will be analyzed and critically discussed.

4.1 Grapes Contribution to Backscattering

To better emphasize the biomass presence and its changes, due to agricultural practices and vine's phenology, a simple model has been developed and applied. The model has got its basis in the hypothesis that each parcel has got a time-invariant structure with the exception of fruit biomass. Simplifying the problem by considering only a first order interaction between all the scattering mechanism, fixing the incidence angle and the frequency, we can write the backscattering of a vineyard as:

$$\sigma_v = \sigma_{soil} + \sigma_{structure} + \sigma_{leaves} + \sigma_{grape} \tag{4.1}$$

where the contribution from the structure can be assumed as a constant during each acquisition, in a multi-temporal scenario. In particular, referring to multi-temporal “Bacchus-DOC” mission, it is possible to make the following consideration.

The measurements taken before and after the grape harvesting are modeled as consisting of a constant backscattering, $\sigma_{0_{5_v}}$ (subscript v stands for vineyard), mainly contributed by poles, wires, stable (mainly wooden) plant components and terrain, and two variable parts, contributed by the grapes and by the variable vineyard parameters (mainly moisture and weed):

$$\sigma_{v_5} + \delta\sigma_g + \Delta v(t) = m_{v_5} \tag{4.2}$$

$$\sigma_{v_{25}} \equiv \sigma_{v_5} \equiv m_{v_5} \tag{4.3}$$

where σ_g is the backscattering variation associated to the grapes (subscript g), only present during the first acquisition, and $\Delta v(t)$ takes into account the variable vineyard parameters. Subscripts 5 and 25 refer to the two acquisition dates. $\sigma_{v_{25}}$ in (4.3) represents the constant backscattering of the stable structures, that are assumed not to vary between the two acquisitions. In an analogous way the backscattering from the bare soil (subscript b) reference parcels can be modeled as:

$$\sigma_{b_5} + \Delta b_t = m_{b_5} \tag{4.4}$$

$$\sigma_{b_{25}} \equiv \sigma_{b_5} \equiv m_{b_5} \tag{4.5}$$

Under the assumption that the bare soil parcels behave like the soil under the stable structures of each vineyard, the difference between the backscattering of the vineyards and that of the bare soil parcels yields:

$$m_{v_5} - m_{v_{25}} - m_{b_5} + m_{b_{25}} = \delta\sigma_g + \Delta v(t) - \Delta b_t \approx \delta\sigma_g + n \tag{4.6}$$

where n is a residual noise. The model’s limitation can be recognized in the term n of Eq. (4.6), which depends on the conditions and position of the bare soil parcels and, after all, is not negligible. Moreover, the different soil condition between the two acquisitions made the model not applicable with a sufficient accuracy to have encouraging results. The particular soil condition during the first acquisition (a storm occurred 2 hours before the Dornier's survey) makes the noise n parameter in the Eq. (4.6) not negligible and strongly dependent by the choice of the reference soil and its conditions.

By the poor results obtained with the fast processing of detected images, a new approach has been selected by means of SLC products; thanks to the fully polarimetric capability of the sensor (L Band), it is possible to synthesize different polarization (Ulaby and Elachi, 1990). After the radiometric calibration and the geocoding procedure, the polarimetric dataset has been integrated into the GIS, together with ground truth information, vintage status and vine orientation map.

Several studies have demonstrated the sensitivity of co-polarization to soil parameters and of cross-polarization to vegetation biomass (Dubois et al. (1995), Ferrazzoli et al. (1997), Mattia et al. (1997)). Hence, the (4.6) can be expressed in term of cross- to co- polarization ratios for the two acquisition dates:

$$\begin{aligned}\sigma_{hv5} - \sigma_{hh5} - \sigma_{hv25} + \sigma_{hh25} = \Delta\sigma_{hv} - \Delta\sigma_{hh} = \\ \Delta\sigma_{cross} - \Delta\sigma_{co} \approx \delta\sigma_g + \delta n\end{aligned} \tag{4.7}$$

where subscript h and v refer to horizontal and vertical polarizations, while *co* and *cross* to co-polar and cross-polar respectively. We expect that $\Delta\sigma_{hv}$ is related to the variation of grape biomass, $\Delta\sigma_{hh}$ depend on the variations of the soil contribution, and other stable scattering sources are canceled. A residual noise δn will still be contributed by unpredictable changes of the backscattering. (4.7) can be extended to any polarization, by referring to the scattering matrix.

4.2 ESAR L-C Band Data

As reported in Chapter 3.1, one of the primary objective of the Bacchus-DOC mission was to investigate the potential of SAR in precision farming purposes, focusing on sensitivity of backscattering to biomass variation of grapes during the harvest period. Indeed, two flights have been planned, the first before the harvest and the second when all the grapes have been collected. The original plan was modified due to other DLR missions' priority and the first acquisition occurred about 2 weeks after the first scheduled overflights; the second mission plan scheduled two flights, the first on the 5^{th} of October (the harvest started in the most part of parcels about 10 days before) and the second on the 25^{th} of October, when the vintage was concluded. Even if the acquisition timing was not optimal, the dataset provided by Bacchus-DOC mission was the first mission dedicated to the grapes' biomass measurement, providing a unique dataset to test algorithms and procedures.

4.2.1 ESAR Detected Products Analysis and Processing

In order to have a fast investigation about the interaction of SAR and biomass variation in a agricultural landscape, only Detected Images were considered. The data set has been processed using L and C Band data of the two acquisition days. The processing chain can be summarized as:

SAR Processing. All the images has been radiometrically calibrated, checked for the position accuracy and a multi-image registration has been performed.

Ground Truth Map Preparation. The vineyard cadaster has been inserted into a G.I.S. and adapted to the SAR Images. The ground truth data (vineyard status during each acquisition) has been integrated into the G.I.S. as a map. Using a QuickBird Image, the cadaster has been updated and grassland and bare soil were located and segmented.

Backscattering Processing. After the GIS integration, the simple model reported in the Chapter 3.2 is applied.

By means of a ground truth map of the Test Site (Figure 4.1), some parcels and bare soils (properly uncultivated grassland to estimate the soil

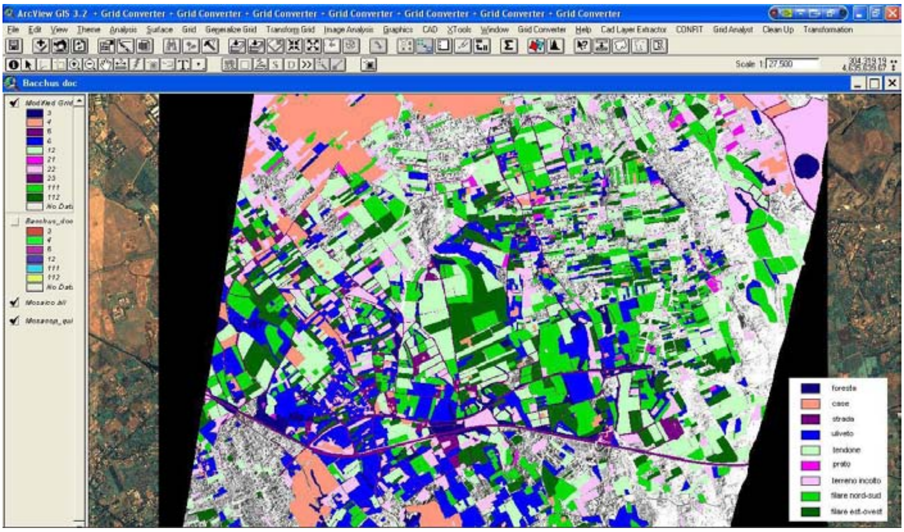

Figure 4.1: Ground Truth Map ovelayed to QuickBird and Radar Data

of each parcel) have been selected and the temporal variation for each radar channel has been reported in Table 4.1

The result is clearly noisy and prevents any conclusion from being drawn from this kind of analysis using HH, VV and HV polarizations and the reference parcels. Further noise could also be contributed by some calibration problems noted in the Geocoded Data, measured on corner reflector deployed during each acquisition. Hence, a different approach has been followed, by using SCL data and better exploiting their polarimetric information.

4.2.2 ESAR SLC Products Analysis and Processing

The simple model expressed by (4.7) has been used to compare backscattering of vineyards before (5^{th} October 2005) and after (25^{th} October 2005) the grape harvesting. Images have been calibrated, converted to ground range and geocoded (using a Nearest Neighbor re-sampling method to avoid

Field ID	**L Band**				**C Band**	
	VV	**VH**	**HV**	**HH**	**VV**	**VH**
F14	-0.16	0.38	0.38	-0.18	0.08	-0.96
F6	1.51	1.53	1.20	3.03	-0.49	-1.00
F3	1.63	0.49	-2.15	0.69	2.54	2.04
F5	0.34	0.79	0.50	-0.30	0.39	-1.06
T4	0.94	0.81	0.60	-0.35	1.56	1.12
T10	0.03	-0.13	-0.43	-1.47	-1.36	-1.98

Table 4.1: Backscattering Differences in Detected Images

uncontrolled changes of the statistics and of the absolute values), then integrated into the GIS.

Three main cross-polarized backscattering have been synthesized: H/V, Circular L/R and Linear +45°/-45°. Only the L-band acquisitions have been considered, since measurements at C-band were not fully polarimetric. The data set has been filtered by an Enhanced Lee Filter to reduce speckle and then masked with the vineyard inventory boundaries both to single out the pixels belonging to the selected vineyards and to separate different cultivation geometries (e.g., row orientation or vine-supporting structures). Results obtained for selected vineyards by this procedure are reported in Table 4.1

Although fluctuations are apparent, a decrease of the cross- and co-polarized backscattering differences is consistently observed between the two acquisition dates. For a further analysis, the data set has been projected onto a color palette to visualize the multi-temporal behavior of backscattering, masking non-vine parcels (Figure 4.2). Due to the dual-pol dataset for C Band, no polarimetric basis change has been performed and no results have been reported.

4.2.3 Conclusions for Bacchus-DOC Mission

The obtained results hint at a sensitivity of L-band backscattering to grape biomass per unit area. To put this feature into evidence, non-conventional

Field ID	$\Delta\sigma_{cross} - \Delta\sigma_{co}$		
	H/V	**Circular L/R**	**Linear ±45°**
F1	2.31	3.95	2.87
F2	0.93	3.94	3.05
F3	3.69	3.03	2.12
F4	2.63	2.87	1.19
F5	1.33	4.49	1.85
T1	0.98	3.99	2.80
T2	2.01	3.82	1.68
T3	1.41	2.82	3.18
T4	2.83	2.55	2.42

Table 4.2: Cross-Polarized Backscattering Differences

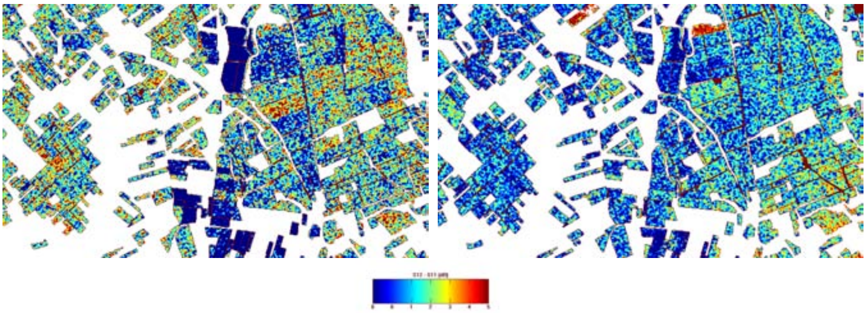

Figure 4.2: $(\delta_{hv} - \delta_{hh})$ difference (in dB) on 5 (left) and 25 (right) October 2005 on a subset of the imaged zone. The vineyard inventory boundaries have been used to display only the vineyards pixels. A clear change of the vineyards backscattering behavior between the two acquisitions is visible.

processing of SAR data has to be carried out, exploiting the pieces of information contained by fully polarimetric measurements. A number of disturbing effects can be detrimental to the result, since the overall vineyard conditions, including soil roughness, weed, moisture on vine supporting structures, number of leaves, water content of wooden parts of the plant and of the leaves, can introduce unpredictable variations of backscattering.

4.3 ALOS PALSAR L Band Data

During last 2 years new space borne sensors (Polarimetric L and C Band) have been successfully lunched and data are now available to test their capability for precision farming. In this section ALOS PALSAR data will be analyzed and discussed.

4.3.1 The ALOS PALSAR Data Set

ALOS was successfully lunched on January, 2006, from the Tanegashima Space Center, carrying on board three instruments: the Panchromatic Remote-sensing Instrument for Stereo Mapping (PRISM) for digital elevation mapping, the Advanced Visible and Near Infrared Radiometer type 2 (AVNIR-2) for precise land coverage observation, and the Phased Array type L-band Synthetic Aperture Radar (PALSAR) for day-and-night and all-weather land observation. Focusing on PALSAR, after a CAL/CAL phase from May to December, 2006, the instrument entered the operational phase and started to provide the first images. The Phased Array L-band Synthetic Aperture Radar (PALSAR) is an enhanced version of the Synthetic Aperture Radar on JERS-1 (L-band; HH-polarization; 35° off-nadir angle) PALSAR is a fully polarimetric instrument, operating in fine-beam mode with single polarization (HH or VV), dual polarization (HH+HV or VV+VH), or full polarimetry (HH+HV+VH+VV). It also features wide-swath ScanSAR mode, with single polarization (HH or VV). The center frequency is 1270 MHz (23.6 cm). The off-nadir angle is variable between 9.9° and 50.8° (at mid-swath), corresponding to a 7.9 - 60.0° incidence angle range. Further details can be found in Rosenqvist et al. (2004).

Thanks to the cooperation between JAXA and ESA, ALOS is an ESA third-part mission and data are available for free, after a CAT-1 project opening. With the aim of vineyard monitoring by means of operational satellite, three images have been acquired during the second half of 2007, building a short, but interesting, time series. Some details on the dataset are reported in Table 4.3. Unfortunately, the time series has got a low time sampling rate, due to the acquisition strategy of JAXA that fix as a priority the acquisition of one of the several sensor acquisition modes during the whole acquisition cycle (46 days). This choice, derived by the need of simplifying the ground segment, does not permit the use of the ALOS data for commercial purposes neither for on-demand operation. Considering all these restrictions, the collected data can be used to test the capability of such instrument in vineyard monitoring.

Date	Mode	Resolution	Incidence Angle
11.05.07	Full Polarimetric	30 m	25°
19.06.07	Dual Pol (HV/HH)	20 m	35°
19.09.07	Dual Pol (HV/HH)	20 m	35°

Table 4.3: ALOS PALSAR Data Set

An overview of the acquired images is reported in Figure 4.3 , where the red box locates the test site. All the images, originally in the Single Look Complex format, have been calibrated, processed and coregistered; the geocoded images have been re-sampled with a 30 m pixel and integrated into the GIS. The processing strategy is more or less the same adopted during the ESAR experience (Chapter 3.1); the backscattering of several vineyards, in a wide area respect to the one imaged during “the Bacchus-Doc Mission”, has been analyzed at field level, distinguishing between the orientation and the parcel geometry (row or tent-like geometry). Some different soils, such as bare soil, forest, and grassland have been analyzed in order to obtain a comparison with vineyards’ backscattering behavior.

Figure 4.3: ALOS PALSAR Data. (left) Dual Pol Image. (right) Full Pol Image

4.3.2 Vine Phenology during the ALOS survey

The agricultural practices' history and vine phenology is crucial to better understand the radar behavior, hence each acquisition will be shortly correlated to what was happening during the satellite survey. The vine phenology timing is strictly linked to the climatology of the wine producing region (Winkler, 1958) and many vine phenological models take the temperature as input to measure the status of vine (Mariani et al., 2007). Focusing on Frascati DOC region and by means of in-situ observations, it is possible to refer to the phenological schema showed in Figure 4.4

11.05.07 - Fully Polarimetric Acquisition. During April and May the vineyard is interested by practices that deeply modify the soil roughness. The grass, that during the previous months wildly grew on the soil, is cut and the soil is deeply plowed to let the oxygen and nitrogen reach the vine's root. After plowing, the soil is again flattened.

19.06.07 - Dual Pol Acquisition. On June no agricultural practice is performed, the field is at the top level of its vigor and the number of leaves will remain constant until late October: during the following months some leaves pruning task can occur to let the leaf biomass at a constant level (Wine Quality is influnced by Leaf Biomass, Chapter 1.2)

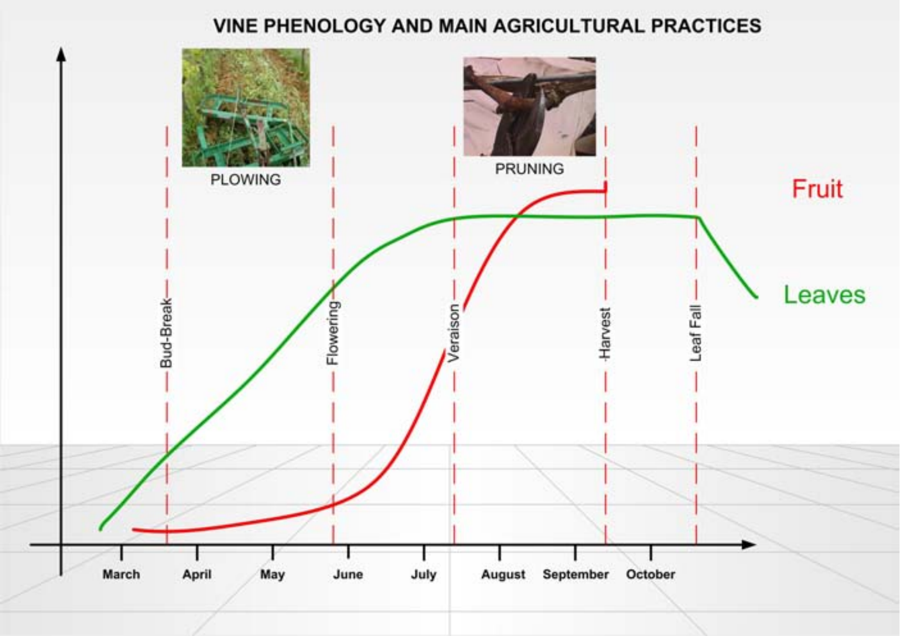

Figure 4.4: Vine Phenology: The graph summarize all the main practices and phenological steps during the observation period

. Grapes are at their initial status (very green and small) and the soil has got a low roughness, because of a previous practice that broke the clods created by the plowing and natural grass, wildly grown during the previous period, is cut to let the vine "breathing" (Oxygen and Nitrogen have to reach the soil and roots without any problems).

19.09.07 - Dual Pol Acquisition. On the second half of September the harvest starts, collecting grapes with different techniques, from the traditional hand-made harvest to the automatic one, performed by a tractors bestriding the row and shaking the grapes. Depending by the consistence of soil and by the weather conditions, this operation usually does not deeply modify the soil roughness.

Moreover, also weather parameters have been monitored during the acquisition period and the weather condition are reported in Table 4.4

Day	$\overline{T}$ $(°C)$	T_{min} $(°C)$	T_{max} $(°C)$	Rain (mm)	Weather Condition	Air Umidity
11.05.07	19.1	14.0	24.4	-	low cloud	78%
19.06.07	26.7	19.0	35.0	-	low cloud	53%
19.09.07	21.3	18.6	24.0	-	low cloud	68%

Table 4.4: Weather condition during ALOS survey

In order to better understand the vineyards' behavior at L Band and with the lack of accurate ground measurements as those available during the "Bacchus-DOC" mission (Chapter 3.3), the study's strategy aims to measure the vineyard's backscattering behavior during the acquisition period and to understand if there is any correlation between radar response and the vine phenological status; in order to perform this ambitious task, some different reference soil has been analyzed and results are shown in Chapter 4.3.6

4.3.3 ALOS PALSAR Processing

As showed in Table 4.3, the ALOS dataset is made of dual and full polarimetric data in SCL format; moreover these two acquisition modes have got two different incidence angles and two different resolutions. To integrate this dataset into the GIS and to use the Quickbird High Resolution to identify the test parcels, the data have been accurately processed.

The ALOS PALSAR Processing chain can be summarized as follow:

Multilooking and Calibration. Data, in a complex format, are converted into a power image and calibrated to obtain the backscattering coefficient. JAXA provides incidence angle corrected products, referred to WGS84 Ellipsoid. Multilook operations have been performed to obtain a square pixel and to reduce the speckle noise.

Image Coregistration The images are coregistered and fused in a multi dimensional radar dataset. Then the dataset is warped on the reference image, the Quickbird image acquired on $25th$ October, 2005.

GIS Integration The radar dataset is now ready to be integrated into the GIS system and to be overlaid with all the other information, such as the well know vine cadaster or the land use and land cover maps of the region.

4.3.4 Reference Soils

Different soils have been analyzed by means of HH and HV observation and using the HV-HH combination to better reduce the soil effect. The selected soils are:

Forest. A forest area of about 5 Ha has been selected in the premises of the “Castelli Romani” volcanic complex. Forest is monitored as a stable reference for biomass and to evaluate the calibration accuracy.

Bare Soil. In the Frascati region there are not any bare soils, because it is an agricultural area with scattered buildings and dense urban centers. We can consider as a bare soil an uncultivated area, never interested by agricultural practices. One “bare soil” has been selected in the neighborhood of the Prataporci Area, for a total area of about 2 Ha.

Grassland Two grasslands have been selected in the Tor Vergata University area and in the Frascati region. Because the vegetation does not grow wild and the grass height is less than 20 cm, the selected grassland can be used as a reference for the vineyard soil monitoring. The grassland can provide indirect information about natural soil roughness and soil moisture.

Arable Land. Two crop parcels have been selected in the agricultural site of “Pantano”, in the Northern part of the Prataporci Area. Arable Land is monitored to have a comparison between the vineyard agricultural practices and practices made on other kind of fields; during the spring time, not only the vineyard is interested by harrowing.

Backscattering behavior for the selected reference soils is reported in Figure 4.5

4.3.5 Analysis of Vineyards

Let’s now consider the backscattering behavior at L band of vineyards. The selected parcels have been divided into three groups, following the same geometric and naming criteria shown in Chapter 3.3.3: *East-West* (for those parcels with a perpendicular row orientation respect to the satellite ground track), *North-South* (for those parcels with a parallel row orientation respect to the satellite ground track) and *“Tent”* (for those parcels with a planar structure).

The backscattering is again computed at parcel level, averaging all the pixels, and only parcels with an area greater than 3 Ha have been selected. The selected parcels are located in an area wider than the one covered during the Bacchus-DOC mission (Chapter 3.1), going from the Prataporci area (in the red box showed in Figure 4.3) to the wine producing area at the south of Ciampino airport, where more extensive vine parcels are present (dotted yellow box in Figure 4.3). Results are reported in Figure 4.6 for EST-WEST parcels, in Figure 4.7 for NORTH-SOUTH parcels and in Figure 4.8 for TENT parcels.

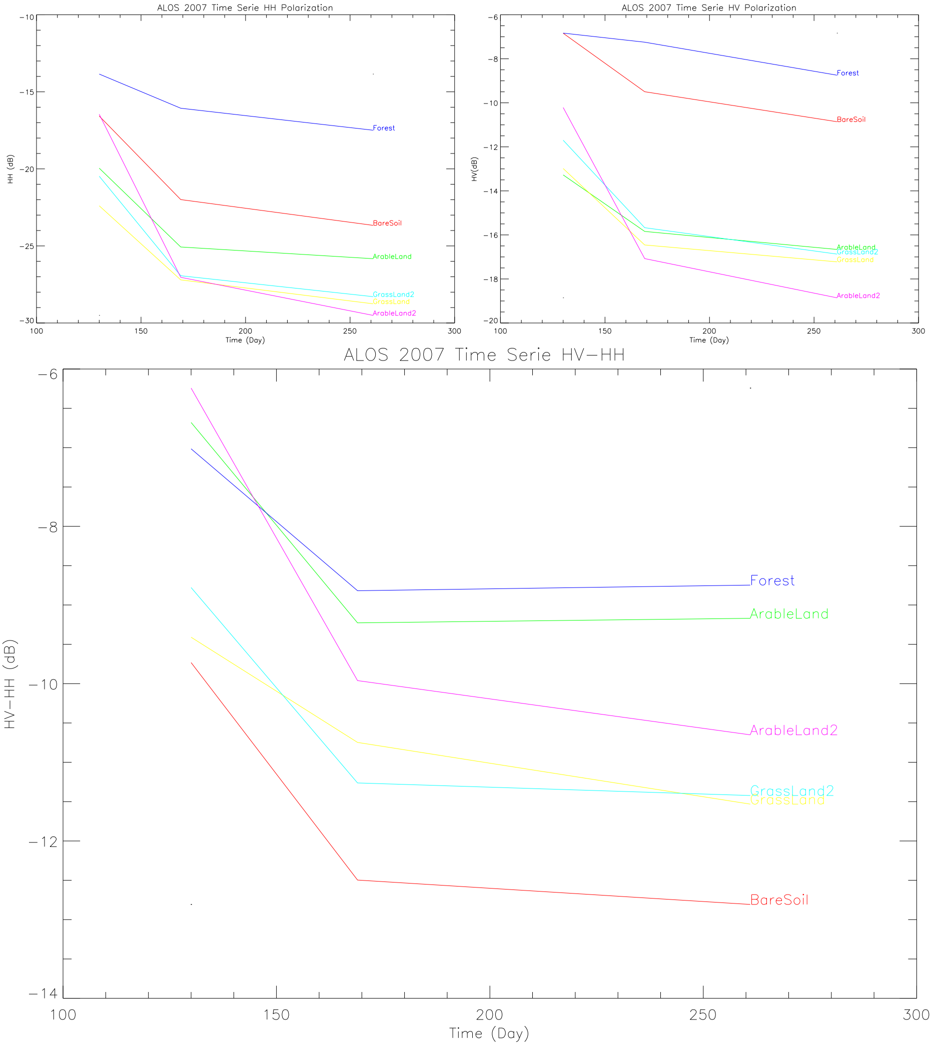

Figure 4.5: Backscattering behavior for the analyzed soils: (top left) HH, (top right) HV, (below) HV-HH

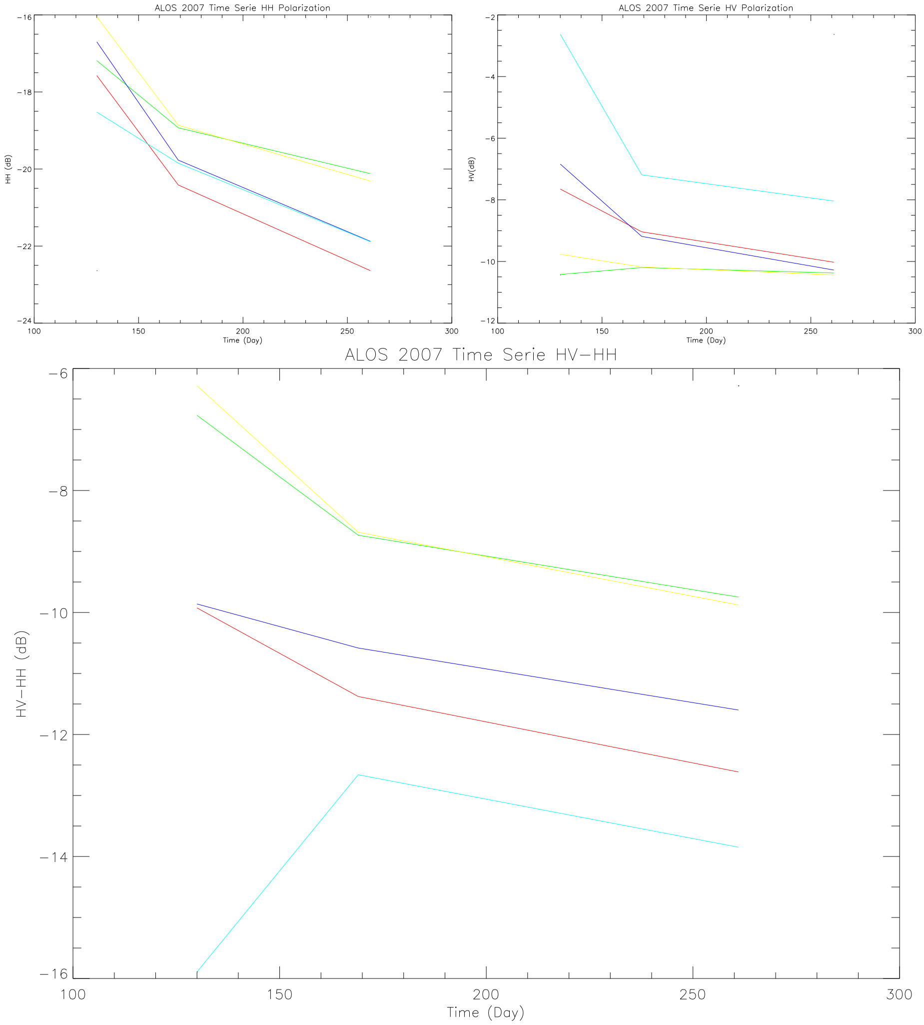

Figure 4.6: Backscattering behavior for the EST-WEST vineyards: (top left) HH, (top right) HV, (below) HV-HH

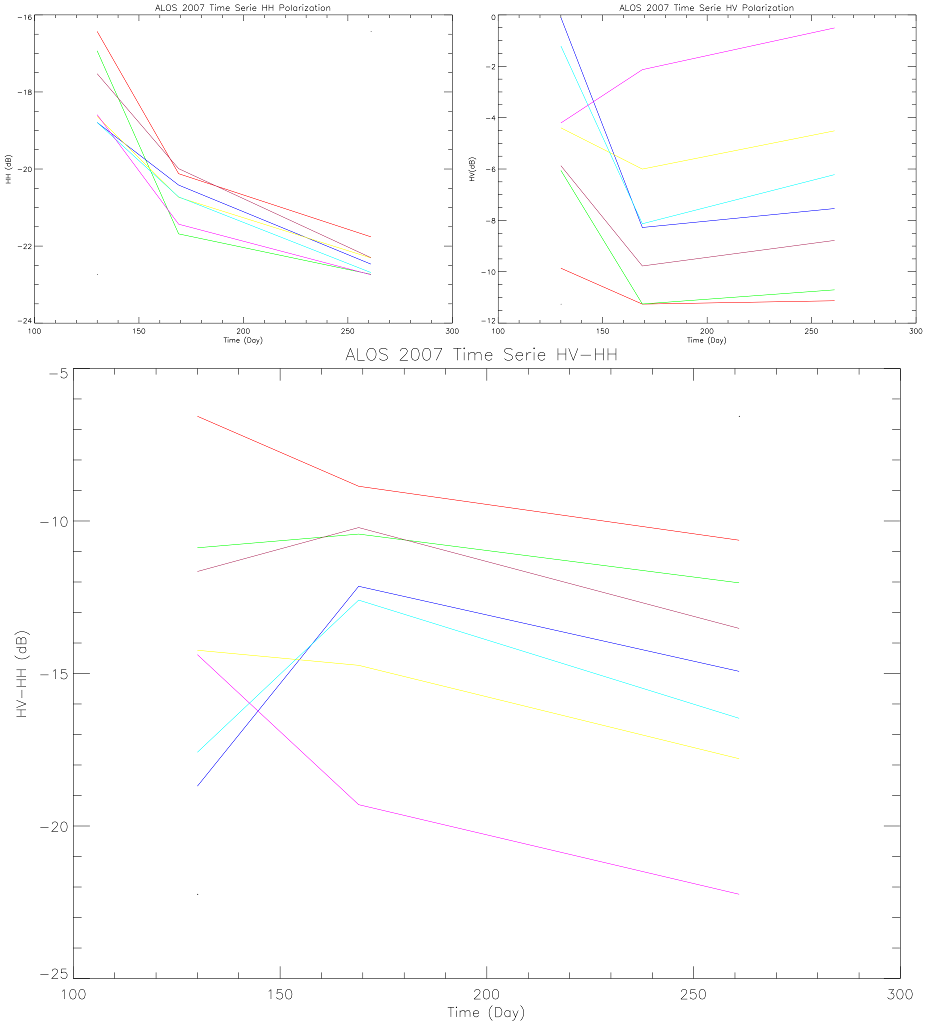

Figure 4.7: Backscattering behavior for the NORTH-SOUTH vineyards: (top left) HH, (top right) HV, (below) HV-HH

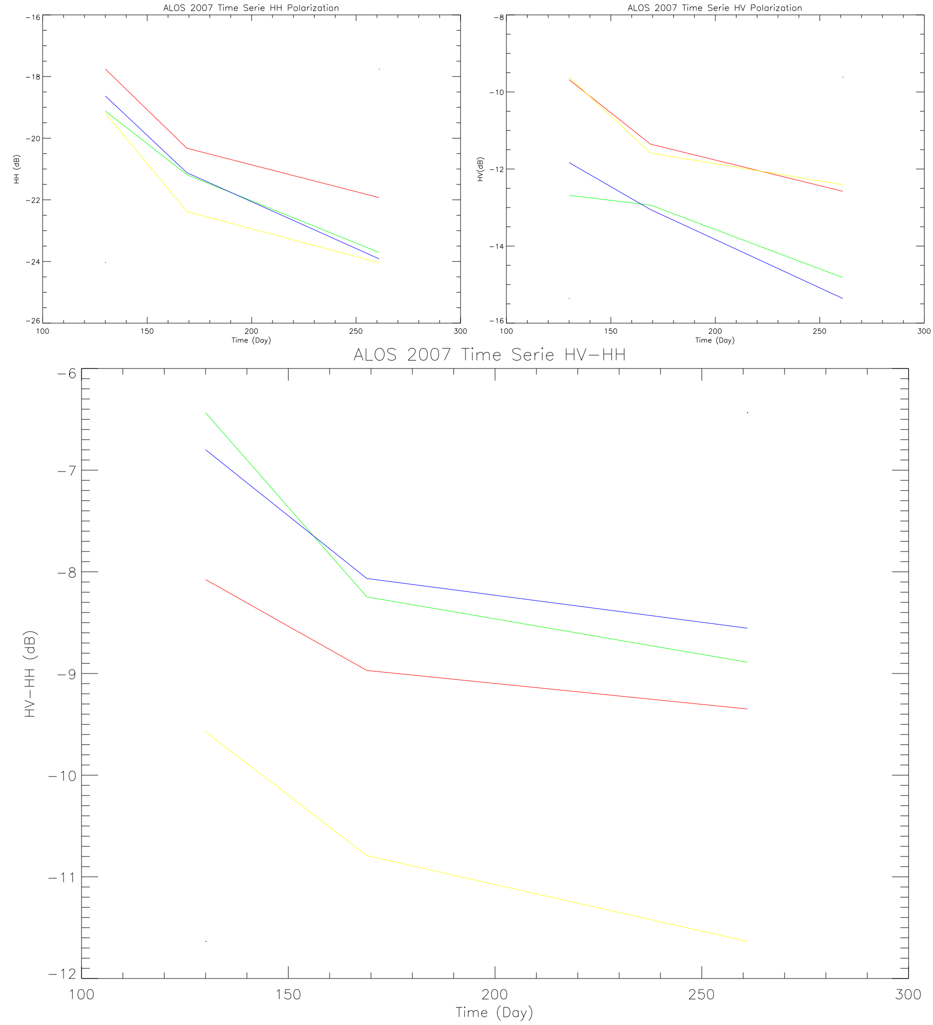

Figure 4.8: Backscattering behavior for the TENT vineyards: (top left) HH, (top right) HV, (below) HV-HH

4.3.6 Discussion and Results.

The graphs reported in the previous section show a very complex environment but some clear topics are clearly visible. Referring to Ulaby and Elachi (1990), we can refer to σ_{HV} as a measurement linked to biomass, to σ_{HV} as linked to soil condition and to σ_{HV-HH} as shown in Chapter 3.2

Reference Soils' Analysis

Considering the image acquired on May, for HH we can notice higher backscattering values than the other two acquisition; with the exception of *Forest*, all the reference soils have got a variability range between May and June of 5 dB. This difference can be partially explained by the difference acquisition geometry (25° and 40° of incidence angle), by some agricultural practices and soil moisture variation; for Forest, this difference is considerably less than the other and can be referred only to different incidence angle effect. In particular, the "ArableLand2" reference soil has got an excursion of 10 dB, due to agricultural practices (harrowing). From June to September, all the reference soils have got a flat behavior, underlying that no significant changes occurred in terms of soil roughness and soil moisture.

For HV polarization, the Forest (oak chestnut) has got a quasi-flat behavior, decreasing from June to September due to the lowering of Plant Water Content (Ferrazzoli et al., 1997). Other soils have got a similar backscattering behavior, with a peak on May (Spring and full growing season) and decreasing slowly during on June and September acquisitions.

For the HV-HH combination, all the reference soils have got a very similar behavior, with a peak on May and no stable measurements on the rest of acquisitions. Focusing on the last two acquisitions, no significant biomass' changes occur during the summer period, with the exception of a slow decreasing behavior due to plant water content (balanced by the decreasing of soil moisture).

“East-Wes” Vineyards

Considering the HH Polarization, all the soils show a common decreasing behavior. The “May-June” difference range is for all the analyzed parcels is between 2 and 3 dB, quite similar to the Forest HH variability during the same period. This effect can be explained by the correlation between the radar measurements and the agricultural practices’ history. On May, after plowing, the soil is restored to its natural roughness and natural short grass is let growing upon it. During the fallowing months, the HH behavior is the same of the reference soils, a slow decreasing due to the decreasing of soil moisture.

For HV Polarization, during May-June we have got quite different behavior: while during the “June-September” period all the parcels show a flat behavior, on May a non homogeneous trend is reported. It is important to underline the orientation of the analyzed parcels that offer a low vines’profile to the incident wave: the HV trend seems more related to the grassland behavior (as showed in Chapter 4.3.6) than to a vine behavior, as showed in the next section.The grass cutting practice and plowing, occurring during the May acquisition, explain the different peak ranges of the parcels.

For the HV-HH combination, a low decreasing trend can be noticed. Again a similarity between grassland, in term of signal range and trend, can be noticed. The most non homogeneous behavior is during the May acquisition, when the parcels are interested by agricultural practices. In the next months an homogeneous trend is clearly visible.

“North-South” Vineyards

Considering the HH Polarization, all the analyzed parcels show a decreasing trend, from high values during May (incidence angle effect and agricultural practices) to the slow decreasing trend of the following acquisition. Focusing on the difference between May and June, we can notice that 3 parcels show values of 4–5 dB, suggesting a late plowing practice and high roughness during the satellite acquisition. Indeed, the agricultural practice of restoring natural soil roughness after the plowing can be done until the late fall of

May. The other two acquisitions show an homogeneous decreasing trend, according with a decreasing of soil moisture, as noticed in the other analyzed soils (Chapter 4.3.6 and 4.3.6).

HV Polarization show the most interesting behavior. Again, focusing on the “May-June” difference, we can find the same behavior of the “East-West” vineyards, where a large number of parcels has got a range between 4-8 dB with a decreasing trend and few parcels show a flat or an increasing trend. Considering the parallel orientation respect to the satellite ground track, the “May” acquisition is affected by the vine fresh growing vegetation and by the grassland; referring to the geometric structure of the vineyard and to its behavior at different incidence angle (Chapter 3.2), this non-homogeneous trend can be related to the different growing status of the parcels and to the grass biomass. For higher incidence angles (June-September), the presence of soil is reduced and the vine biomass is emphasized: with the exception of two parcels with a flat behavior, all the analyzed parcels have got the same growing trend, with a range between 1.5–3 dB. Considering the vine phenology in Figure 4.4, the leaves’ growth stops at June (when the hot season is going to start) and the leaves’biomass remain constant until the harvest, while from the grapes point of view, they start to store water until the maturation is completed in the fall of September. By these consideration, this behavior could be related to the grapes’ maturation.

For HV-HH combination, focusing directly on the “June-September” period, an homogeneous decreasing trend with a range between 1.5–3 dB is reported. It is important to notice two main differences between vineyards with orthogonal and parallel orientation to the incidence wave:

HV “North-South” and “East-West” parcels have got an opposite trend

HV-HH The range of the signal of “North-South” parcels, during the “June-September” acquisition is sensibly greater than the one presented by “East-West” parcels (2 dB).

This confirm the hypothesis of a backscattering sensitivity to biomass dependent by the rows’geometric orientations.

“Tent” Vineyards

The analysis of “tent” vineyard is particularly interesting. At HH Polarization, the “May-June” peak has got a 2 dB range (the same measured for he Forest) to gently decrease during the summer period. At HV Polarization we can measure a quasi-flat behavior, with signal range of 1–1.5 dB. HV-HH shows an homogeneous flat behavior during the grapes’ development period. This lack of sensitivity to the grapes’ development and the low sensitivity to the soil variation (in term of biomass of grass, soil moisture and soil roughness) can be explained by its geometric structure. A “tent” vineyard has got all the leaves on the top of the geometrical structure and leaves’ density can be so high that also the sun light cannot directly reach the soil (Figure 4.9). Because of the leaves’density and leaves cover thickness (from 30 to 50 cm), soil and grapes’ contribution is strongly attenuated.

4.3.7 Conclusions for ALOS PALSAR

The analysis of ALOS PALSAR data showed a very interesting behavior during the “grapes’ maturation” period for parallel oriented rows. Moreover, the geometric structure dependence of the parcels has been clearly showed. In particular, the “tent” vineyards’ analysis showed that the backscattering of agricultural surfaces is particularly complex and linked to the geometry of the observed parcels. The soil contribution decreases with the increase of the incidence angle and it is dependent on the row orientation and the vineyard’geometric structure. Backscattering at L-Band showed a sensitivity to grapes maturation but, due to the short and inappropriate time series, it is not possible to clearly demonstrate the sensitivity of L band to grape presence.

Figure 4.9: View of one of the analyzed ”tent” vineyards

Chapter 5

RADARSAT-2 detecting grapes

In this section RADARSAT-2 results will be presented and discussed. RADARSAT-2 showed a great capability in mission planning and data delivering, two important aspects in a precision farming system; its polarimetric capability, its resolution and its short revisit time make the RADARSAT-2 a good candidate for vineyard monitoring

5.1 The RADARSAT-2 data set

RADARSAT-2 is Canada's next-generation commercial SAR satellite, the follow-on to RADARSAT-1. The new satellite was launched in December, 2007 on a Soyuz vehicle from Russia's Baikonur Cosmodrome in Kazakhstan. RADARSAT-2 has been designed with significant and powerful technical advancements which include 3 m high-resolution imaging, flexibility in selection of polarization, left and right-looking imaging options, superior data storage and more precise measurements of spacecraft position and attitude. The SAR Payload includes the SAR antenna and associated sensor electronics required for imaging.Fully computer-controlled, the antenna is capable of being steered electronically over the full range of the swath and can switch between operating modes virtually instantaneously. Thanks to the Science and Operational Applications Research for RADARSAT-2 Program (SOAR),a joint partnership program between MDA and the Canadian Government through the Canadian Space Agency (CSA) and the Natural Resource Canada's Canada Centre for Remote Sensing (CCRS), an interesting fully polarimetric time series has been planned during the pre-launch activities and successfully acquired during the last 6 months of 2008. The SOAR project (SOAR-1488) aims to the monitoring of grapes' development toward estimating the yield of vineyards and olive groves, providing 10 acquisitions, from August to December, 2008. The Area of Interest is reported in Figure 5.1, while the full time series' details can be found at Table 5.1.

Date	Beam	Polar	Inc. Ang.
08.08.2008	FQ9	H+HV+V	28.20
25.08.2008	FQ4	H+HV+V	22.33
08.09.2008	FQ14	H+HV+V	33.60
15.09.2008	FQ19	H+HV+V	38.51
25.09.2008	FQ9	H+HV+V	28.20
02.10.2008	FQ14	H+HV+V	33.60
09.10.2008	FQ19	H+HV+V	38.51
19.10.2008	FQ9	H+HV+V	28.20
12.11.2008	FQ9	H+HV+V	28.20
13.12.2008	FQ14	H+HV+V	33.60

Table 5.1: RADARSAT-2 Time Series

During each satellite acquisition, weather, soil and plants' phenological conditions have been annotated by means of in-field observations. Weather conditions are reported in Table 5.2, while the monthly summary for rain rate is reported in Figure 5.2

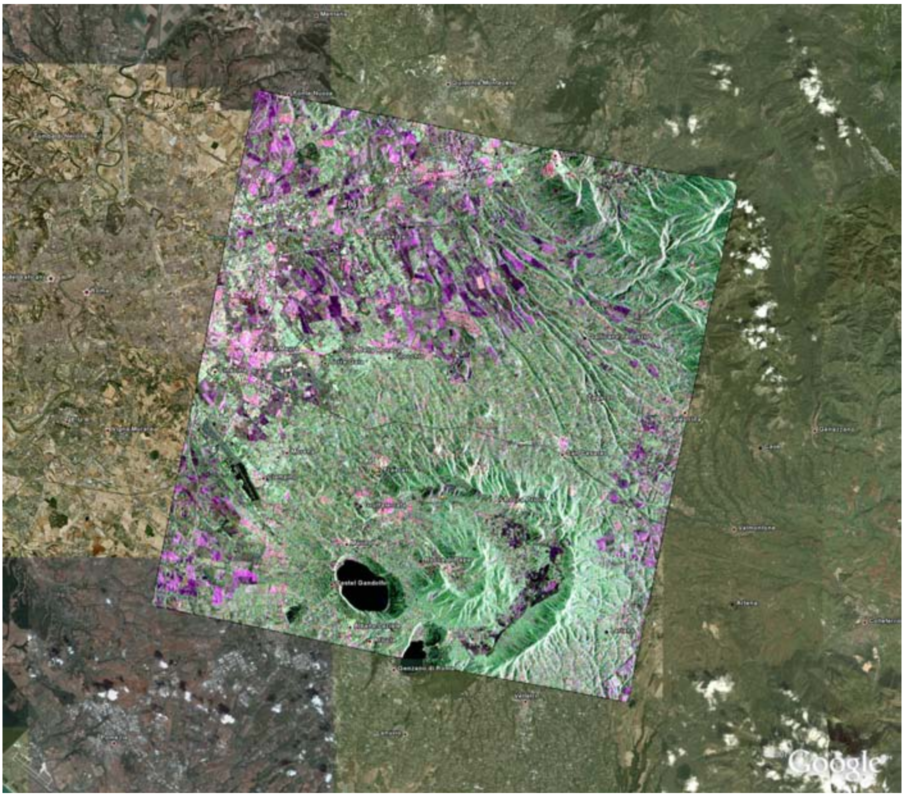

Figure 5.1: The Area of Interest for the SOAR-1488 project

Day	$\overline{T}$ $(^\circ C)$	T_{min} $(^\circ C)$	T_{max} $(^\circ C)$	Rain	Weather Condition	Mean Air Umidity
08.08.2008	28.0	23.0	33.0	-	Clear	62%
25.08.2008	25.0	20.0	30.0	-	Clear	66%
08.09.2008	27.0	22.0	31.0	-	Clear	64%
15.09.2008	19.0	14.0	25.0	Storm	Cloudy	70%
25.09.2008	17.0	11.0	23.0	-	Clear	62%
02.10.2008	17.0	13.0	22.0	-	Clear	66%
09.10.2008	17.0	11.0	25.0	-	Clear	70%
19.10.2008	17.0	12.0	23.0	-	Clear	77%
12.11.2008	13.0	7.0	17.0	Rain	Cloudy	82%
13.12.2008	28.0	23.0	33.0	-	Clear	62%

Table 5.2: SOAR-1488 Mission: Weather Conditions as measured by the ESA/ESRIN Meteorologic Station

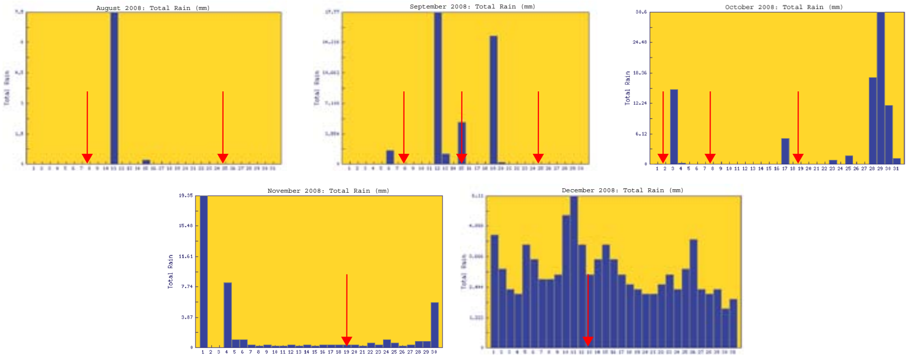

Figure 5.2: Monthly Summuary for Rain rate

5.2 Vine Phenology during RADARSAT-2 survey

As previously done for ALOS (Chapter 4.3.2), each acquisition has been put in relation with the vine phenological status and agricultural practices. Short revisit time of the RADARSAT-2 acquisitions offers an unique chance to monitor the harvest period.

Veraison Period. 3 images acquired on 8^{th} and 25^{th} of August and 8^{th} of September. No agricultural practices are reported. The leaves' biomass is constant while all the water collected by the roots is stored into the grapes. On August, vine is in the “Veraison” phase, where grapes change their color and their sugar concentration.

Harvest Period. 4 images acquired on 15^{th} and 25^{th} of September, 2^{th} and 9^{th} of October. The harvest period officially started on the 15^{th} of September, but, because of the storm occurred the same day, the harvest started some days after. Grapes collecting operation are vine quality dependent and the starting time can change from parcel to parcel; it is possible to affirm that in one month all the grapes'collecting operations are completed.

Breathing Space 1 image acquired on 19^{th} of October. The “Breathing Space” is a 10 days long period, where the plants are preparing to the Autumn. The biomass is quite constant while the leaves are loosing their vigor and water content.

Leaf Falling Period 2 images acquired on 12^{th} of November and on 13^{th} of December. The leaves are loosing completely their photosynthetic capability and gradually falling to the ground. The vine is preparing to the hibernation and all the leaves biomass will be lost before the end of December. No agricultural practices are reported to clean up the parcels, the leaves are let on the ground.

The only agricultural practice that could modify the soil roughness is the harvest; tractors moving on the field and people picking grapes could modify the soil profile.

5.3 RADARSAT-2 Processing

Because of the fast data delivering (1–3 days after the acquisition) and large amount of data, a traditional processing, as the one used for ALOS and ESAR data, cannot be used in a fast way. A Processor has been built to perform a fast GIS integration. The block diagram can be found in Figure 5.3

The dataset, composed by 10 Radarsat-2 Fully polarimetric acquisitions, is processed to obtain two different products, one focused on the backscattering analysis and the other on the polarimetric characterization of each field. The main steps for the first processing chain are:

- **RADARSAT-2 SLC Format.** The SLC data is composed by two main sub-product: The *Scattering Matrix* and the *header*.
    - *Scattering Matrix.* In a standard TIFF file, in a "complex-like" format; one band for the Real Part and one for the Imaginary Part
    - *Header.* Delivered in XML ASCII format, it contains all the information to correctly process the data.
- **Complex to Amplitude.** Amplitude images are computed by the Complex Dataset
- **Multilook.** The Multilook factor is computed considering the ground resolution linked to slant resolution by $G_r = \frac{S_r}{\sin\theta}$ and spatial multilook factor can be easily computed by means of $M = G_r \mathrm{MOD}(A_r)$, where A_r is the resolution in the azimuth direction and $\mathrm{MOD}(A_r)$ is the module operator.
- **Geocoding.** The Geocoded is performed by means of Orbital Parameters and Tie Point. The dataset is then warped by means of a polynomial transformation.
- **Coregistration.** Once all the images have been processed, an automatic coregistration tool has been integrated.

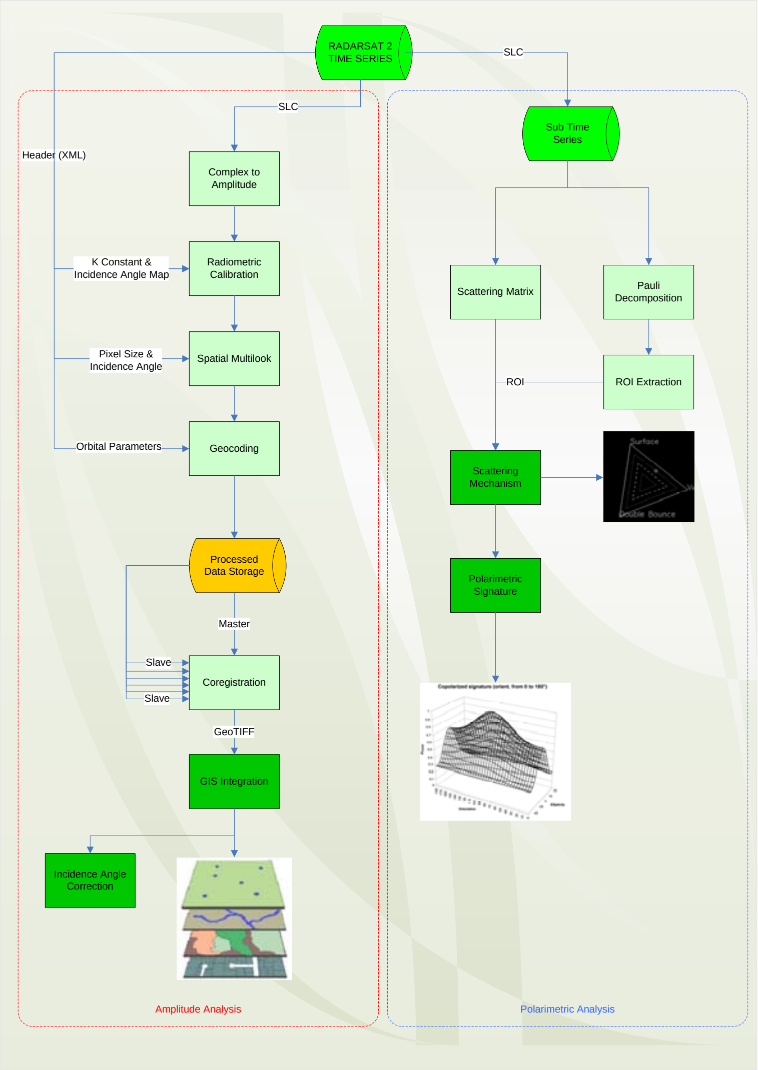

Figure 5.3: Block Diagram for the RADARSAT-2 Processor

- **GIS Integration** The data stack is integrated into a GIS system, containing all the cadastral information to accurately select each analyzed parcel. Once selected, the average multi-temporal backscattering value is sent to the "incidence angle correction" module, where the incidence angle dependence of the backscattering is normalized to a reference value.

- **Incidence Angle Correction.** The new generation spaceborne radar have got the capability of enhance the revisit time over a target steering and tilting the antenna beam, changing the incidence angle of the transmitted wave. If we want to monitor a target during the whole acquisition period, the incidence angle dependence has to be taken into account and corrected (Brown et al., 1993). The incidence angle correction module is based on the statistical measurements reported in Ulaby and Dobson (1989), improved by some simulations provided by the Mark Williams Coherent Model, integrated into the PolSarPro tool (Williams, 2006). All this information has been integrated into a database and used to correct the incidence angle effect by soil type. It is important to underline that this operation is performed on the mean backscattering values of the analyzed parcel and not made per pixel.

This processing chain is performed both for H-V and Circular R-L polarimetric basis, but only H-V data has been incidence angle corrected, because of good amount of statistical information.

The second processing chain is focused on the polarimetric characterization of each analyzed soil to better understand the change of backscattering interaction with vines during the harvest period and grapes' contribution to this change. The processing flow can be summarized as follow:

- **Scattering Matrix Extraction.** The Scattering Matrix is extracted by the storage and converted in a complex data format to easily retrieve all the polarimetric information.

- **Pauli Decomposition.** The Pauli Decomposition is calculated in order to provide a reference for the parcel individuation and segmentation. All the operations for the identification of parcels are performed by visual inspection of the radar image in a slant-range geometry, with the visual support of an high resolution optical image.

- **Scattering Mechanism.** By means of RAT[1], the average scattering mechanism over the analyzed parcel is computed and plotted in the plane Volume-Double Bounce-Surface plane, as proposed in Freeman and Durden (1998).

- **Polarimetric Signature** To perform the Polarimetric Signature Analysis the tool provided by the CSA [2] is used (Fiset and Farhat, 2001); this tool accepts as input the Kennaugh Matrix averaged by pixels contained in the ROI and the Co-Polarized and Cross-Polarized Polarimetric Signature is produced.

5.3.1 Region of Interest

In order to better understand the backscattering behavior of vineyards during the harvest period, several reference soils have been selected and monitored during the Radarsat-2 acquisitions. 25 ROIs have been selected, further details can be found in the Table 5.3. Figure 5.4 shows how the ROIs are located in the observed area.

In the next paragraph, the full incidence angle corrected time series will be presented and results will be discussed.

5.3.2 Multi-temporal Soil Analysis

As reported in Chapter 5.3, after the coregistration of each acquisition with a master image (acquired on 08/08/08), the average value of backscattering over each ROI has been calculated and then corrected by the incidence angle dependence. In this section will be reported the analysis for each selected ROI after the incidence angle correction.

---

[1] RAdar Tool

[2] Canadian Space Agency

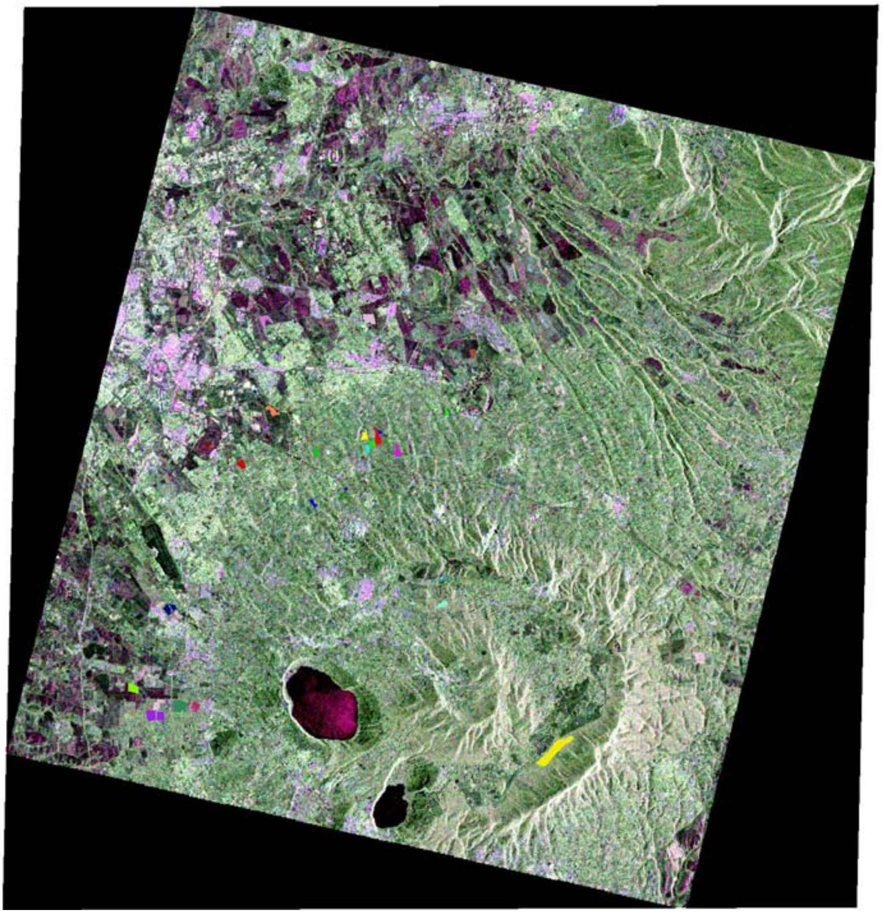

Figure 5.4: Overview of the ROIs' distribution over the observed area.

Nr. ROI	ROI Type	Zone
4	Arable Land	Pantano, Gotto d'Oro
2	Forest	Monte Cavo Vulcanic Complex
3	Grassland	Tor Vergata, Gotto d'Oro
3	Olive Groves	Pietra Porzia
4	North-South Row Vineyards	Pietra Porzia, Gotto d'Oro
5	East-West Row Vineyards	Pietra Porzia, Gotto d'Oro
4	Tent Vineyards	Pietra Porzia, Gotto d'Oro

Table 5.3: Details on selected ROIS

North-South Row Vineyards

Four parcels have been selected and analyzed. Results are reported in Figure 5.5. For three of them, the harvest timing has been accurately observed and plotted together with the backscattering measurements. All the analyzed parcels have got the same behavior during the observation period and, focusing on the harvest period, they show a clear sensitivity to grapes' presence; in particular, the behavior of the red parcel has to be noticed ("Santini"), with a delayed harvest: this effect is clearly visible with a temporally shifted decrease of the quantity $HV - HH$ for this parcel. A general increase of the backscattering at HH polarization during the November-December period can be noticed, due of the increase of the soil moisture and of the presence of rain (Figure 5.2). Anyway, the $HV - HH$ seems to take into account these variations and to good underline the grapes' effect during the harvest period. It is important to notice that only after the incidence angle correction, the "grapes' signal" was put in evidence and showed a clear effect during the observation period; when a multi-temporal and multi-angle observation is performed, this operation is strongly suggested.

East-West Row Vineyards

Five parcels have been selected and analyzed. Results are reported in Figure 5.6. It is also important to analyze the backscattering response to the orientation of the rows respect to the satellite flight heading. Taking into account the considerations made in Chapter 3.2 on the influence of the geometry on the backscattering response, it has been noticed that the grapes' signal during the harvest period is not anymore clear and visible and the parcel's response is closer to the one presented by a grassland parcel than to the one observed in the Chapter 5.3.2 and in Figure 5.5. The orientation of a vineyard respect to the satellite heading is crucial in terms of soil contribution to the backscattering mechanism: dealing with East-West Row Vineyards (perpendicularly oriented respect to the satellite ground track) the soil effect is maximum, hiding the contribution from the canopy, while for the North-South Row Vineyards, the soil effect is still present but lowered by the canopy.

Tent Vineyards

Four parcels have been selected. In a Tent Vineyard, the grapes are located under the top leaves' layer and this can attenuate their presence; on the other side, the biomass of grapes in a tent vineyard is greater than in a row vineyard, such as the water content of the grapes, so the backscattering could be sensible to the grapes' effect, even if shadowed by the leaves. The observations are reported in Figure 5.7; during the harvest period, a decrease of the $HV - HH$ signal is reported, underlying a sensitivity to the grapes' biomass; the soil contribution is lowered by leaves, growing during the last observations, during the fall of autumn, when leaves loose their vigor and fall on the ground.

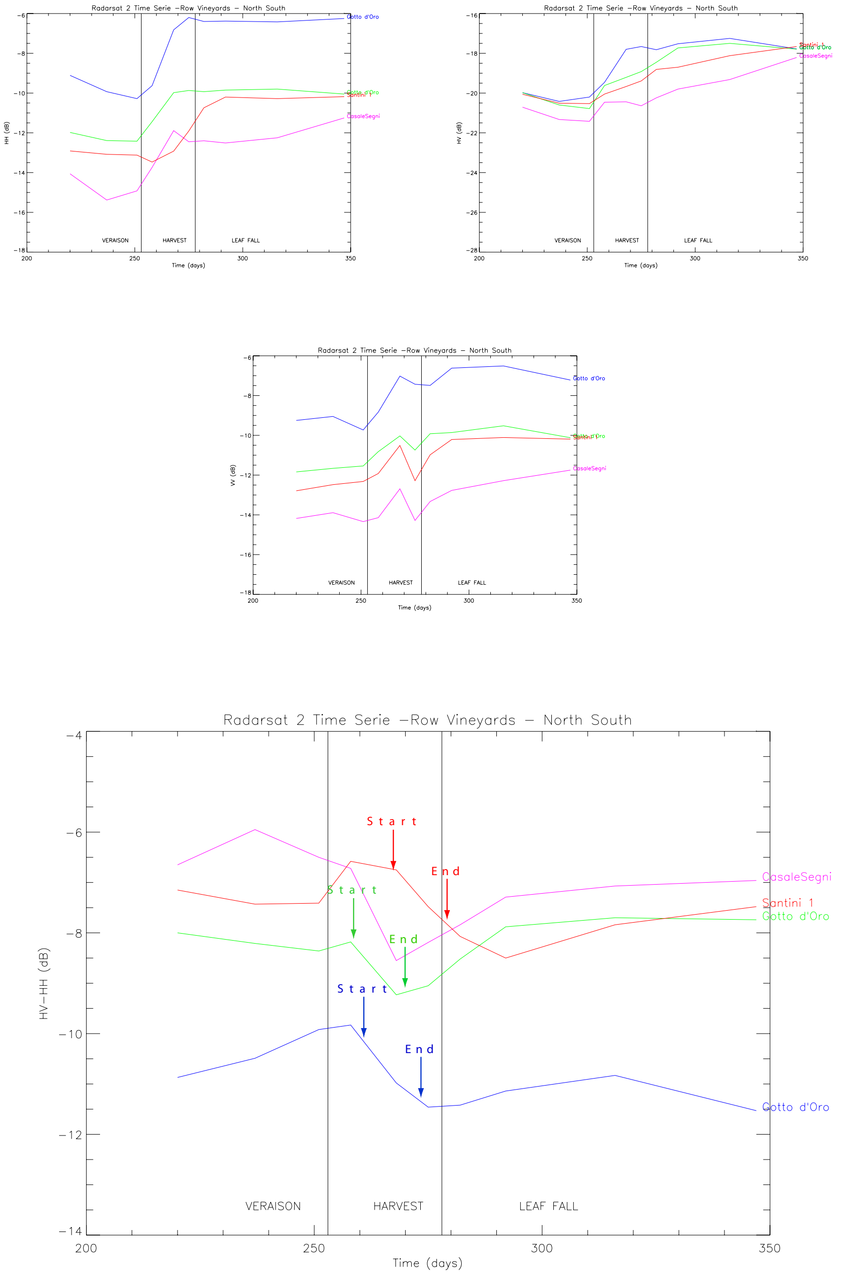

Figure 5.5: Observation of North-South Row Vineyards. “Start” and “End” labels show on the time line the measured time location of the harvest for each analyzed parcel.

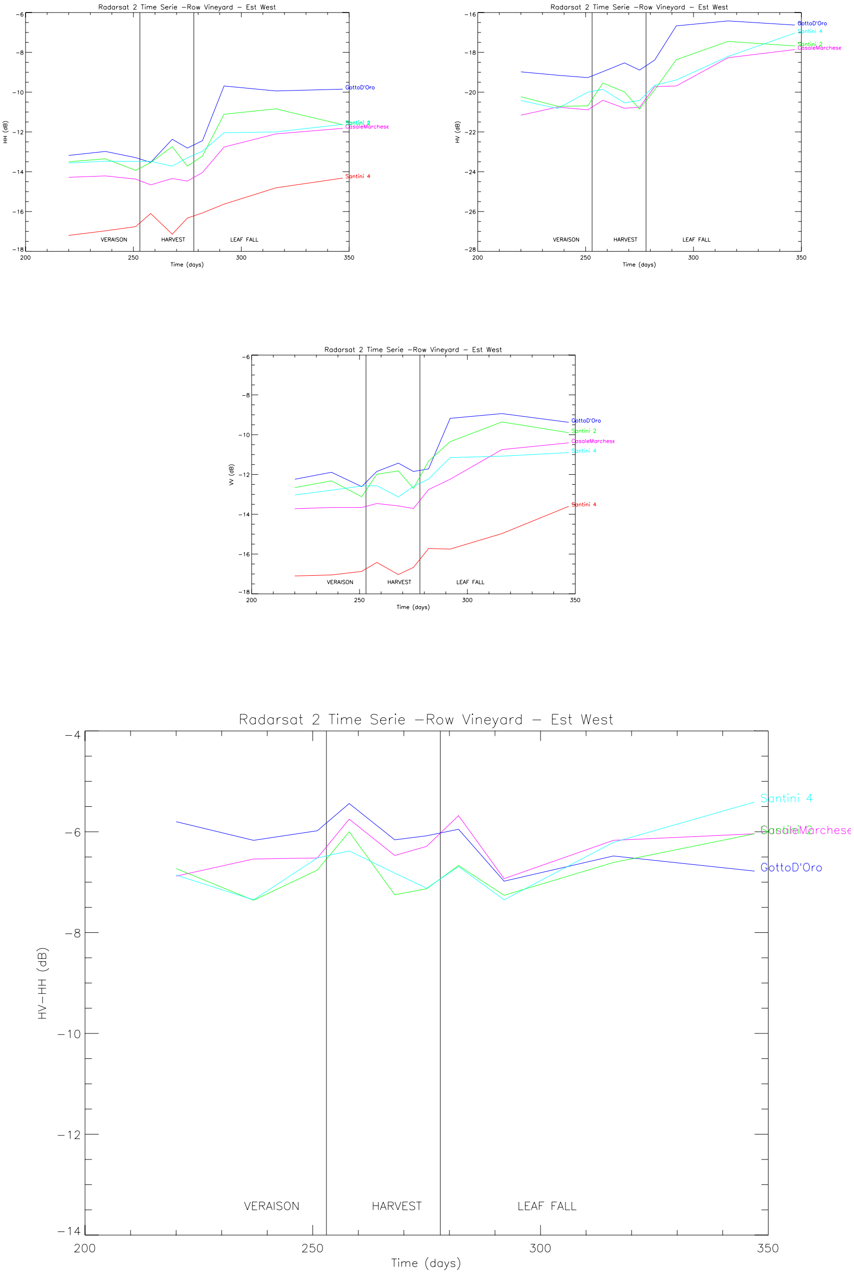

Figure 5.6: Observation of East-West Row Vineyards

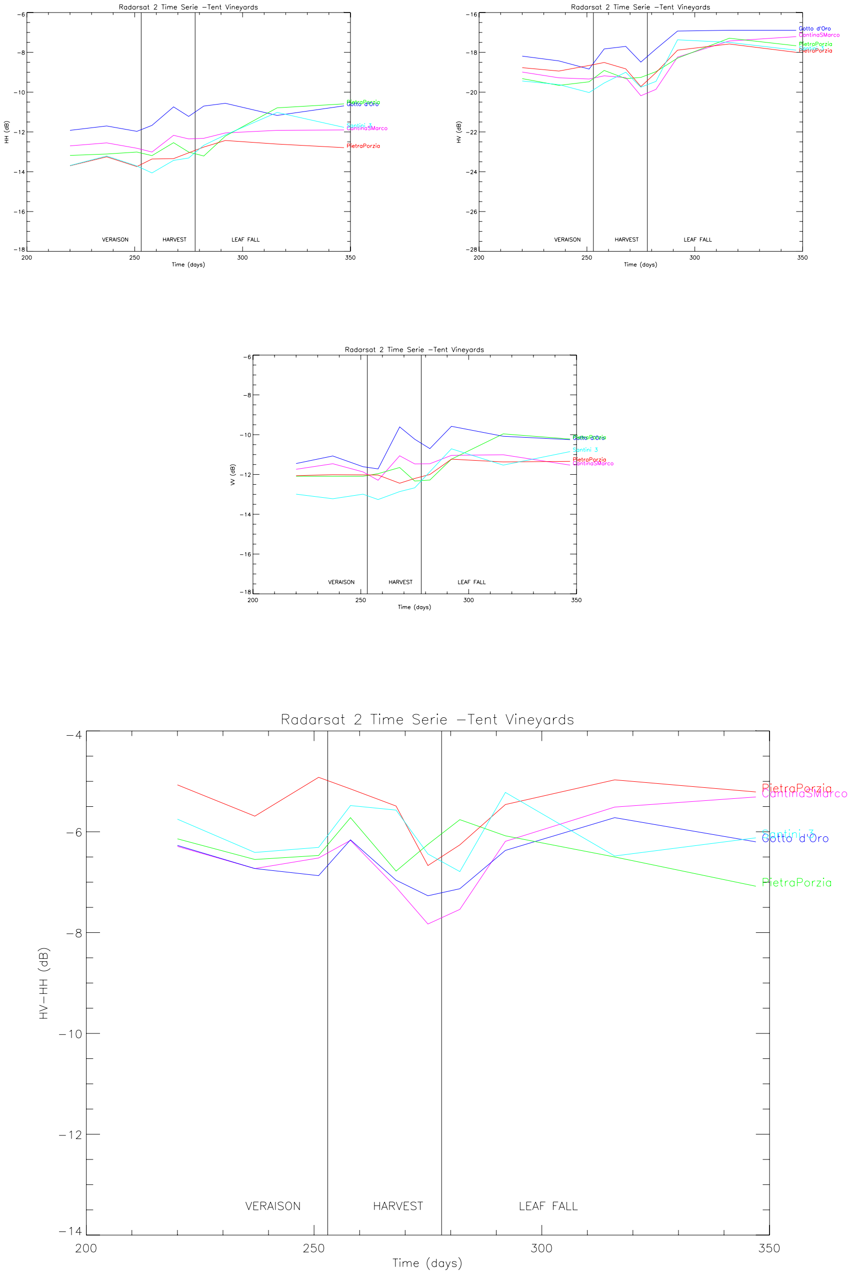

Figure 5.7: Observation of Tent Vineyards

Forest

Two parcels have been selected in the area surrounding the ancient volcanic complex of “Colli Albani”. Chestnut trees are wildly growing in this area, with a stable leaves’ biomass until early November; the observation of such parcels is used as a reference. Specially for the forest, the Williams’ backscattering model (Williams, 2006) has been used to set up the backscattering incidence angle dependence. Results are reported in Figure 5.8; a flat behavior of the backscattering can be noticed all over the observation period.

Grassland

Three parcels have been selected; grassland is used as a reference for the soil contribution to the backscattering mechanism of a vineyard. Observation of grassland is also used to understand the effect of soil moisture, precipitations, natural soil roughness and grass biomass. As can be noticed in the Figure 5.9, focusing on the HH polarization, a flat behavior can be reported for the first acquisitions, until the mid of October; after that, with the growing of the soil moisture due to the rain phenomena (Figure 5.2), a general growth of the backscattering is noticed. Anyway, it has to be noticed that the $HV - HH$ quantity remains constant during the harvest period and grows lightly during the fall of the year, due of the increasing of grass biomass and high soil moisture level. It is important to notice the differences between the North-South Vineyards, East-West Vineyards and Grassland. While for the North-South parcels there is a clear difference with the backscattering of grassland, during the harvest period the East-West Parcels have got a very similar behavior to grassland, in terms of absolute value and trend of the graphs. This effect can be explained taking into account the effect of row orientation during the interaction between the incidence wave and the vineyard.

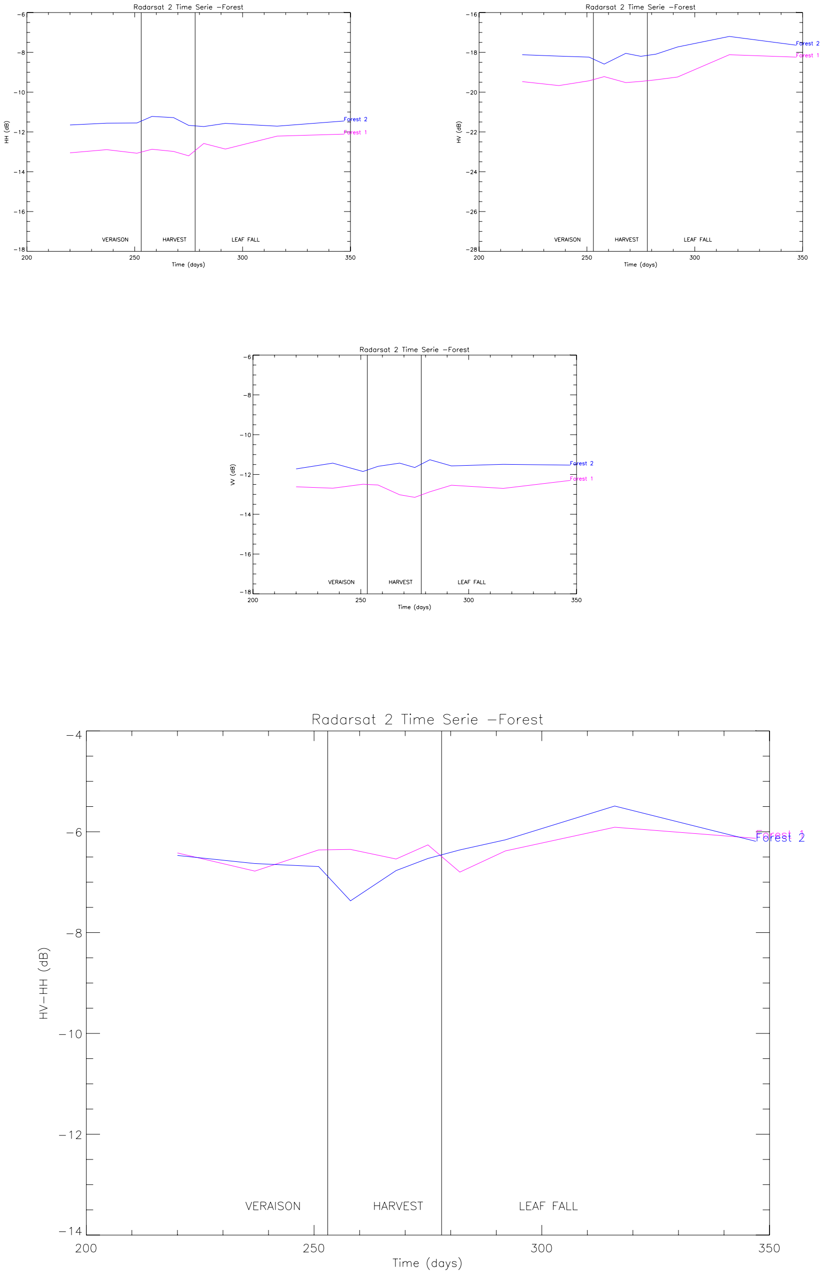

Figure 5.8: Observation of Forest

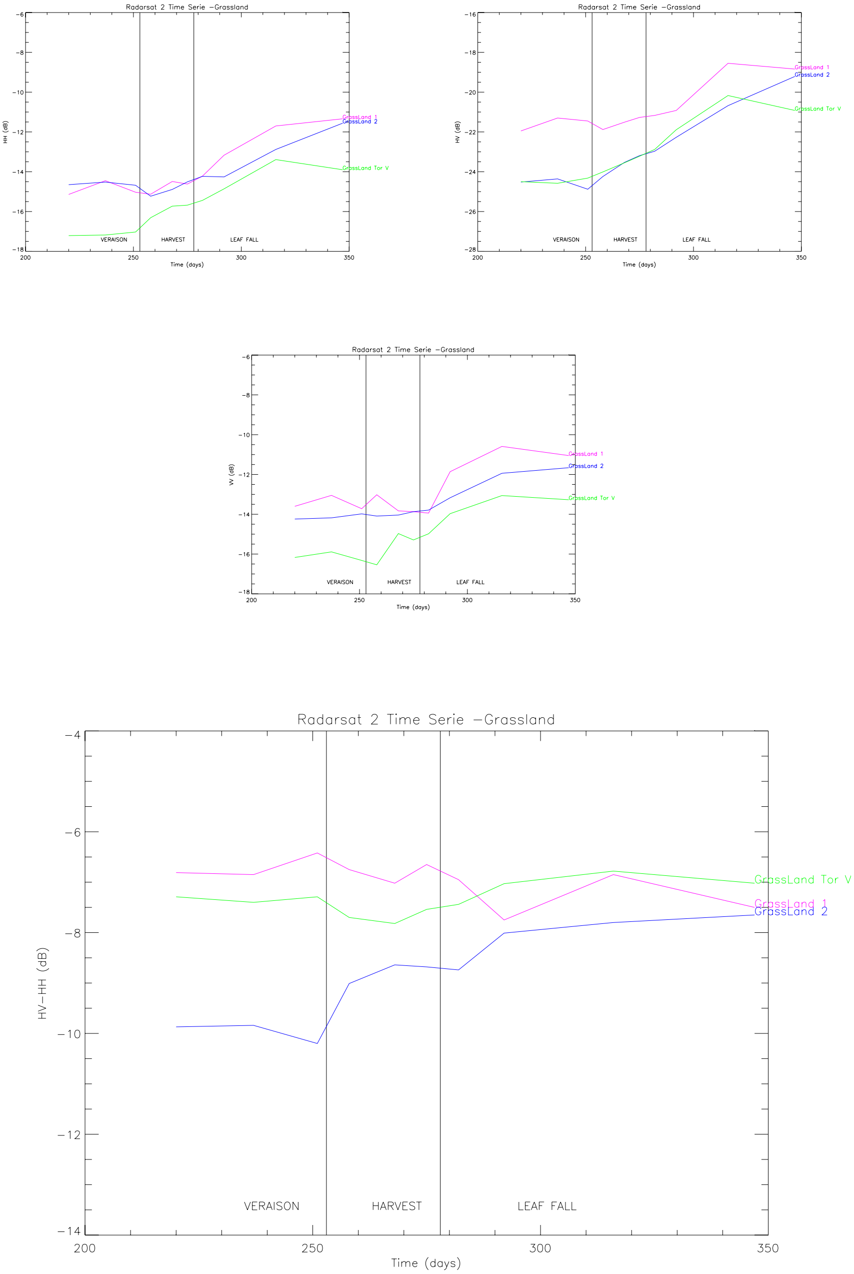

Figure 5.9: Observation of Grassland

Arable Land

Four parcels have been selected. As reported in Figure 5.10 an heterogeneous behavior can be noticed due to the different nature of the parcels, but again a different behavior respect to the one observed for vineyards is reported. A difference respect the grassland parcels is reported, due to probable practices during the observation period. On the last acquisitions, an increase of the soil moisture can be noticed.

Olive Groves

Three parcels have been selected. A constant behavior is reported during the harvest period, while during the last acquisitions an heterogeneous behavior is reported. No sensitivity to the olive presence can be clearly reported;such kind of heterogeneous behavior during the November-December period can be explained with an heterogeneous soil condition due to different grass cover; indeed the grass biomass and the soil practices can be different from parcel to parcel. Results are reported in Figure 5.11

5.4 Polarimetric Analysis and Characterization of Vineyards

To discuss in detail the backscattering sensitivity to grapes, two acquisitions have been chosen, the first on the 8^{th} of September, with grapes still present and just before the harvest, and the second one on the 2^{nd} of October, when the majority of the vine parcels had been harvested. The aim of this section is to understand, focusing on a short well known period, the effect of grapes on scattering mechanism and on the polarimetric signature of each parcel. The main steps of this study can be summarized as follow:

- Extraction of Scattering Matrix starting from original SLC Polarimetric Data
- Pauli Decomposition and segmentation of the target parcel

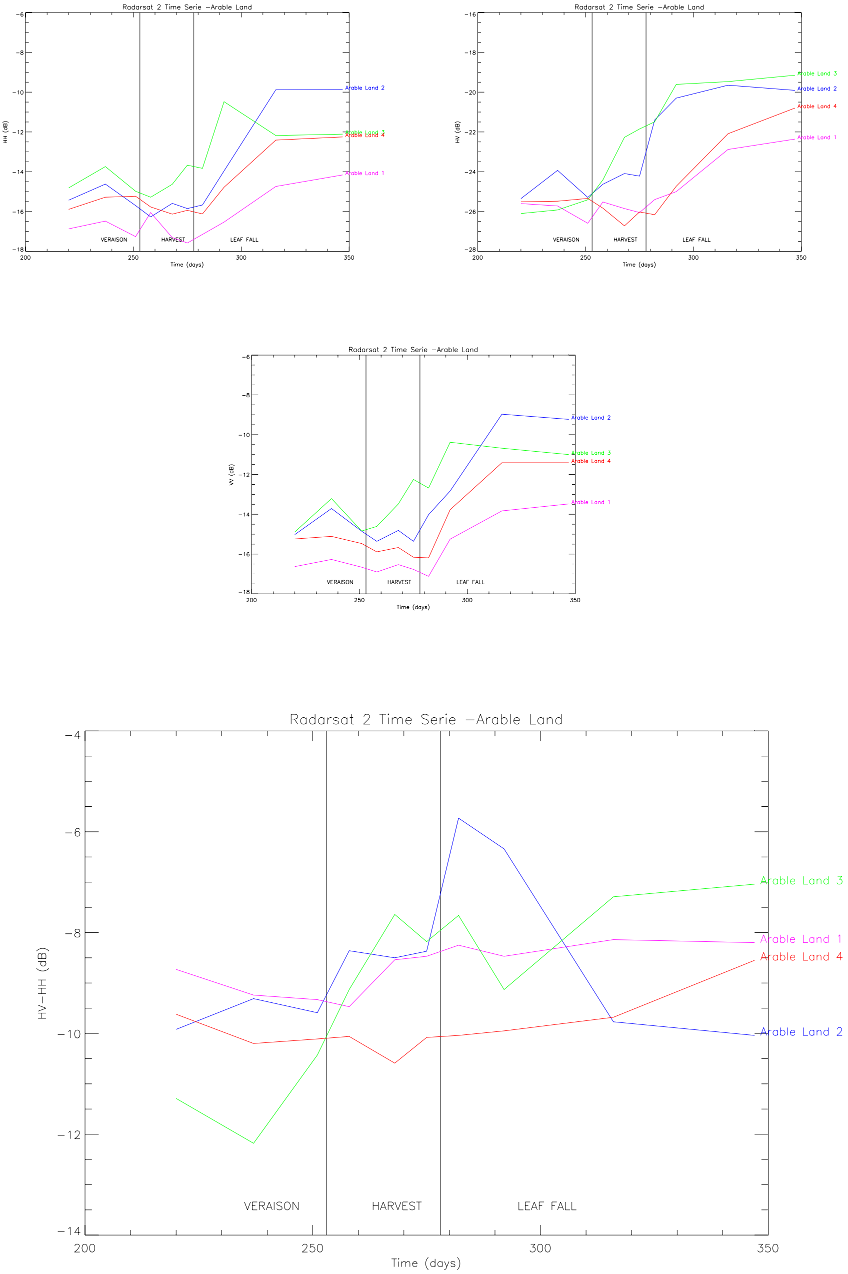

Figure 5.10: Observation of Arable Land

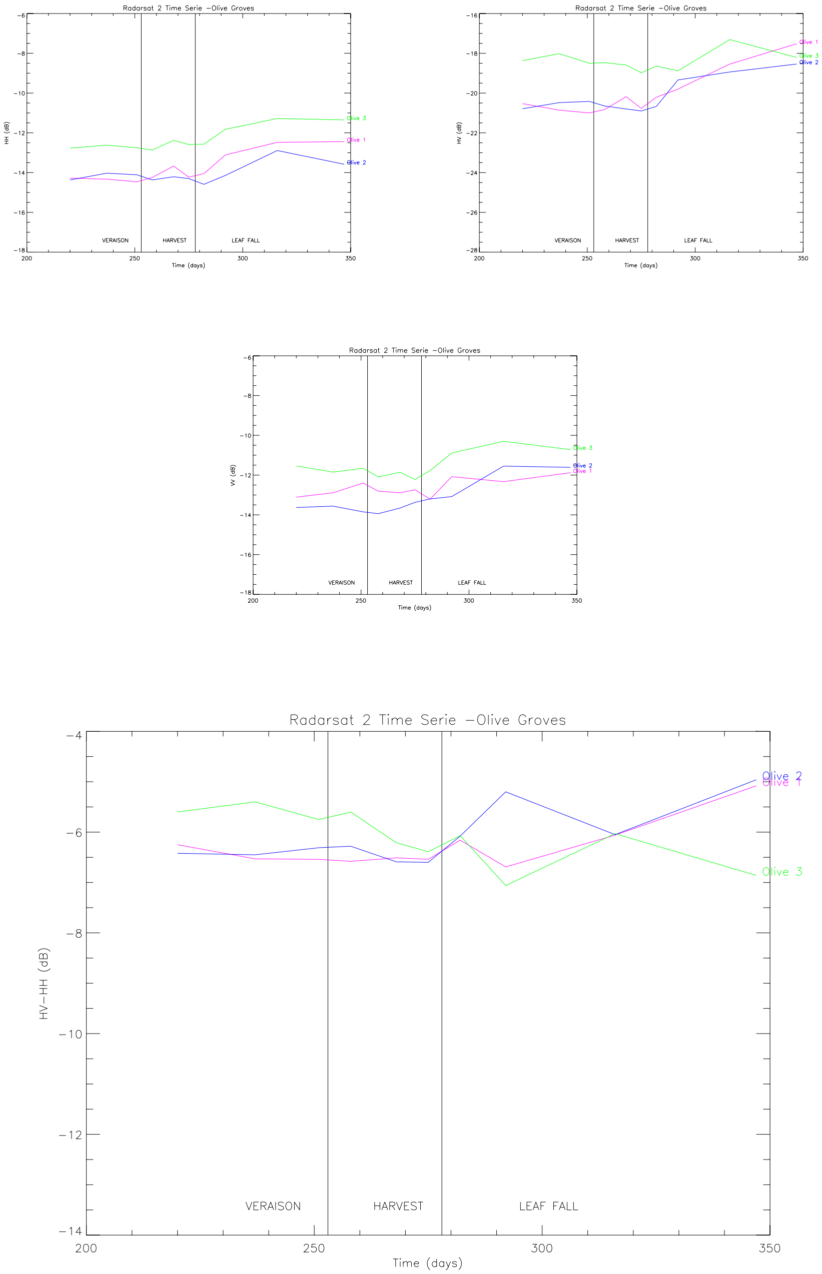

Figure 5.11: Observation of Olive Groves

- Freeman Decomposition (Freeman and Durden, 1998) and Mean Scattering Mechanism Identification
- Mean Polarimetric Signature

Each parcel has been analyzed and the full study is reported in Annex. In this section two North-South vineyards will be presented, the first one with grapes still present in both acquisitions and the second one with grapes' biomass variation. Moreover, a bare soil and a forest parcel will be analyzed and used as reference.

Polarimetric Analysis of "Gotto d'Oro 1"

A ROI of about 200 pixels has been extracted by the parcel, labeled as *"Gotto d'Oro NS 1"*. The scattering mechanism is reported in Figure 5.12, while the Co-Polarimetric Signature is shown in Figure 5.13. This parcels has been harvested before the second acquisition (02.10.08), a change in the scattering mechanism can be easily noticed, from volume to surface. Also a change in the shape of the polarimetric signature can be noticed

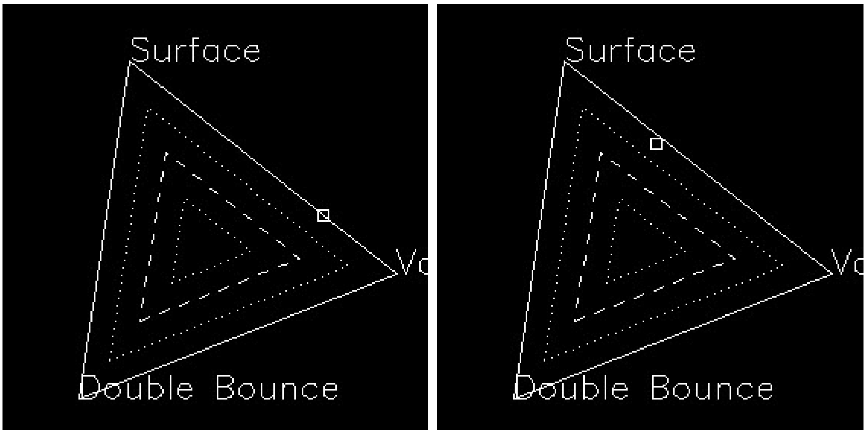

Figure 5.12: Scattering Mechanism for the "Gotto d'Oro 1" parcel before (left) and after the harvest (right)

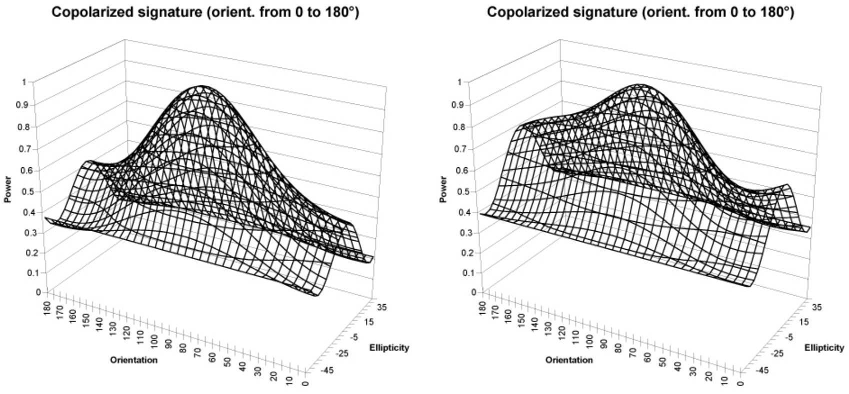
Copolarized signature (orient. from 0 to 180°)

Copolarized signature (orient. from 0 to 180°)

Figure 5.13: Co-Polarimetric Signature for the “Gotto d’Oro 1” parcel before (left) and after the harvest (right)

Polarimetric Analysis of “Santini 1”

A ROI of about 150 pixels has been extracted by the parcel, labeled as *“Santini1”*. The scattering mechanism is reported in Figure 5.14, while the Co-Polarimetric Signature is shown in Figure 5.15. Grapes are still present in both acquisitions: no change in the scattering mechanism and in the polarimetric signature can be reported.

Polarimetric Analysis of Bare Soil

A ROI of about 240 pixels has been extracted by the parcel, labeled as *“Bare Soil Gotto d’Oro”*. The scattering mechanism is reported in Figure 5.16, while the Co-Polarimetric Signature is shown in Figure 5.17. No change in the scattering mechanism and in the polarimetric signature is reported. No changes happened in the soil conditions (soil moisture, roughness, etc . . .) between the two acquisitions.

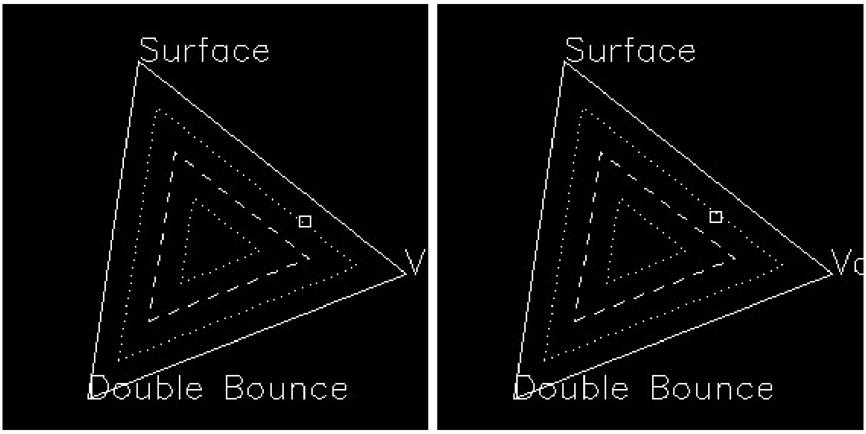

Figure 5.14: Scattering Mechanism for the "Santini 1" parcel before (left) and after the harvest (right)

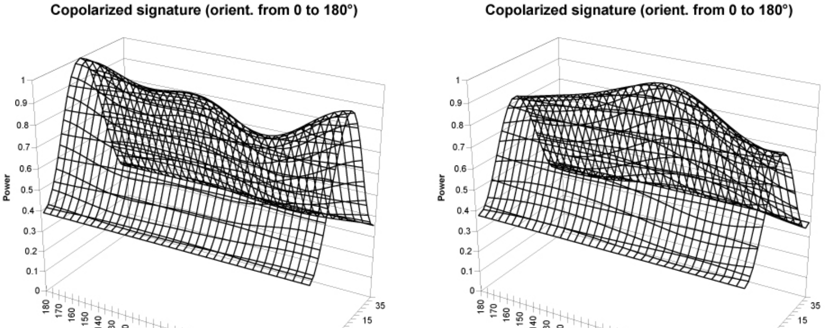

Figure 5.15: Co-Polarimetric Signature for the "Santini 1" parcel before (left) and after the harvest (right)

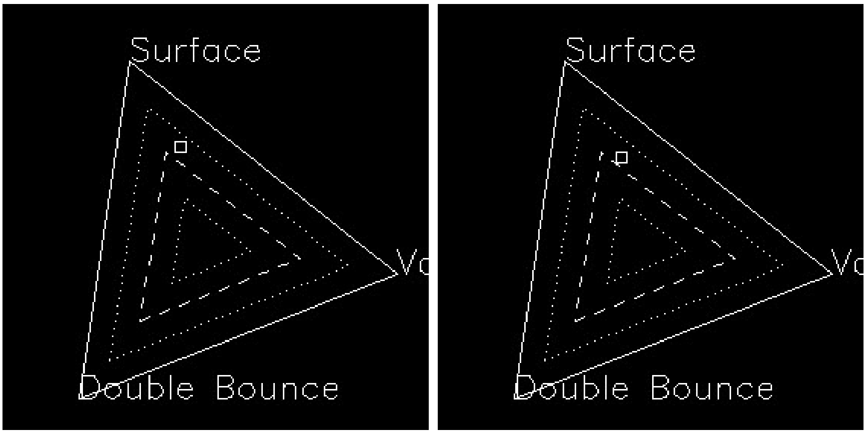

Figure 5.16: Scattering Mechanism of bare soil, on the first (left) and on the second aquisition(right)

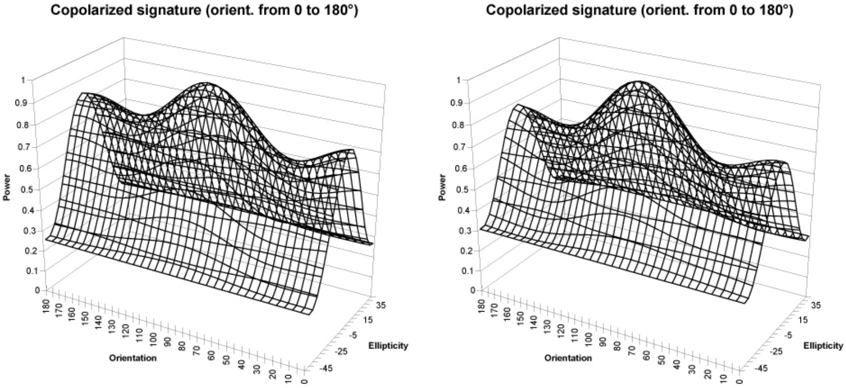

Figure 5.17: Co-Polarimetric Signature of bare soil, on the first (left) and on the second aquisition(right)

5.4.1 Polarimetric Analysis of Forest

A ROI of about 250 pixels has been extracted by the parcel, labeled as *"Forest 2"*. The scattering mechanism is reported in Figure 5.18, while the Co-Polarimetric Signature is shown in Figure 5.19. No change in the scattering mechanism and in the polarimetric signature is reported. As expected, in both acquisitions, the forest shows a constant volume scattering mechanism.

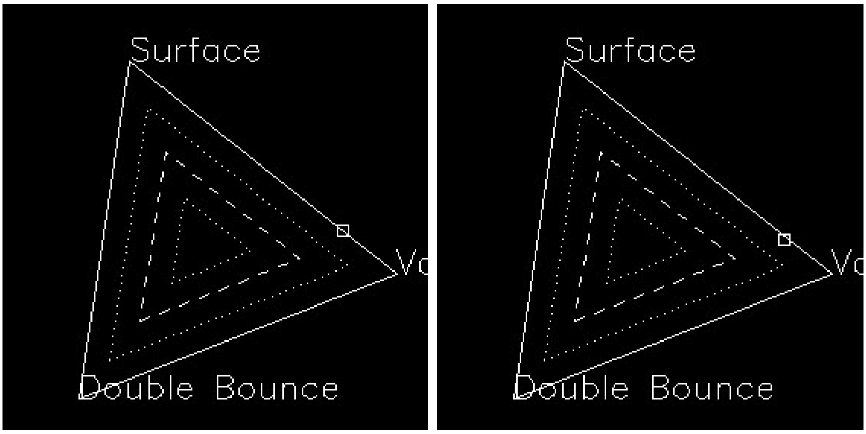

Figure 5.18: Scattering Mechanism of Forest, on the first (left) and on the second aquisition(right)

5.5 Conclusions for RADARSAT-2

The polarimetic capability of RADARSAT-2 and its short revisit time played a key role in the study of sensitivity of backscattering to grapes and the characterization of vineyards from a polarimetric point of view. Even if C-Band tends to saturation when vegetation is observed, RADARSAT-2 data showed a clear sensitivity to grapes' biomass variations. The effect of grapes on the scattering mechanism can be modeled as an attenuator of the soil contribution to the general scattering mechanism: when grapes

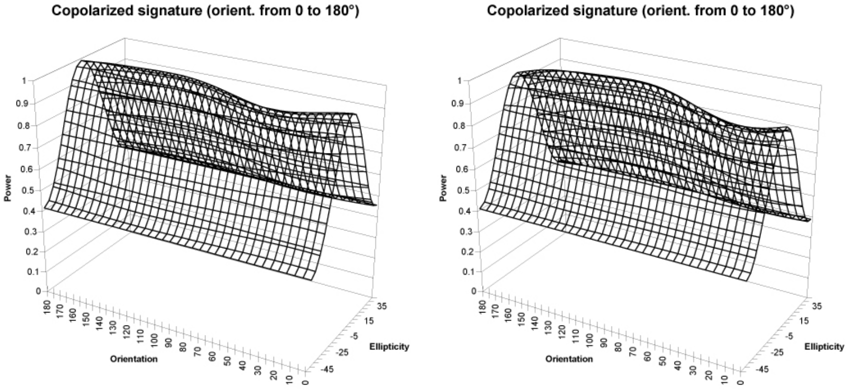
Copolarized signature (orient. from 0 to 180°)

Copolarized signature (orient. from 0 to 180°)

Figure 5.19: Co-Polarimetric Signature of Forest, on the first (left) and on the second aquisition(right)

are present, the soil contribution is lowered, while after the harvest, the soil contribution grows. This has been observed both in the complete time series and in the multi-temporal polarimetric analysis. The backscattering sensitivity to grapes is also dependent on the orientation of rows: for those parcels, with rows orthogonally oriented respect to the flight track, the sensitivity to grapes is almost zero and the scattering mechanism is similar to the one presented by grassland. Sensitivity to grapes for tent vineyard has been observed, even if leaf presence attenuates it. The study of reference surfaces, such as forest, grassland and bare soil, the monitoring of atmospheric phenomena together with ground based observations, had been used to identify variations in the observed targets and to better understand the changes occurring during the harvest period.

Chapter 6

A System for Vine Precision Farming

In this chapter will be shortly shown a precision farming system implementation, the instruments and technologies involved to provide a Precision Farming platform for the Frascati D.O.C. area. This experiment has been supported by the Frascati Living Lab and ESA/ESRIN. After the state of art and the multi-platform and frequency radar analysis, this chapter wants to propose solution for vine precision farming in the Frascati D.O.C. area.

6.1 The Geovine Experience

The idea of making a precision farming platform was born at end of the *"BACCHUS"* project and of other related projects to provide an on-going service to the wine community and to keep updated all the collected information. As already presented in the Chapter 1.1, remote sensing cannot be a "stand-alone" system, but it has to related to other technologies.

Geovine aims to implement a system based on earth observation products and agricultural sensors with a WebGIS component, designed to support vineyards management and precision farming. Specifically, Geovine provides the possibility to visualize via WEB several satellite products (Quickbird, Ikonos, Proba, SPOT and SAR) and different vector layers, building a multi sensor and multi capability platform to support the vineyard management.

6.1.1 Setting up the platform

One of the most important aspects of a precision farming system is its sustainability: no future is granted if the sustainability is not considered. To perform this task, an open-source web-GIS platform seemed to be the best choice. Several open-source systems are available, but not many easily perform the managing of huge amount of data (such as the web-GIS proposed by Google, Google Earth); Ka-Map has been individuate as a possibile solution.

Ka-Map is an open source project that is aimed at providing a javascript API for developing highly interactive web-mapping interfaces using features available in modern web browsers. Ka-Map has got a number of interesting features. It supports the usual array of user interface elements such as:

- interactive, continuous panning without reloading the page
- keyboard navigation options (zooming, panning)
- zooming to pre-set scales
- scalebar, legend and keymap support
- optional layer control on client side (layers are made visible instantly but at reduced performance due to more images, and potentially slower browser interactivity)

Anyway, its most important characteristics is the asynchronous server-client communication, image caching and image tiling. These performances perfectly fitted the Geovine's platform needs. Further and more detailed information can be found at `http://ka-map.maptools.org/`

During this task, the work and professionalism of Antonio Biscuso and Pablo Navarro Farinos has to be acknowledged.

6.1.2 The Dataset

Once set all parameters of the web-platform, all the informative layers have been integrated. The data stored can be summarized as follow:

- **Vine Cadaster.** Vectorial layer providing information about the official parcels' boundary, plants' density, vine quality and other important stuffs.

- **QuickBird data**. 3 images have been already integrated (April 2002, July 2004 and June 2005) and other data will be processed in the next future.

- **IKONOS.** 1 image acquired on 2000, used as an historical high-resolution reference.

- **Brix Index and Acidity Map.** Based on the semi-empirical model discussed in Chapter 1.3, a Brix Index and Acidity map have been processed.

- **Vigor Index Map.** Based on the QuickBird image, acquired on 2005, a Vigor Index Map is processed.

6.1.3 A Weather Forecast Ingrated Service

After a first satellite data and cadastral data integration, A weather Forecast service has been integrated into the Geovine platform: weather data are collected by TuttoMeteo, a partner of the Frascati Living Lab, and processed by the "MeteoFLLab" tool: following the information provided by a forecast weather model and by satellite and ground measured data, the tool creates maps for air pressure at sea level, temperature and air humidity; moreover, the main phenomena forecast is provided. Some example of the output is reported in Figure 6.1. This service is crucial if we consider the next step of vine phenological models' integration.

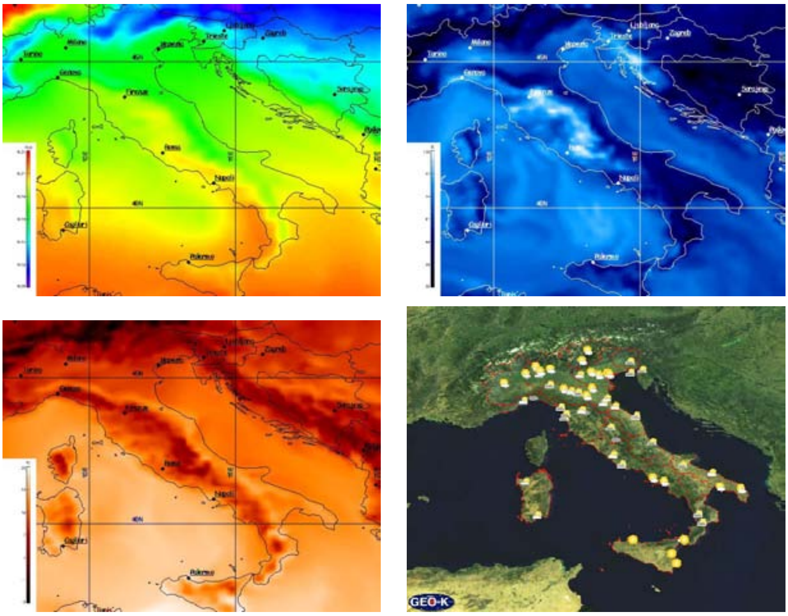

Figure 6.1: Output example for the Weather Forecast Tool: (Top Left) Pressure Map, (Top Right) Humidity Map, (Bottom Left) Temperature Map and (Bottom Right) Weather Map

6.1.4 Sensors' Network

Geovine allows the integration of a ground sensors' network. Nowadays, only one Meteo Station has been integrated, providing in-field conditions. The system is designed to be upgraded with other sensors of different types (e.g. On April 2008, for two weeks a network of 5 wireless sensors carrying on board instruments for incidence solar radiance measurements has been successfully deployed and tested). Actually, Sensors Network has been used to collect precise in-field weather condition during the SAR acquisitions (mainly for RADARSAT-2), but the aim of this block is to provide input data to biological models to deliver precise information about the parcels phenological status, probability of attack of bugs and agricultural practices timing. An example of the user interface for the Sensor Network is reported in Figure 6.2 . In Figure 6.3 the rain rate during the RADARSAT-2 acquisition on 15^{th} of September, 2008, is reported.

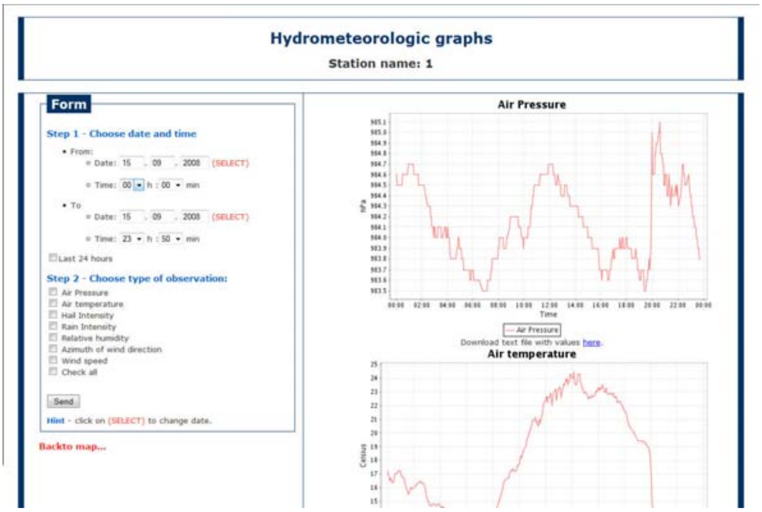

Hydrometeorologic graphs

Station name: 1

Form

Step 1 - Choose date and time

- From:
  - Date: 15 . 09 . 2008 (SELECT)
  - Time: 00 h : 00 min
- To
  - Date: 15 . 09 . 2008 (SELECT)
  - Time: 23 h : 50 min

☐ Last 24 hours

Step 2 - Choose type of observation:

☐ Air Pressure
☐ Air temperature
☐ Hail Intensity
☐ Rain Intensity
☐ Relative humidity
☐ Azimuth of wind direction
☐ Wind speed
☐ Check all

Hint - click on (SELECT) to change date.

Download text file with values here.

Figure 6.2: Sensors' Network User Interface

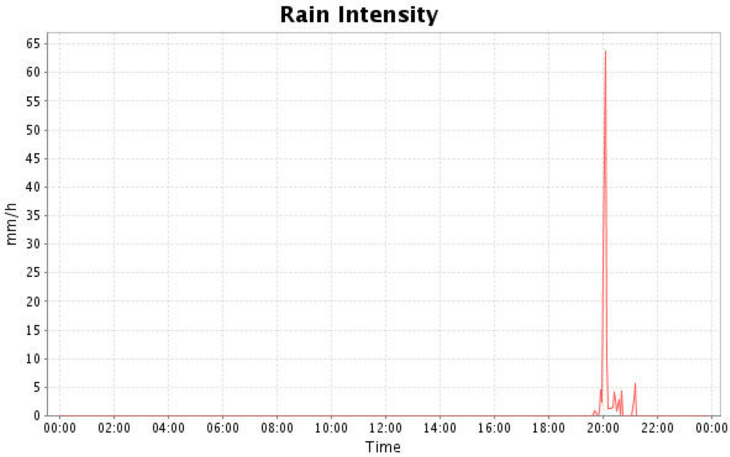

Figure 6.3: Rain Rate on the RADARSAT-2 survey, 15th of September, 2008

6.1.5 Geovine User Interface

The User Interface, designed to be friendly for a non skilled user, has got all the basic capabilities of a GIS viewer. The User Interface (Figure 6.4) is divided into three main section: the image area, the Toolbar and the StatusBar.

The **Image Area**, in the yellow box, displays all the data, vector or raster layer, overlaid according their geographic informations. By means of *Toobar*, in the light green box, the user can easily interact directly with information stored into the database, perform query, zoom, interact with the Sensors' Network and other standard tasks. The *Status Bar* shows all the geographic information of the Image Area and the instantaneous cursor position. By means of *Status Bar*, the user can interactively access the Weather Forecasting Service.

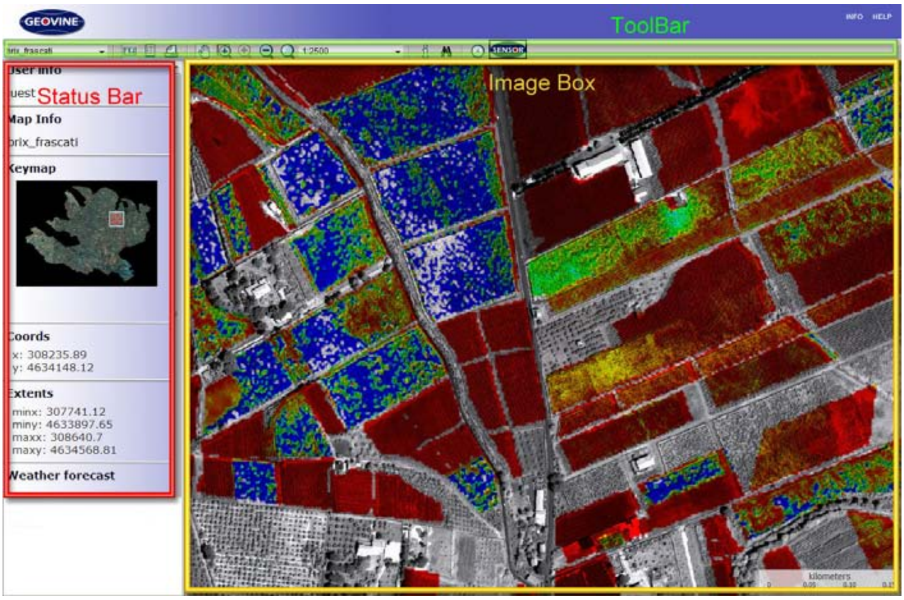

Jser info
uest

Map Info
rix_frascati

Keymap

Coords
x: 308235.89
y: 4634148.12

Extents
minx: 307741.12
miny: 4633897.65
maxx: 308640.7
maxy: 4634568.81

Weather forecast

Figure 6.4: Geovine User Interface

6.2 The Geovine Future

Nowadays, Geovine is in the initial phase of the precision farming start up process, with other important functionalities to be developed. A simple scheme about the full capabilities of this system is reported in Figure 6.5. We can summarize each functionality as follow:

- **Ground Truth Informations.** Cadastral Information are needed to properly identify each parcel and to have a clear reference about the real condition of the wine producing area. Moreover, some ground campaign are needed to properly calibrate the several satellite data and models involved into the precision farming process.

- **Multi-Spectral Processing.** As reported in Chapter 1 and in Chapter 3.3.2, it has been shown the capability of commercial space-borne sensors in providing value added information about the grapes'quality, Leaf Area Index or plants'vigor status, also at metric resolutions.

- **SAR Processing.** The sensitivity of backscattering to phenological and biomass variations has been proved; it is possible to imagine a scenario where radars are used to measure the grape biomass.

- **Hyper-Spectral Processing.** Hyper-Spectral sensors can provide informations on hydrological stress or wine variety, depending on their spatial resolution. Nowadays, space-borne hyper-spectral sensors cannot provide a real service for precision farming, but in a next future it will be possible to use their full capabilities (as reported in Chapter 1.4). The use of airborne sensors is not sustainable because of the complex economic and geographical context.

- **Biological Models.** The newest vine phenological models are based on temperature (Mariani et al., 2007) and incidence radiance measurements; a ground based sensors' network can provide real time data with high spatial resolution (Micro-Climate Analysis) and be used also as a reference for space-borne data calibration.

Nowadays, only *Ground Truth Informations* and *Multi-Spectral Processing* blocks are operational and available for a free use; *Biological Models* is in the development phase, dealing with the sensors' network, while at a study's phase from the biological models' point of view. The *SAR* and *Hyper-Spectral* blocks are in the R&D[1] phase, with promising performances and capabilities.

---

[1] Research and Development

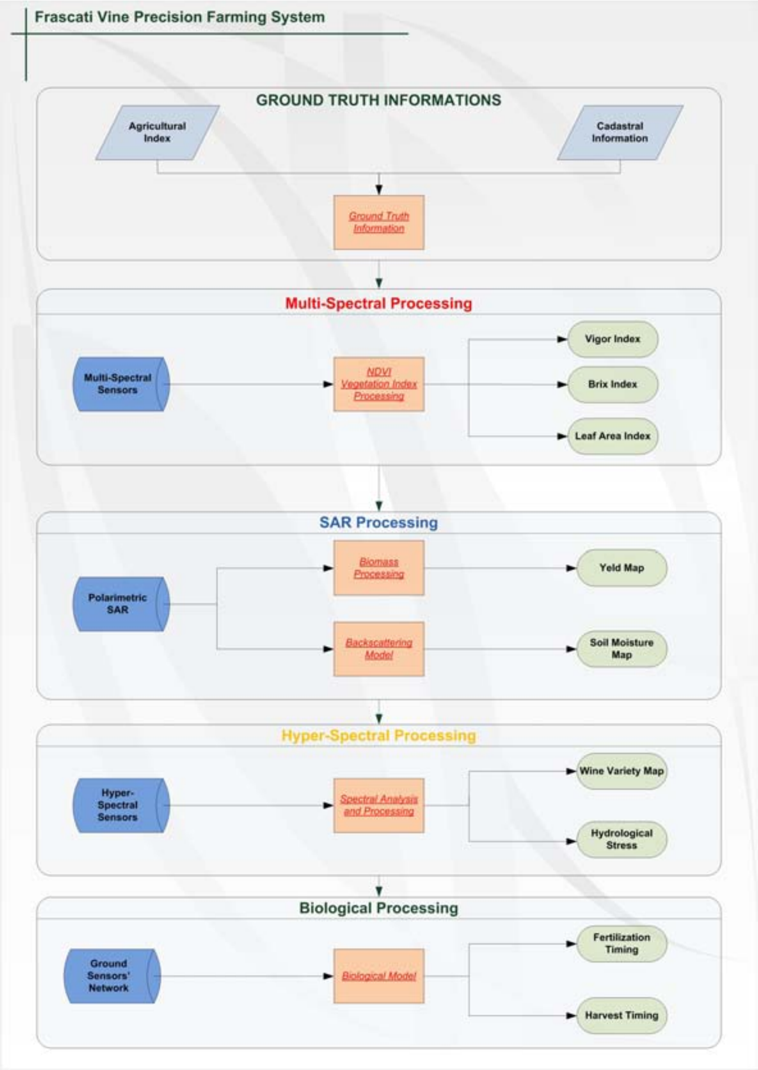

Figure 6.5: Block Diagram for the Frascati Vine Precision Farming System

Chapter 7

Conclusions

The use of SAR images as a support to vine precision farming has been examined from several points of view. Very-high resolution optical maps of the test area were used in combination with the radar ones for comparison, ground truth and synergistic measurements.

The mapping capability of metric-resolution images has been first examined. The agriculture-oriented 5-class pixel-based mapping capability of SAR has been evaluated: accuracy above 85% is attained by L-band polarimetric data at both low (25 degrees) and high (45 degrees) incidence angles. The accuracy is further enhanced when co- and cross-polar C-band data are added, especially for the higher incidence angle, at which the accuracy exceeds 90%. Both L- and C-band images show sensitivity to the geometry of the vineyard and discriminate between row and tent plantations. The orientation of the rows is also clearly identified, although the Bragg effect at L-band has been noted to yield some unexpected appearance of the periodic vine structure for given plantation geometry and observation direction. It is interesting to point out that SAR was able to discriminate between adjacent parcels, one with stable and productive vines, the other with young unproductive vines, that were not distinguished by optical data.

The use of SAR for characterizing some relevant bio-physical features of vines has then been considered. In particular, the correlation of backscattering with the Vigor Index has been analyzed at the different frequencies and incidence angles. L-band appears more sensitive to VI than C-band. An exercise has been carried out to retrieve VI from the ratio of cross-polar to co-polar backscattering. To this end, ground truth measurements have trained a Neural Network algorithm for inverting the radar data. The VI retrieved values compare well with those from the optical data, estimated by the technique proposed in a previous experiment on vineyards. As expected, the spread of retrieved values was observed to decrease with the increasing number of looks, i.e., with degrading spatial resolution, due to the effect of speckle.

The study on the sensitivity of backscattering to the grape biomass is the core topic of this project, It has been extensively developed in three experiments with different sensors, following a previous approach utilizing ERS data.

The analysis of E-SAR measurements hint at some sensitivity of L-band backscattering to grape biomass per unit area, but the short time series (only two acquisitions, with the first one corrupted by rain) does not allow to demonstrate a manifest dependence of backscattering to the variation of grape biomass, in spite of the rather sophisticated processing trying to exploit the pieces of information contained in fully polarimetric measurements. Indeed, a number of rain disturbing effects were detrimental to the result, including water pools, and films and drops on weed, vine wooden parts and leaves, and on supporting structures.

Also the ALOS PALSAR series of images was inadequate, given the limitations in acquisitions over the Frascati test site. The full polarimetric mode was active only in May, when cultivation practices deeply modify the soil roughness, weed wildly grows and grapes are not developed. Together with the other few available acquisitions, the time series allows a quite limited confidence in the sensitivity to grape mass.

On the contrary, the acquisitions by RADARSAT-2 within a Canadian Space Agency Science and Operational Applications Research (SOAR) Program project covered the most significant period of time, with data of good quality and timely delivered. The fully polarimetric nature of the images and the short revisit time interval add value to this excellent set of data.

The analysis of the ratio between cross-polar and co-polar backscattering coefficient for different vineyards appears to demonstrate the sensitivity of C-band radar to the grape mass. Given the complicated structure of the vineyard and the further hindrance by the changing climatic conditions, the interpretation of the observed time trend is not straightforward. The proposed explanation is based on the idea that the grapes attenuate the co-polar scattering contributions from the soil surface and the larger fixed structures, like poles and stalks. The cross-polar scattering of the twigs and leaves is mainly contributed by the higher parts of the plants and suffers less or no attenuation by the grapes. Hence, when the attenuating grapes are harvested, the co-polar scattering increases relatively to the cross-polar one and a peculiar signal is observed in the time series. This interpretation is supported by the quite different trend which is contemporarily observed in the backscattering from other kinds of surfaces, like forest, grass and bare soil.

This experiment seems to have demonstrated for the first time the sensitivity of radar to grape biomass, thus opening the road towards monitoring the potential quantity of wine from space.

Annex: Polarimetric Analysis of Vineyards

The analyzed parcels are listed below:

1. North-South Row Vineyard - Santini 1 - Figure 7.1 and 7.2
2. North-South Row Vineyard - Gotto d'Oro 1 - Figure 7.3 and 7.4
3. North-South Row Vineyards - Gotto d'Oro 2 - Figure 7.5 and 7.6
4. East-West Row Vineyard - Santini 4 - Figure 7.7 and 7.8
5. East-West Row Vineyard - Gotto d'Oro 3 - Figure 7.9 and 7.10
6. East-West Row Vineyard - Santini 2 - Figure 7.11 and 7.12
7. Tent Vineyards - Gotto d'Oro Tendone - Figure 7.13 and7.14
8. Tent Vineyard - Pietra Porzia 1 - Figure 7.15 and7.16
9. Tent Vineyard - Pietra Porzia 2 - Figure 7.17 and 7.18

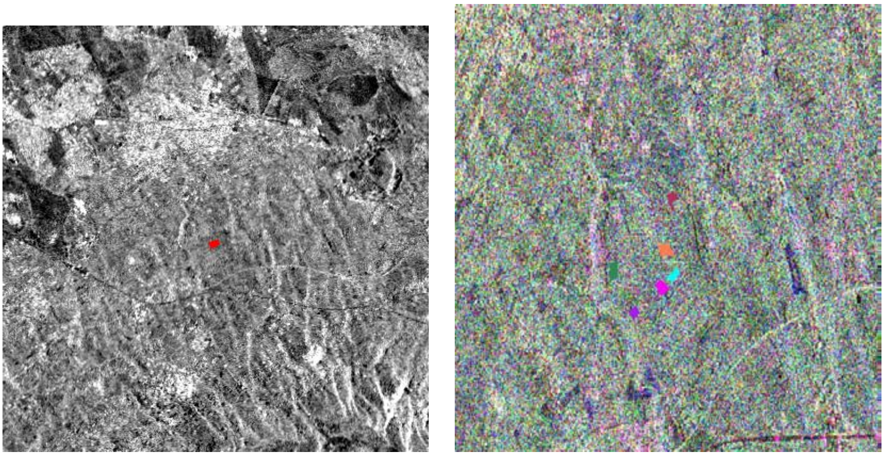

Ground Range Image

Pauli Decomposition

08.09.08

02.10.08

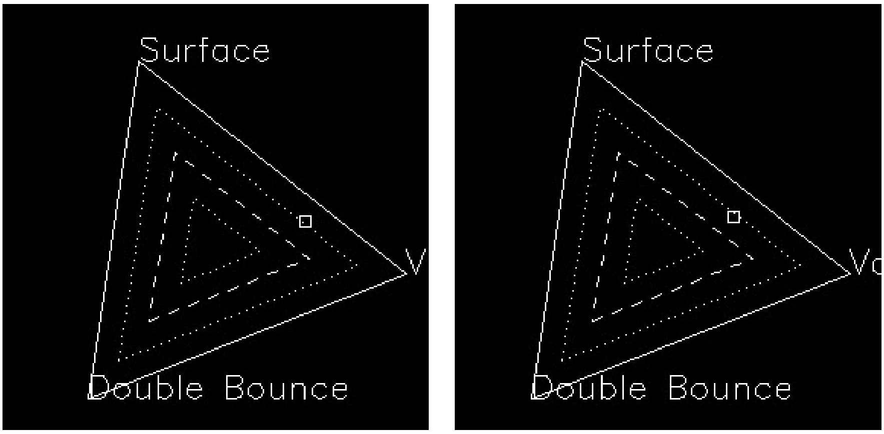

Scattering Mechanism

Scattering Mechanism

Figure 7.1: North-South Row Vineyard - Santini 1.Scattering Mechanism

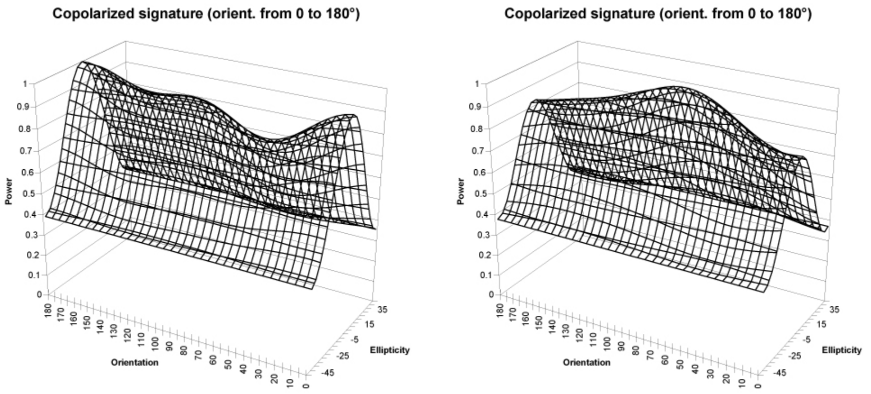

Copolarized signature (orient. from 0 to 180°)

Copolarized signature (orient. from 0 to 180°)

Copolarized Signature Copolarized Signature

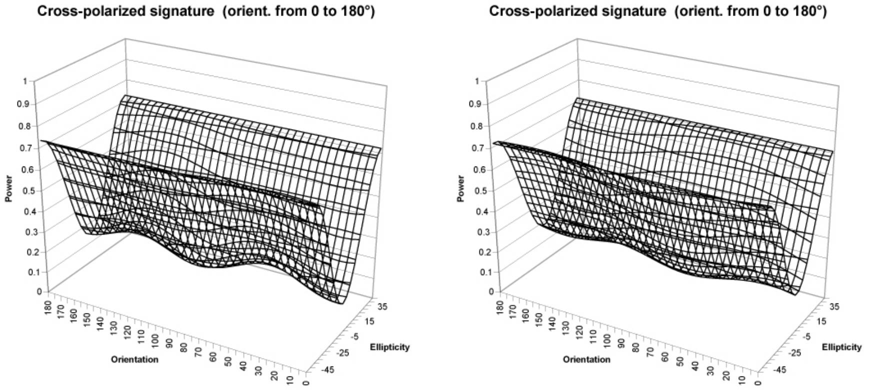

Cross-polarized signature (orient. from 0 to 180°)

Cross-polarized signature (orient. from 0 to 180°)

Cross Polarized Signature Cross Polarized Signature

Figure 7.2: North-South Row Vineyard - Santini 1. Polarimetric Signature

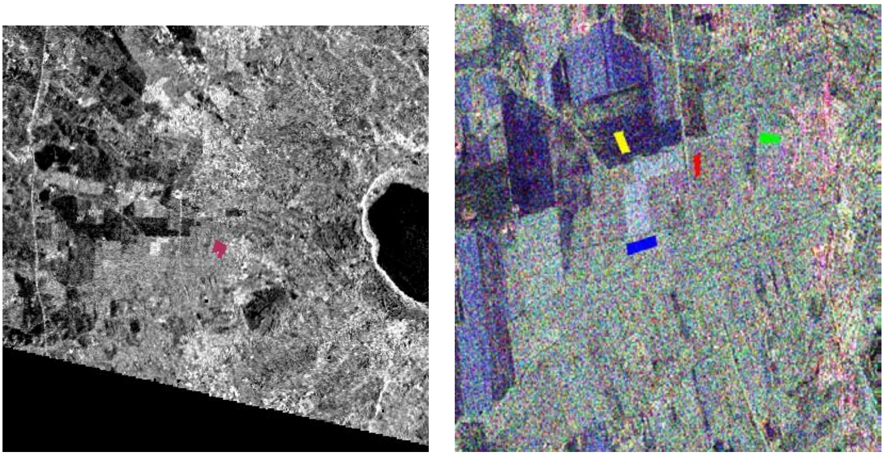

Ground Range Image

Pauli Decomposition

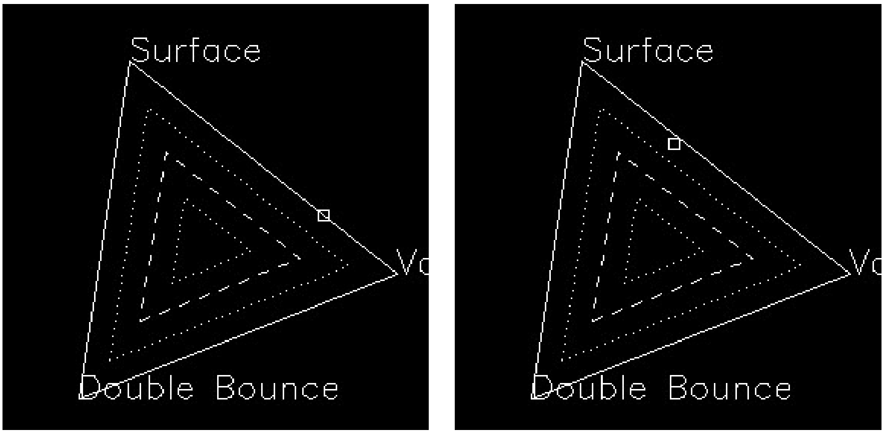

08.09.08

02.10.08

Scattering Mechanism

Scattering Mechanism

Figure 7.3: North-South Row Vineyard - Gotto d'Oro 1. Scattering Mechanism

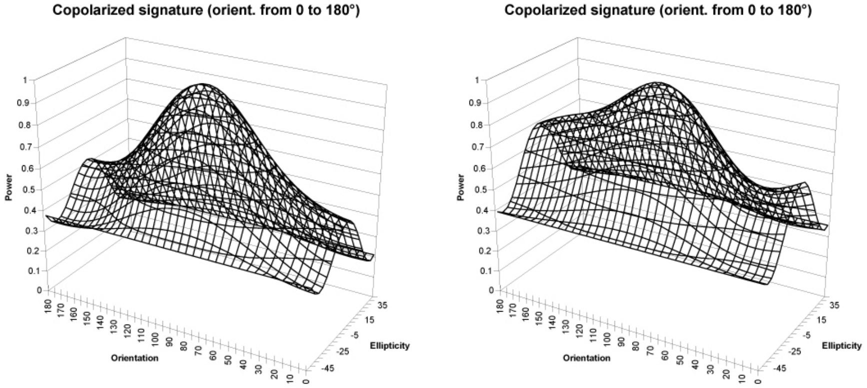

Copolarized Signature Copolarized Signature

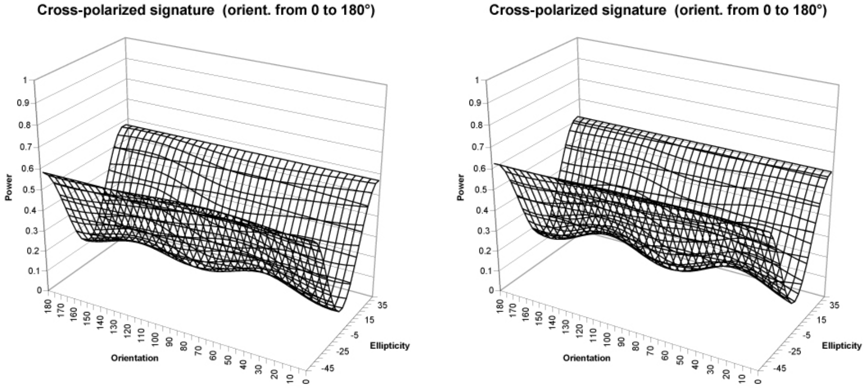

Cross Polarized Signature Cross Polarized Signature

Figure 7.4: North-South Row Vineyard - Gotto d'Oro 1. Polarimetric Signature

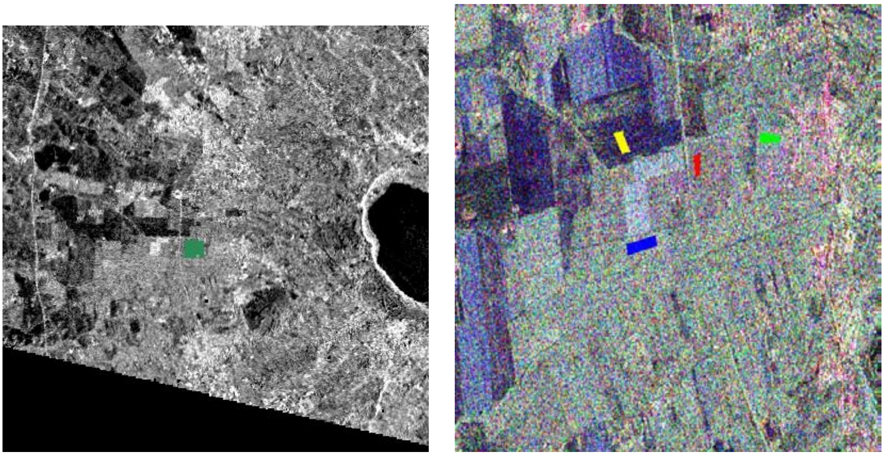

Ground Range Image

Pauli Decomposition

08.09.08

02.10.08

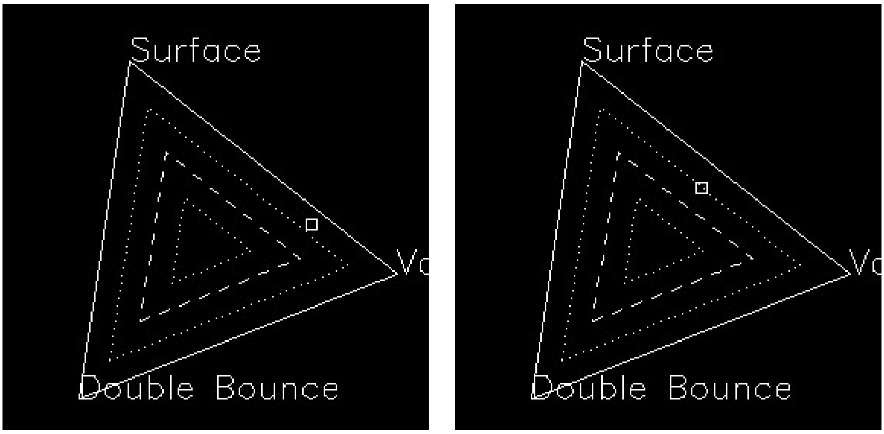

Scattering Mechanism

Scattering Mechanism

Figure 7.5: North-South Row Vineyard - Gotto d'Oro 2. Scattering Mechanism

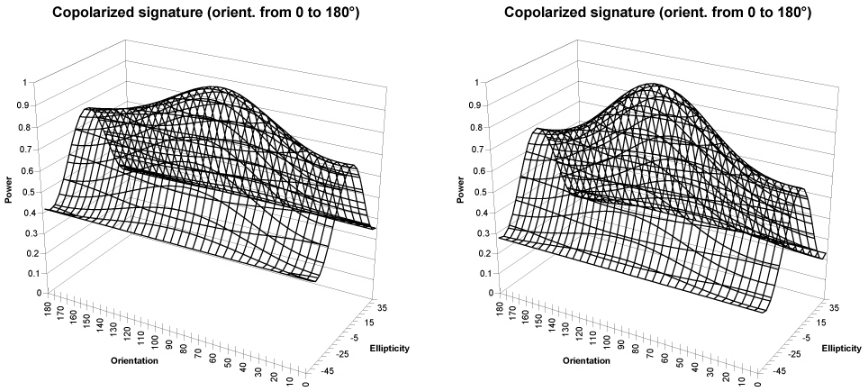
Copolarized signature (orient. from 0 to 180°)

Copolarized signature (orient. from 0 to 180°)

Copolarized Signature Copolarized Signature

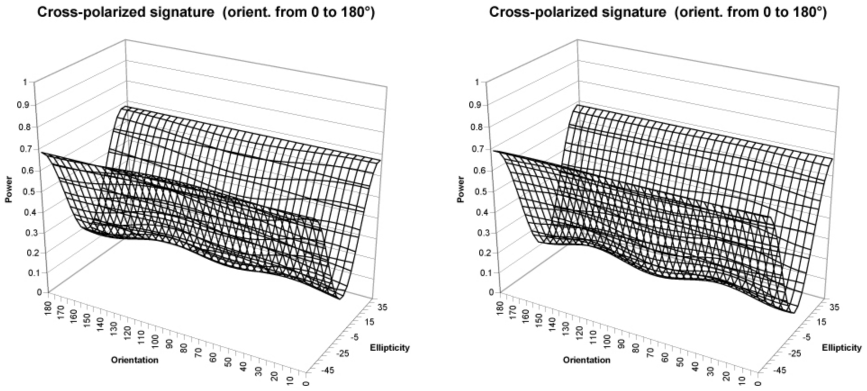
Cross-polarized signature (orient. from 0 to 180°)

Cross-polarized signature (orient. from 0 to 180°)

Cross Polarized Signature Cross Polarized Signature

Figure 7.6: North-South Row Vineyard - Gotto d'Oro 2. Polarimetric Signature

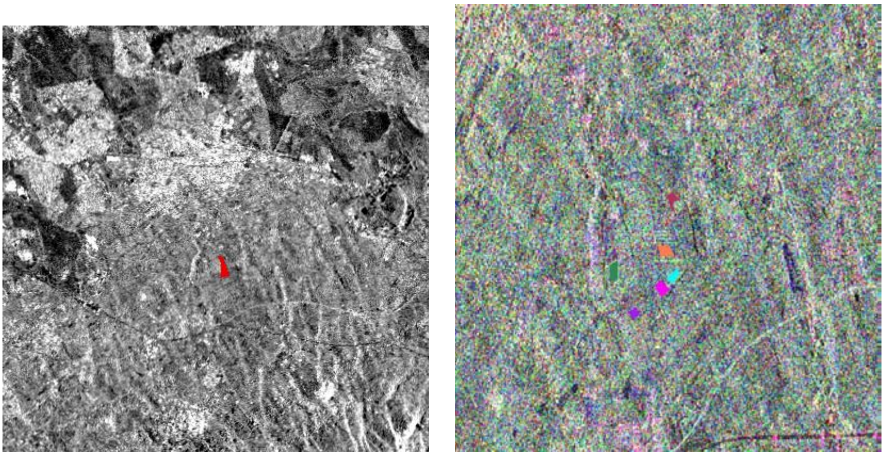

Ground Range Image

Pauli Decomposition

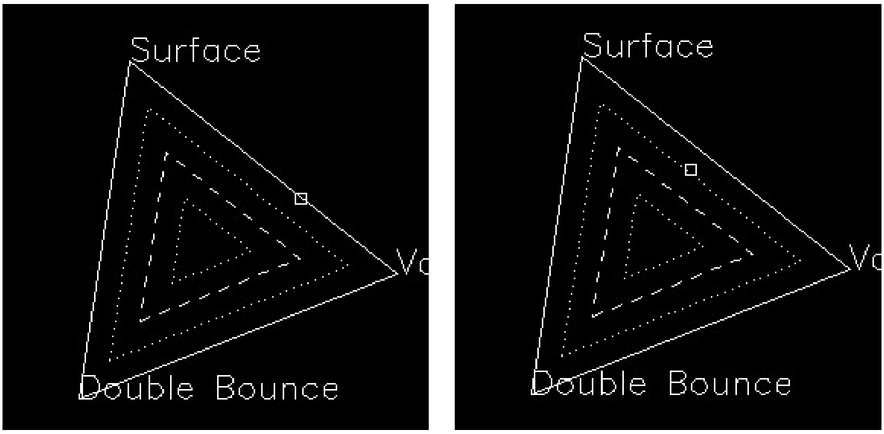

08.09.08

02.10.08

Scattering Mechanism

Scattering Mechanism

Figure 7.7: East-West Row Vineyard - Santini 4. Scattering Mechanism

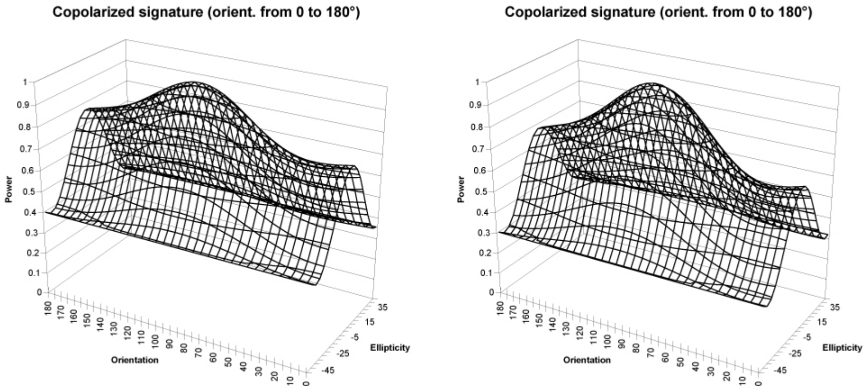

Copolarized Signature Copolarized Signature

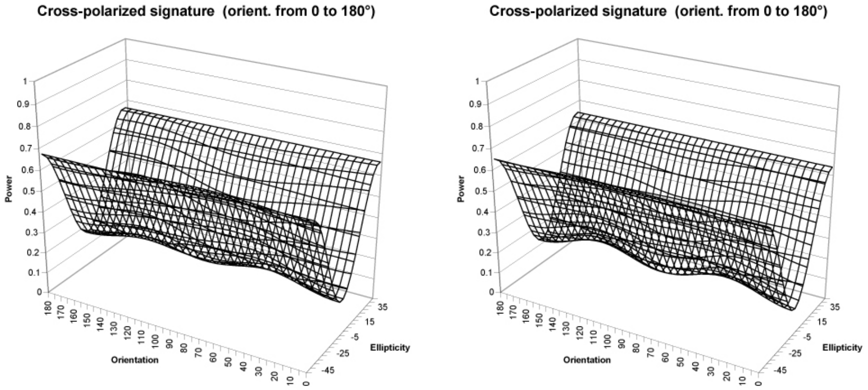

Cross Polarized Signature Cross Polarized Signature

Figure 7.8: East-West Row Vineyard - Santini 4. Polarimetric Signature

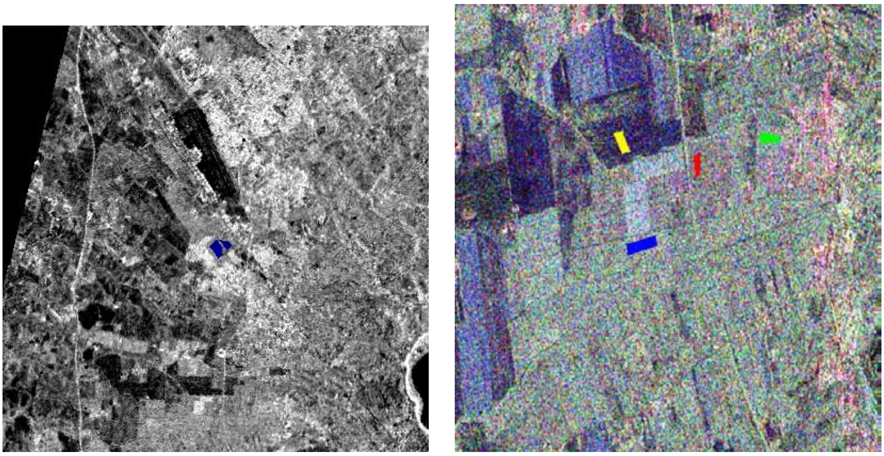

Ground Range Image　　Pauli Decomposition

08.09.08　　02.10.08

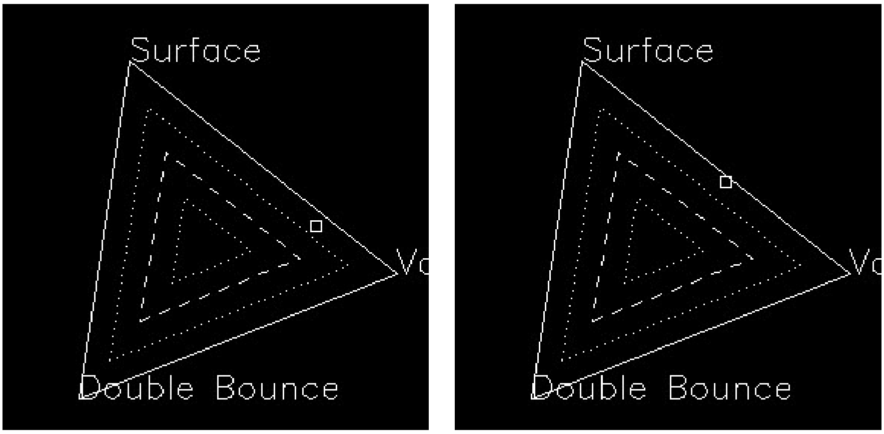

Scattering Mechanism　　Scattering Mechanism

Figure 7.9: East-West Row Vineyard - Gotto d'Oro 3. Scattering Mechanism

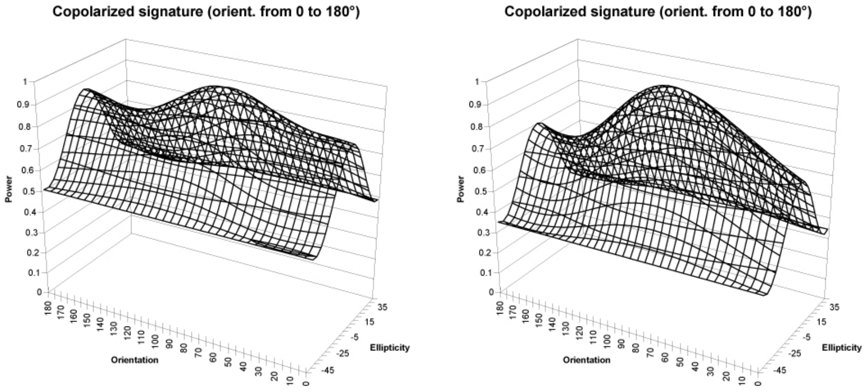

Copolarized Signature Copolarized Signature

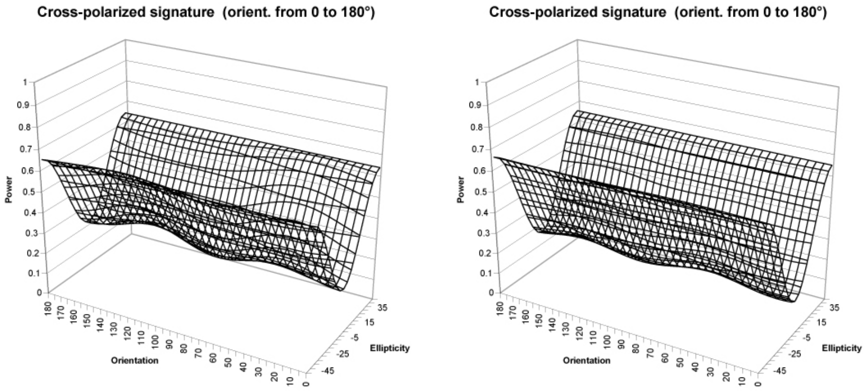

Cross Polarized Signature Cross Polarized Signature

Figure 7.10: East-West Row Vineyard - Gotto d'oro 3. Polarimetric Signature

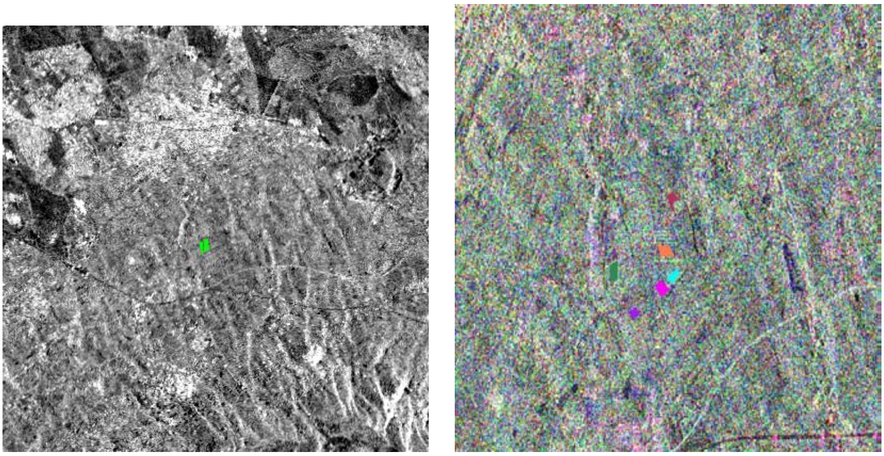

Ground Range Image

Pauli Decomposition

08.09.08

02.10.08

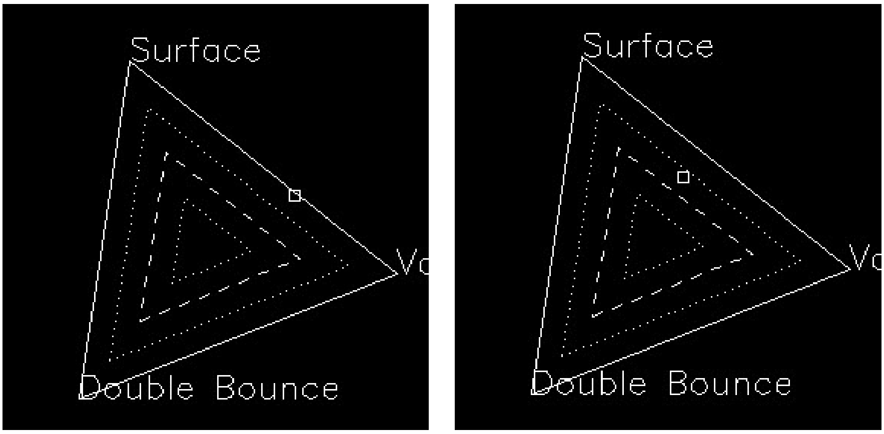

Scattering Mechanism

Scattering Mechanism

Figure 7.11: East-West Row Vineyard - Santini 2. Scattering Mechanism

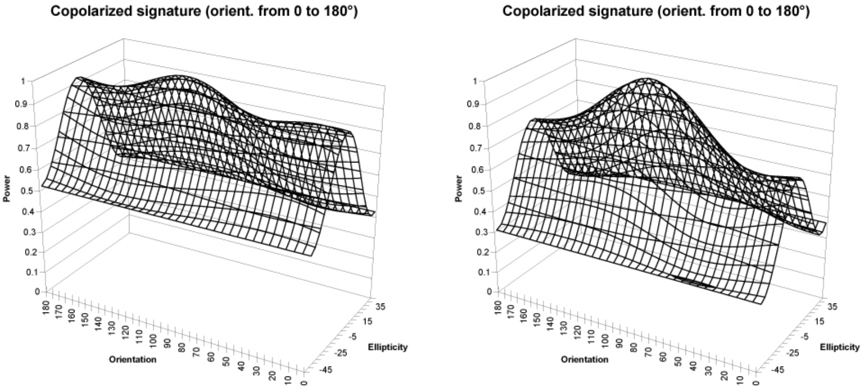

Copolarized Signature Copolarized Signature

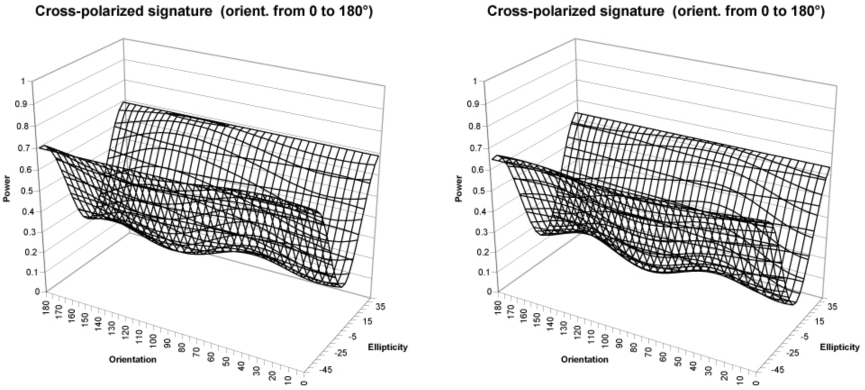

Cross Polarized Signature Cross Polarized Signature

Figure 7.12: East-West Row Vineyard - Santini 2. Polarimetric Signature

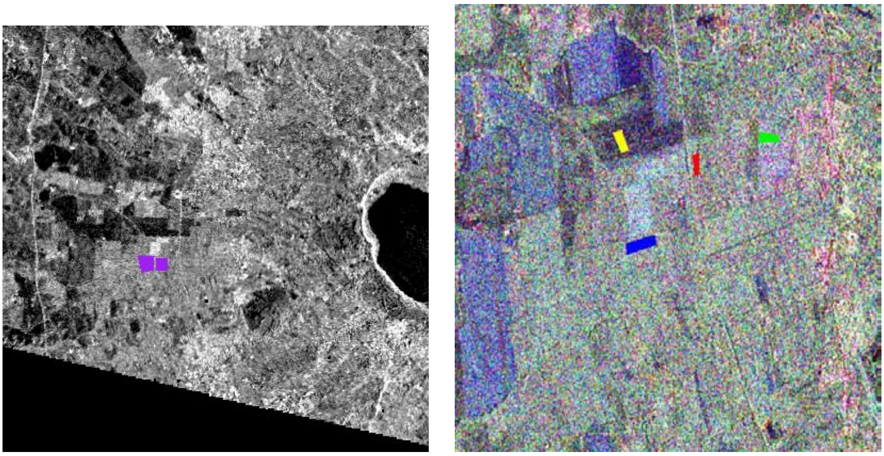

Ground Range Image

Pauli Decomposition

08.09.08

02.10.08

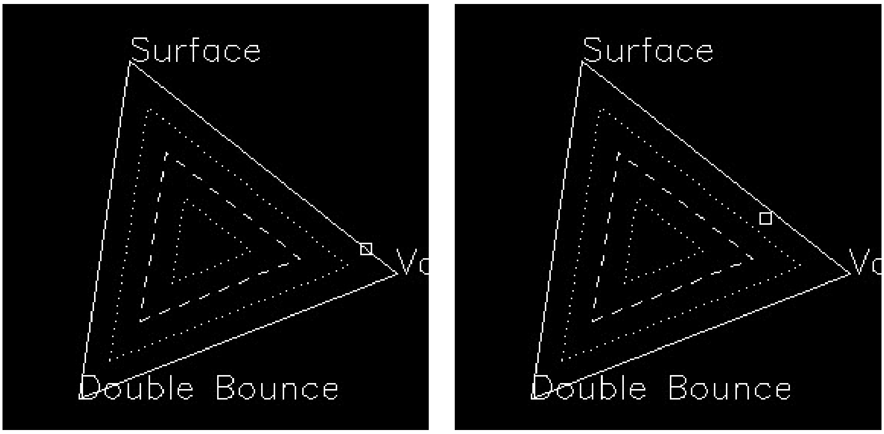

Scattering Mechanism

Scattering Mechanism

Figure 7.13: Tent Vineyard - Gotto d'Oro Tendone. Scattering Mechanism

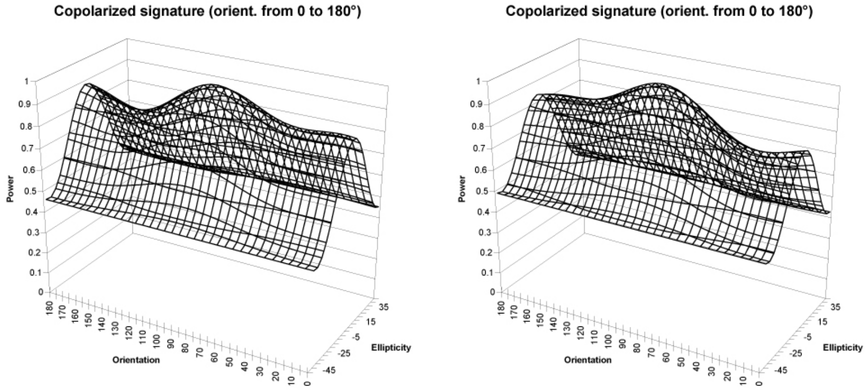

Copolarized Signature Copolarized Signature

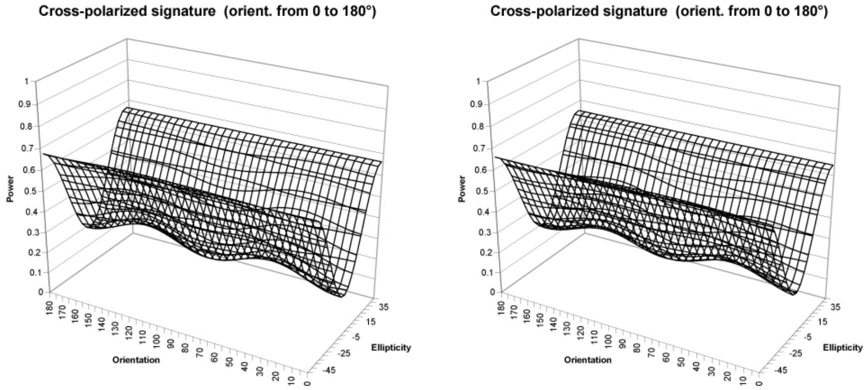

Cross Polarized Signature Cross Polarized Signature

Figure 7.14: Tent Vineyard - Gotto d'Oro Tendone. Polarimetric Signature

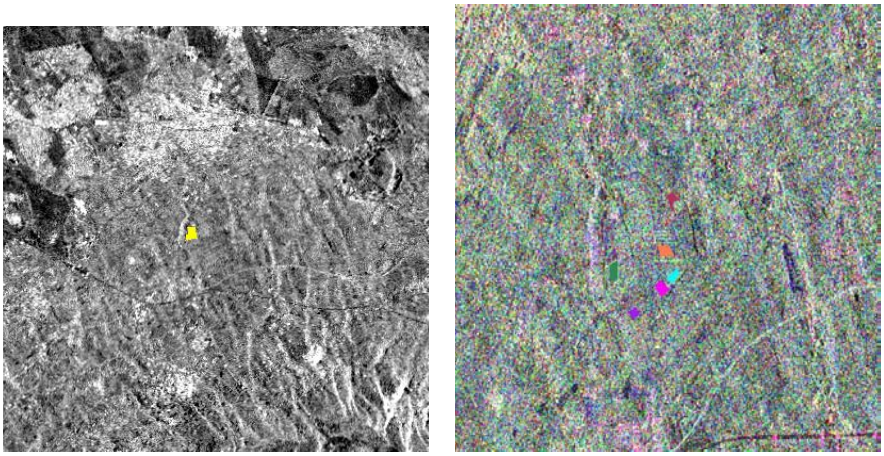

Ground Range Image Pauli Decomposition

08.09.08 02.10.08

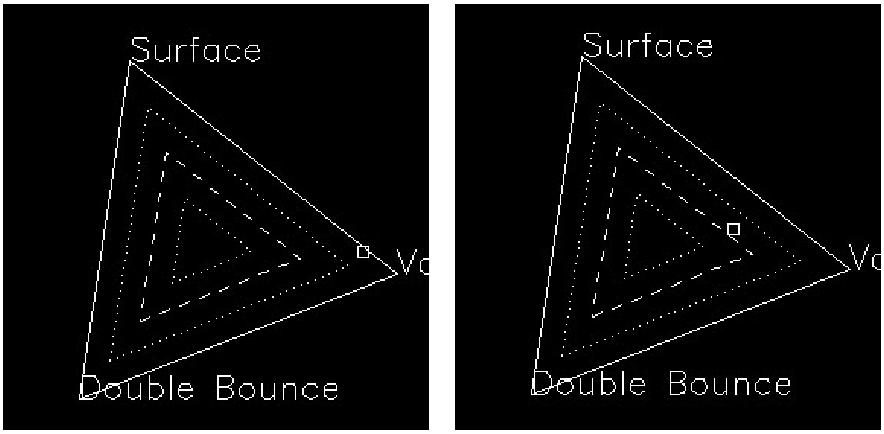

Scattering Mechanism Scattering Mechanism

Figure 7.15: Tent Vineyard - Pietra Porzia 1. Scattering Mechanism

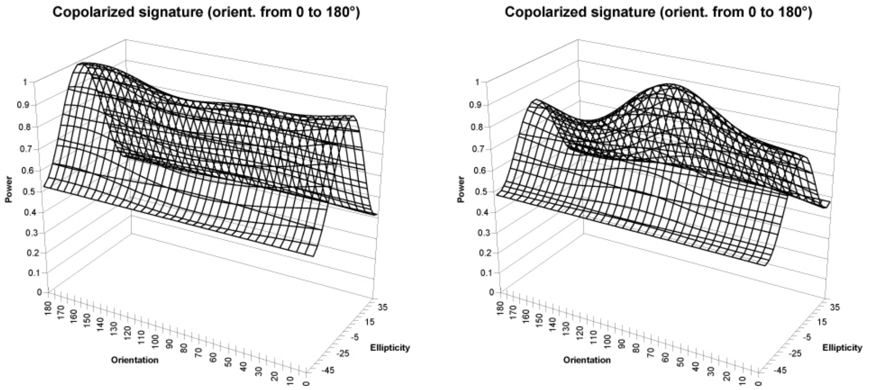

Copolarized Signature Copolarized Signature

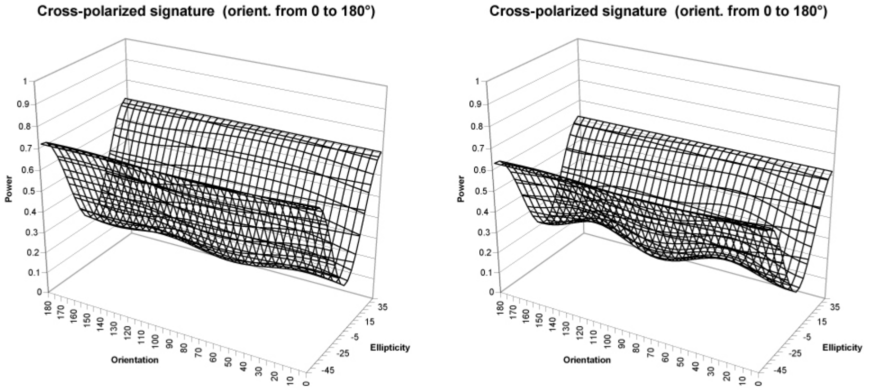

Cross Polarized Signature Cross Polarized Signature

Figure 7.16: Tent Vineyard - Pietra Porzia 1. Polarimetric Signature

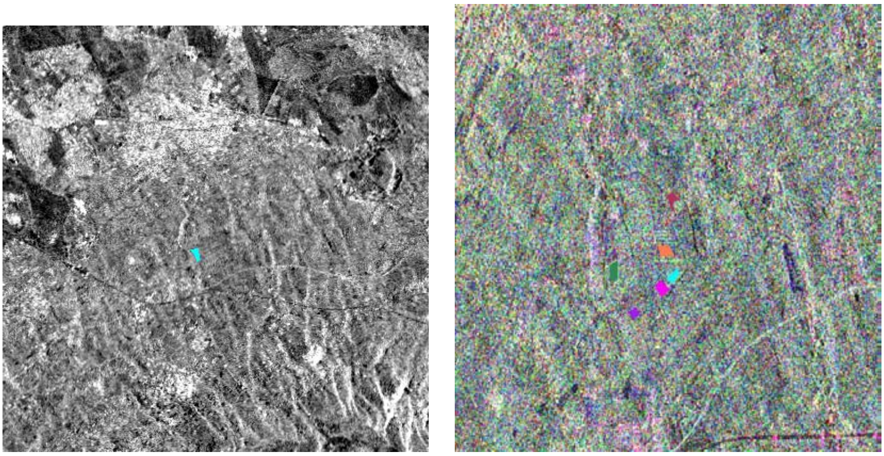

Ground Range Image Pauli Decomposition

08.09.08 02.10.08

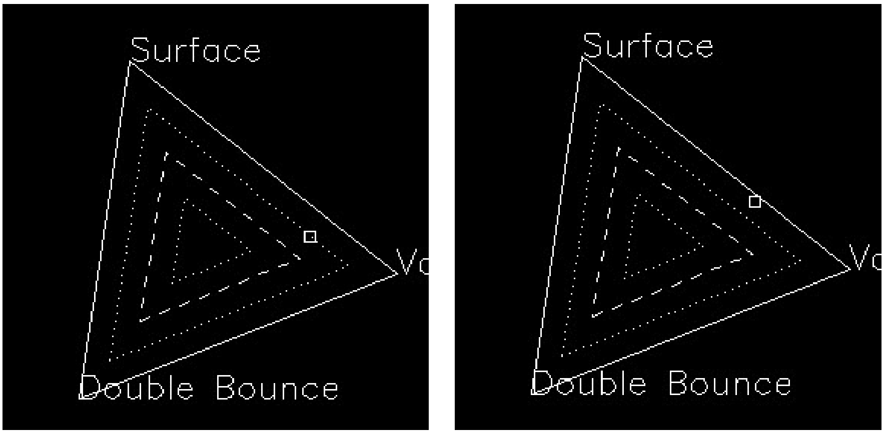

Scattering Mechanism Scattering Mechanism

Figure 7.17: Tent Vineyard - Pietra Porzia 2. Scattering Mechanism

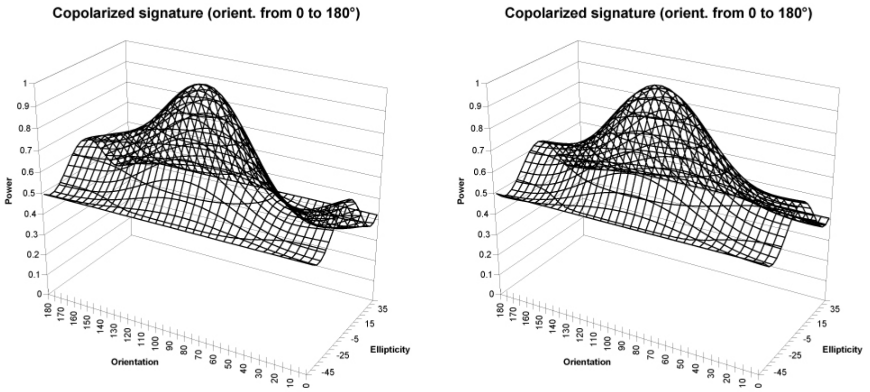

Copolarized signature (orient. from 0 to 180°)

Copolarized signature (orient. from 0 to 180°)

Copolarized Signature Copolarized Signature

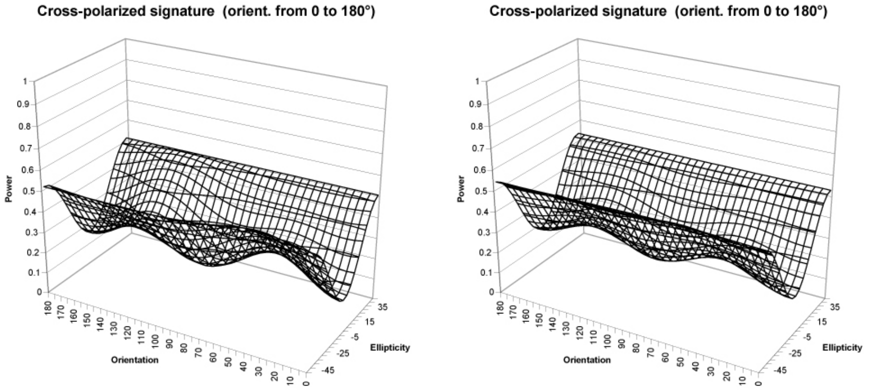

Cross-polarized signature (orient. from 0 to 180°)

Cross-polarized signature (orient. from 0 to 180°)

Cross Polarized Signature Cross Polarized Signature

Figure 7.18: Tent Vineyard - Pietra Porzia 2. Polarimetric Signature

Annex: Polarimetric Analysis of Forest

The analyzed parcels are listed below:

1. Forest 1 - Figure 7.19 and 7.20
2. Forest 2 - Figure 7.21 and 7.22

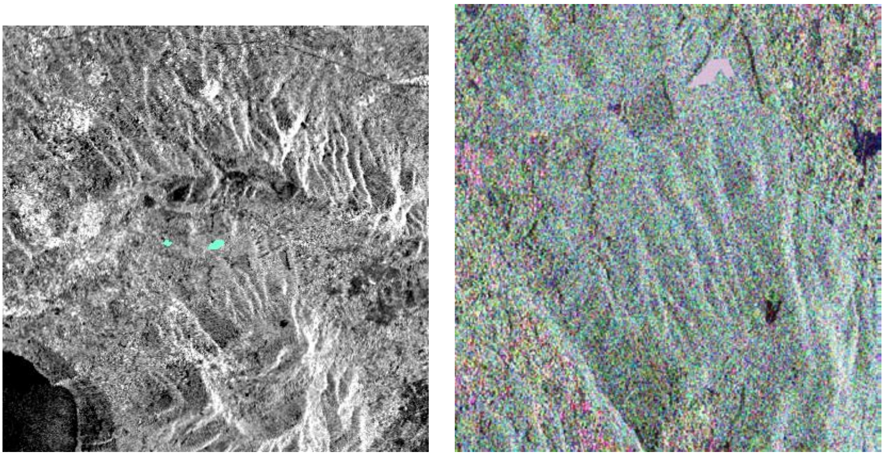

Ground Range Image

Pauli Decomposition

08.09.08

02.10.08

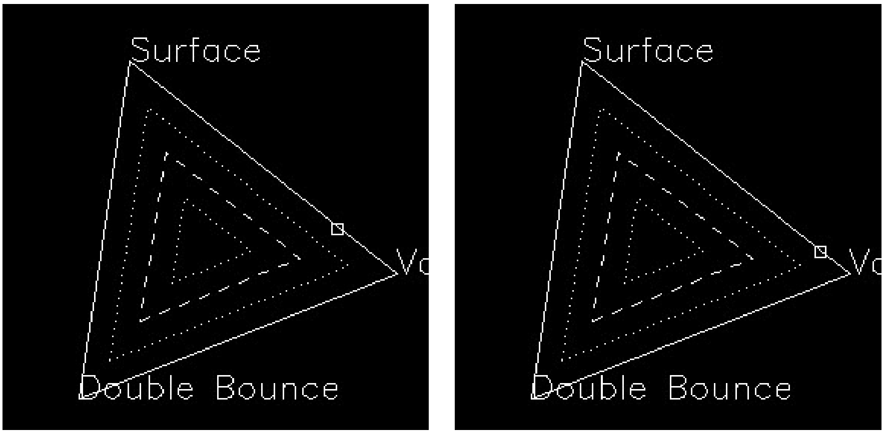

Scattering Mechanism

Scattering Mechanism

Figure 7.19: Forest 1.Scattering Mechanism

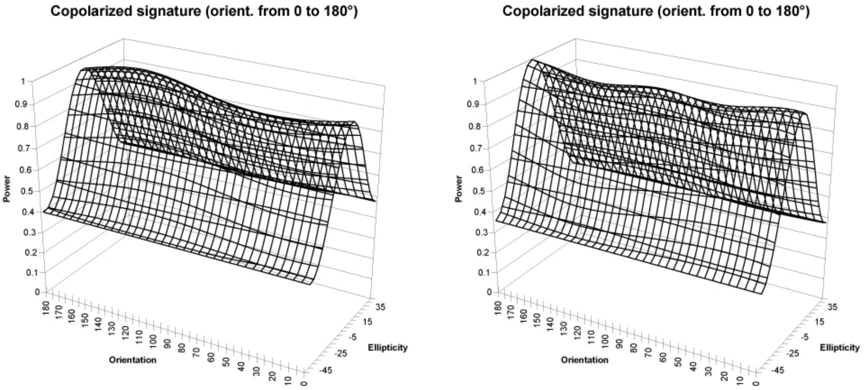

Copolarized Signature Copolarized Signature

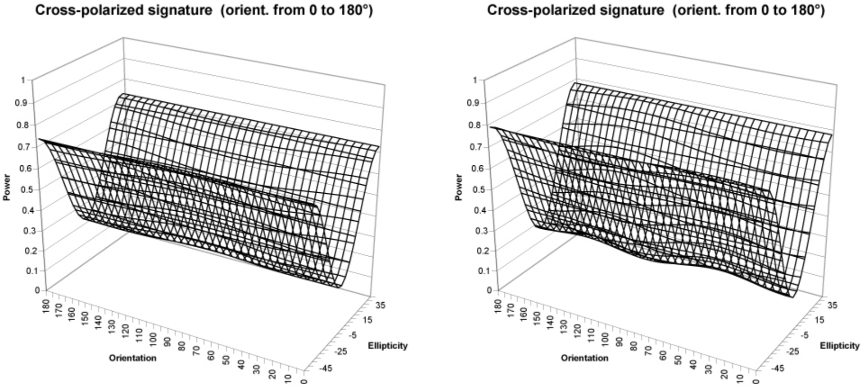

Cross Polarized Signature Cross Polarized Signature

Figure 7.20: Forest 1. Polarimetric Signature

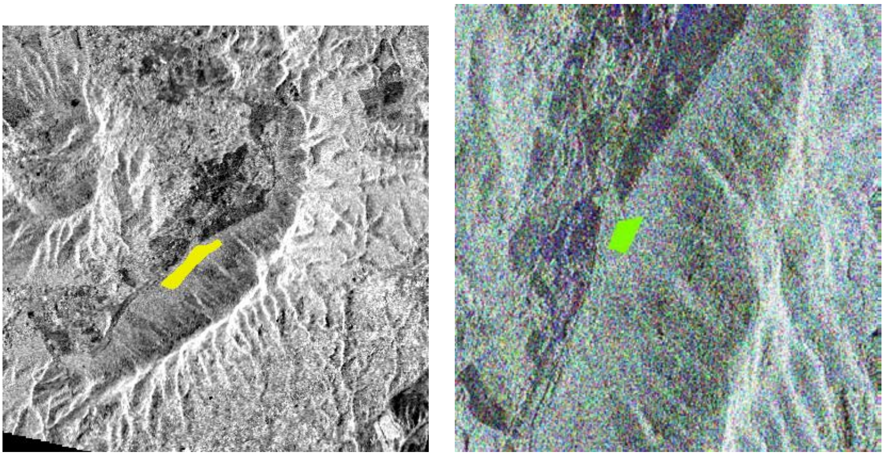

Ground Range Image Pauli Decomposition

08.09.08 02.10.08

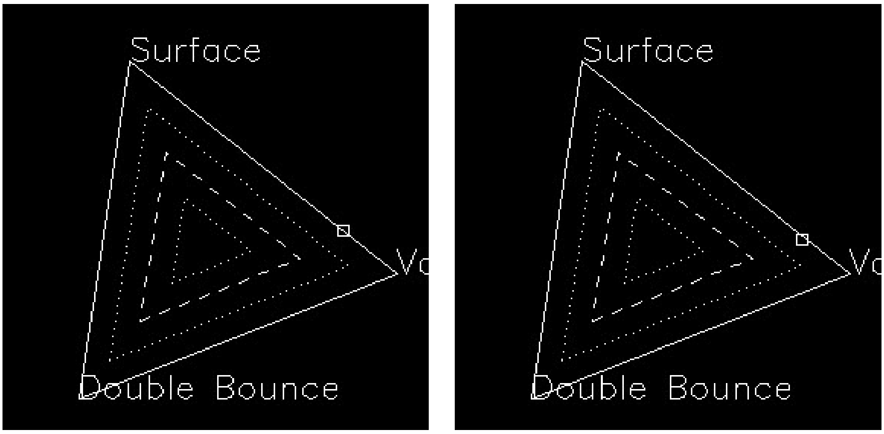

Scattering Mechanism Scattering Mechanism

Figure 7.21: Forest 2.Scattering Mechanism

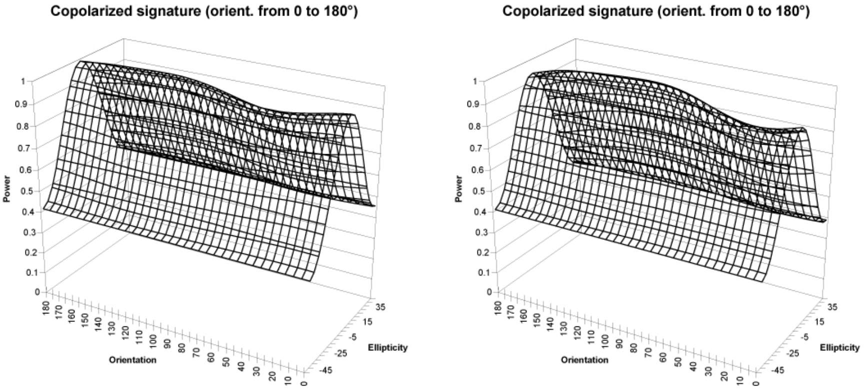

Copolarized Signature Copolarized Signature

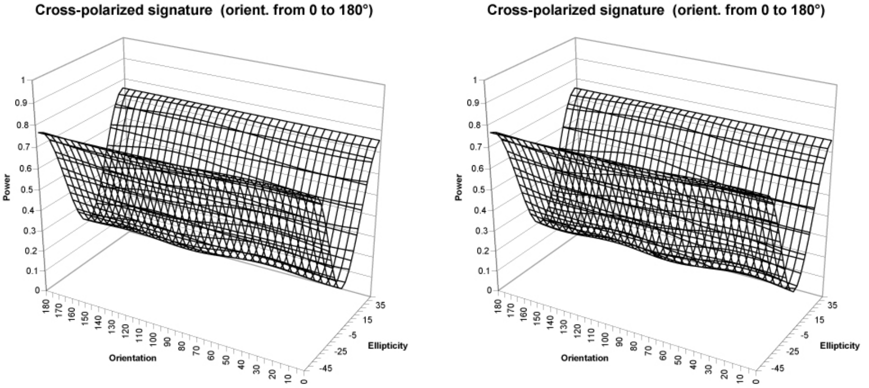

Cross Polarized Signature Cross Polarized Signature

Figure 7.22: Forest 2. Polarimetric Signature

Annex: Polarimetric Analysis of Bare Soil

The analyzed parcel are listed below:

1. Bare Soil - Capannelle - Figure 7.23 and 7.24
2. Bare Soil - Gotto d'Oro - Figure 7.25 and 7.26

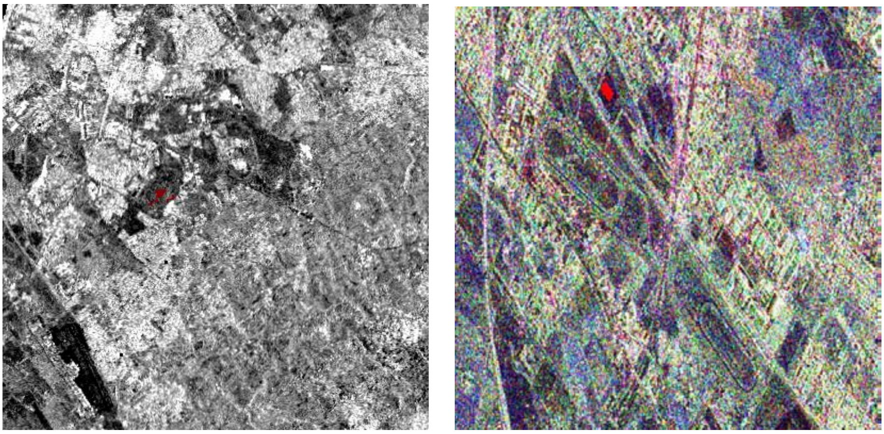

Ground Range Image

Pauli Decomposition

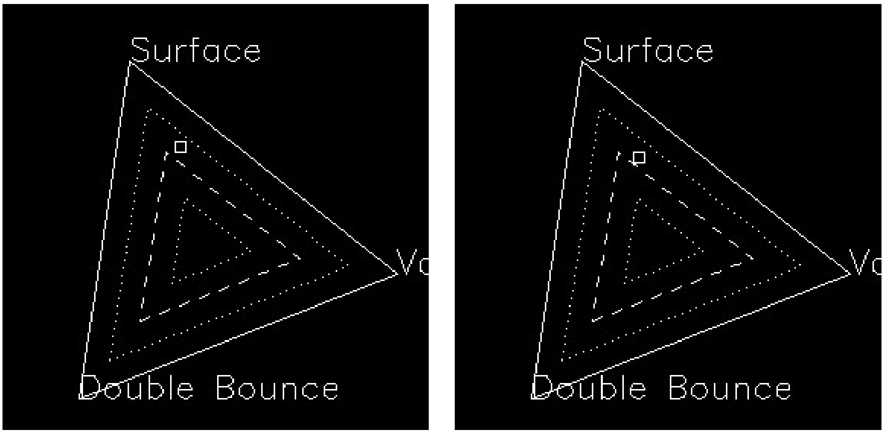

08.09.08

02.10.08

Scattering Mechanism

Scattering Mechanism

Figure 7.23: Bare Soil - Capannelle. Scattering Mechanism

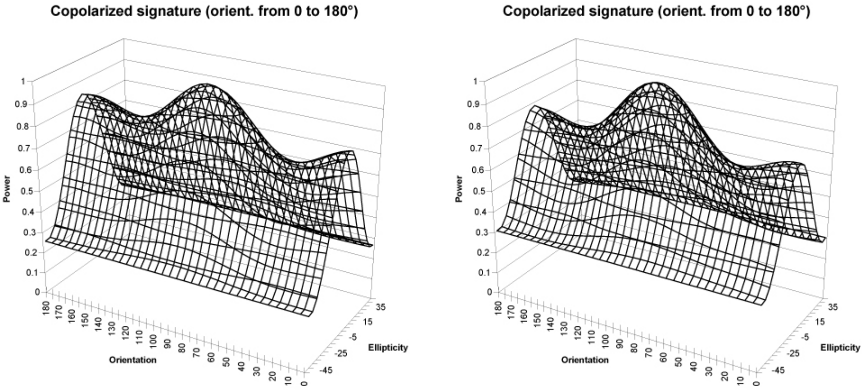

Copolarized Signature Copolarized Signature

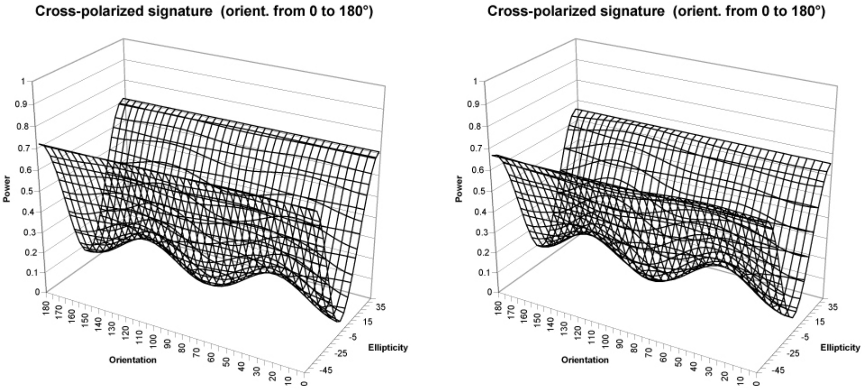

Cross Polarized Signature Cross Polarized Signature

Figure 7.24: Bare Soil - Capannelle. Polarimetric Signature

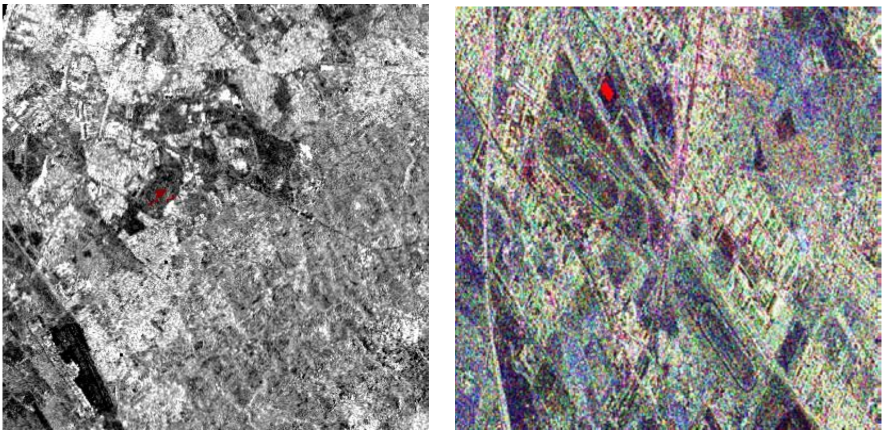

Ground Range Image Pauli Decomposition

08.09.08 02.10.08

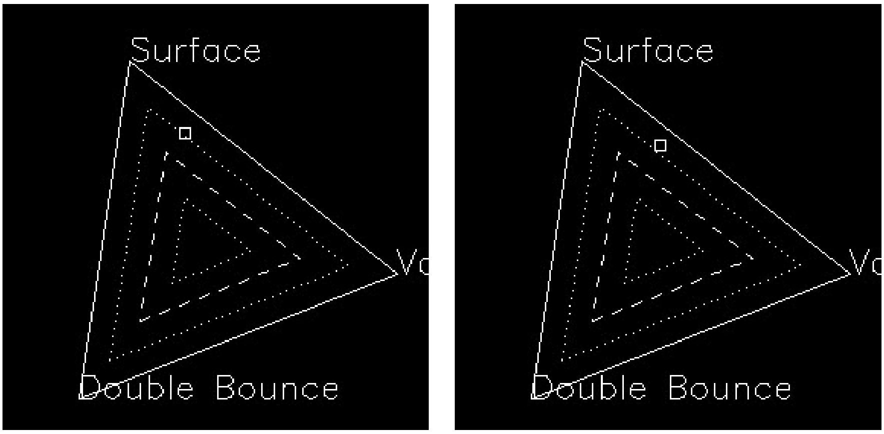

Scattering Mechanism Scattering Mechanism

Figure 7.25: Bare Soil - Gotto d'Oro. Scattering Mechanism

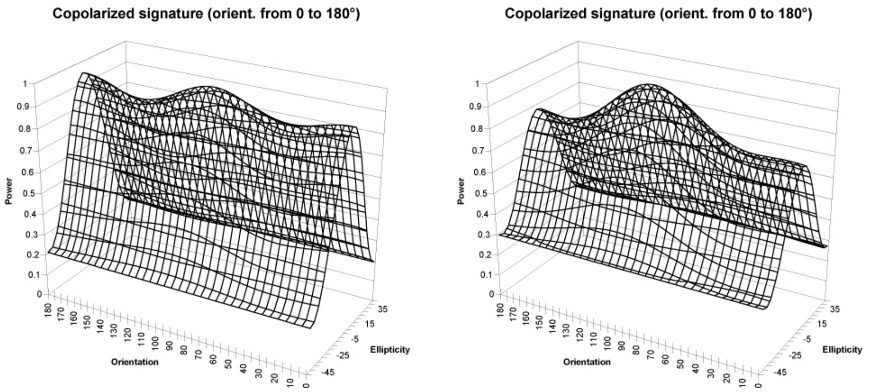

Copolarized signature (orient. from 0 to 180°)

Copolarized signature (orient. from 0 to 180°)

Copolarized Signature

Copolarized Signature

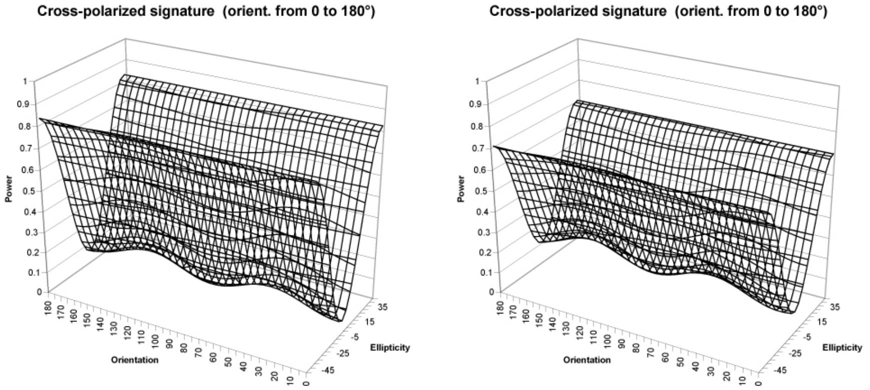

Cross-polarized signature (orient. from 0 to 180°)

Cross-polarized signature (orient. from 0 to 180°)

Cross Polarized Signature

Cross Polarized Signature

Figure 7.26: Bare Soil - Gotto d'Oro. Polarimetric Signature

Annex: Polarimetric Analysis of Grassland

The analyzed parcels are listed below:

1. Grassland - Tor Vergata - Figure 7.27 and 7.28
2. Grassland - Ciampino Zone - Figure 7.29 and 7.30

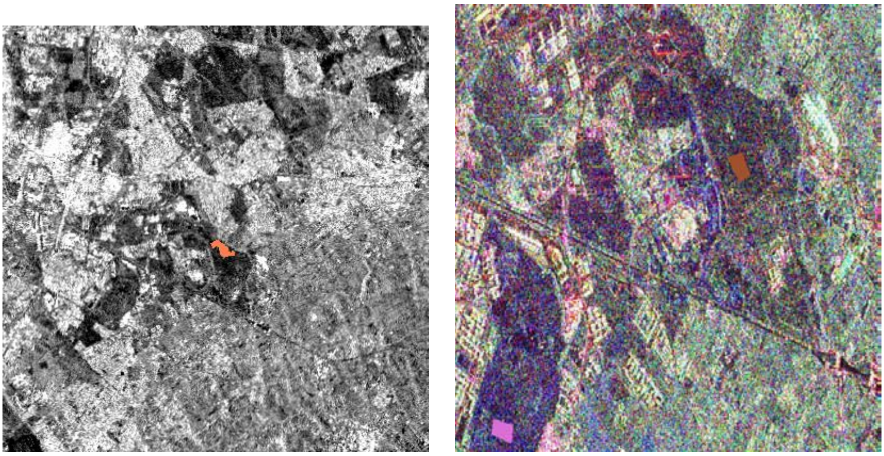

Ground Range Image

Pauli Decomposition

08.09.08

02.10.08

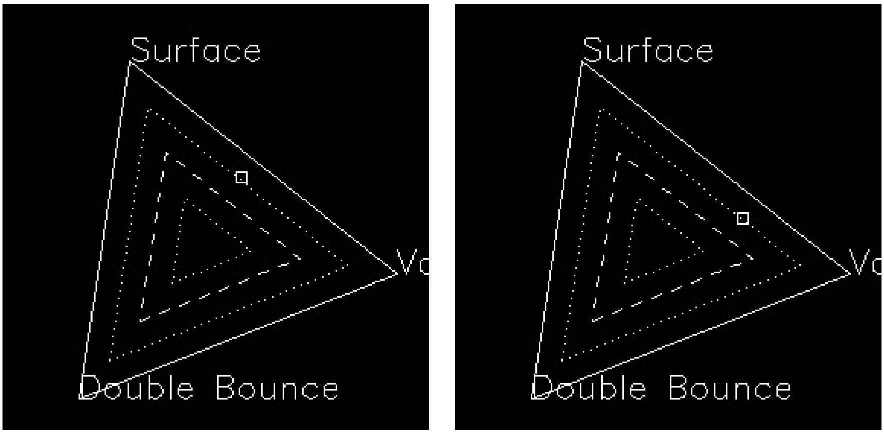

Scattering Mechanism

Scattering Mechanism

Figure 7.27: Grassland - Tor Vergata. Scattering Mechanism

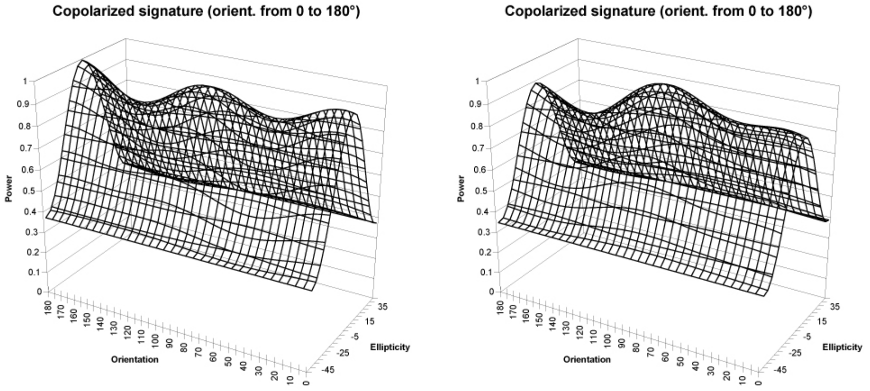

Copolarized Signature Copolarized Signature

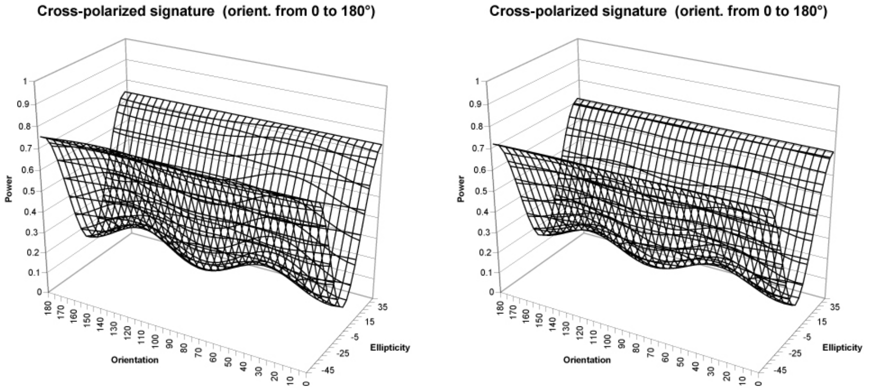

Cross Polarized Signature Cross Polarized Signature

Figure 7.28: Grassland - Tor Vergata. Polarimetric Signature

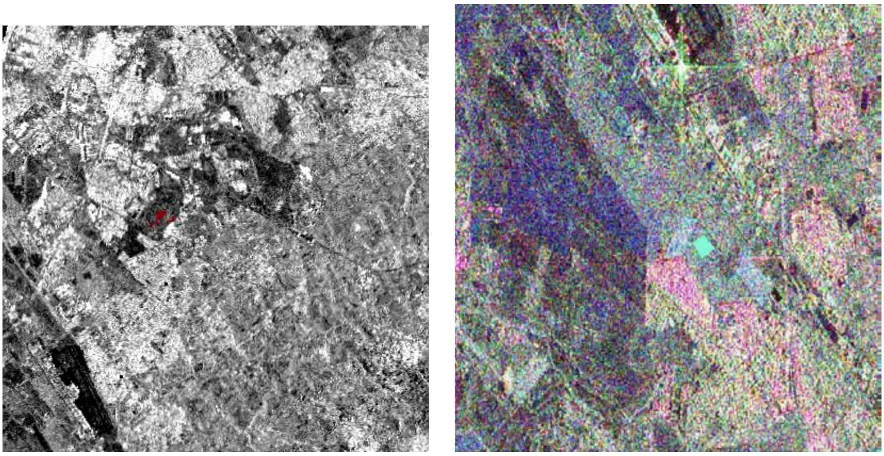

Ground Range Image | Pauli Decomposition

08.09.08 | 02.10.08

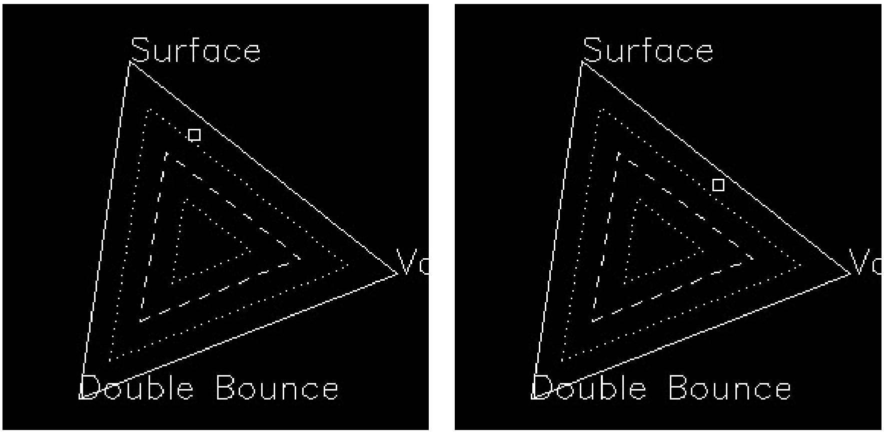

Scattering Mechanism | Scattering Mechanism

Figure 7.29: Grassland - Ciampino Zone. Scattering Mechanism

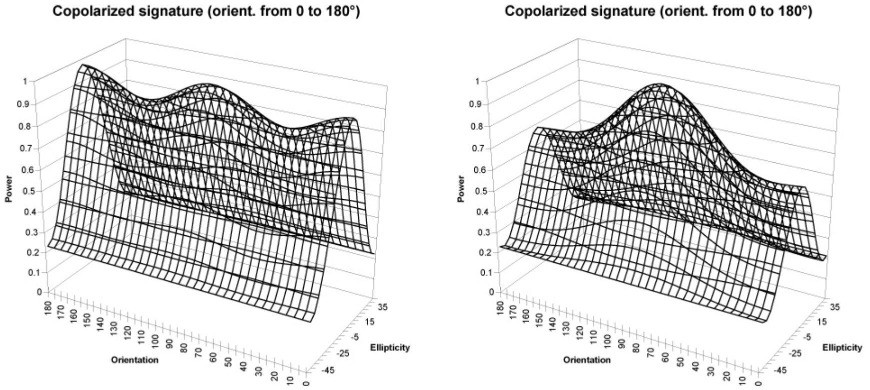

Copolarized Signature Copolarized Signature

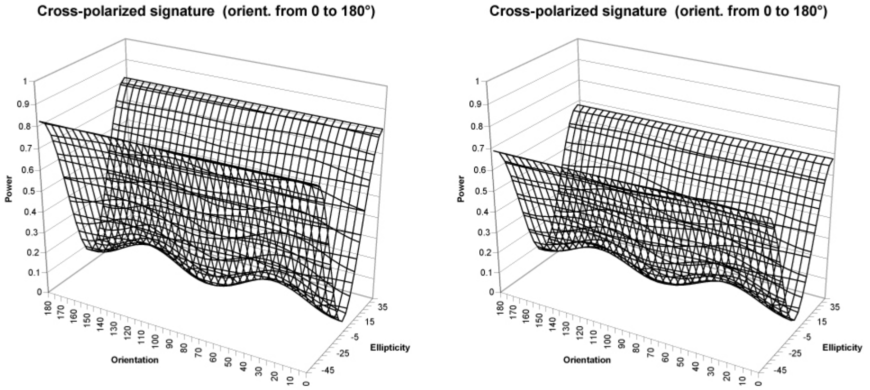

Cross Polarized Signature Cross Polarized Signature

Figure 7.30: Grassland - Ciampino Zone. Polarimetric Signature

Annex: Polarimetric Analysis of Shrubs

The analyzed parcel is :

1. Shrubs - Monte Cavo - Figure 7.31 and 7.32

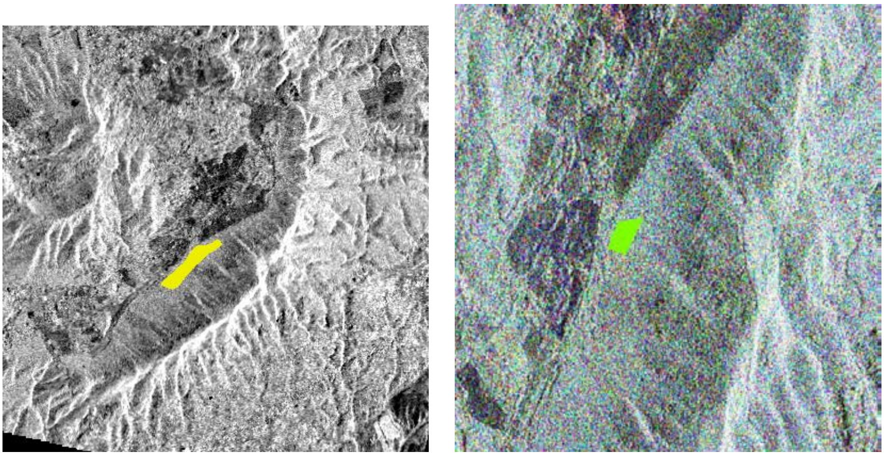

Ground Range Image

Pauli Decomposition

08.09.08

02.10.08

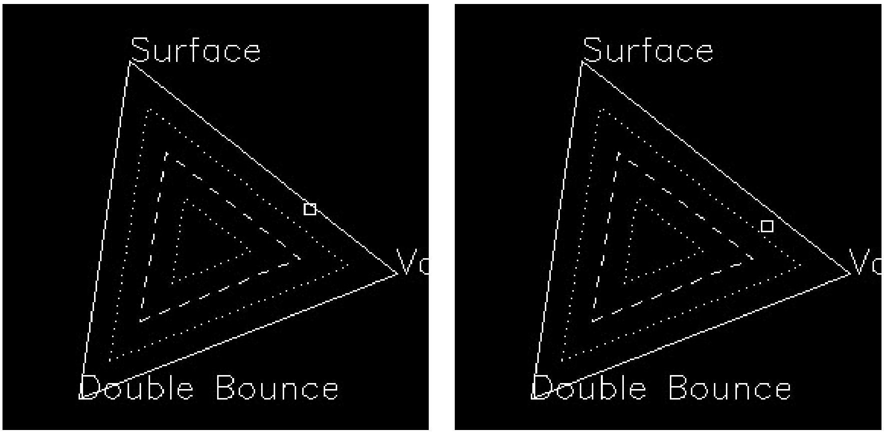

Scattering Mechanism

Scattering Mechanism

Figure 7.31: Shrubs - Monte Cavo. Scattering Mechanism

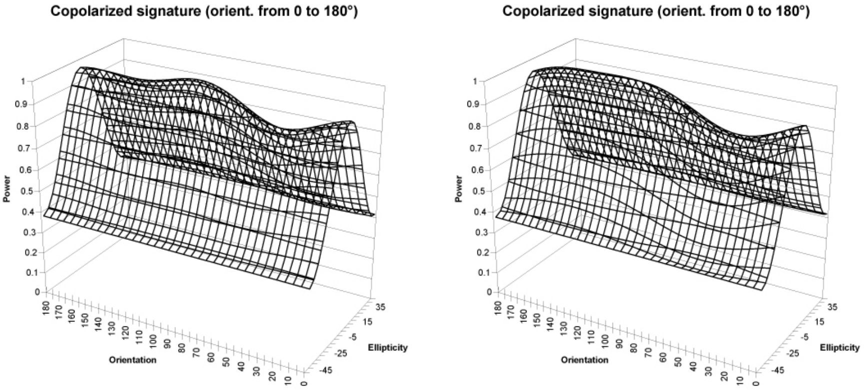

Copolarized Signature Copolarized Signature

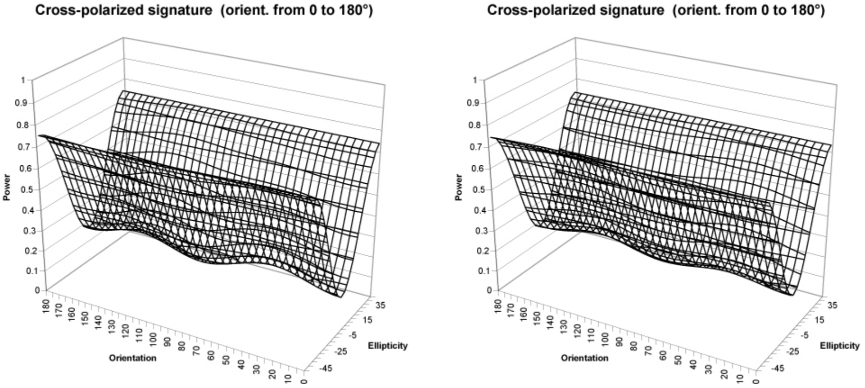

Cross Polarized Signature Cross Polarized Signature

Figure 7.32: Shrubs - Monte Cavo. Polarimetric Signature

Bibliography

Agriculture Committee, U. (2000). Agriculture glossary. Technical report, House Committee of Agriculture.

Arkun, S., Dunk, I., and Ranson, S. (2005). Hyperspectral remote sensing for vineyard management. *The Regional Institute Ltd.*

Baret, F. and Guyot, G. (1991). Potential and limits of vegetation indices for lai and apar assesment. *Remote Sensing of Environment*, 35:161–173.

Bobillet, W., Da Costa, J.-P., Germain, C., Lavialle, O., and Grenier (2003). Row detection in high resolution remote sensing images of vine fields. *European Conference on Precision Agriculture, Berlin*, 1:81–87.

Bracaglia, P., Ferrazzoli, P., and Guerriero, L. (1995). A fully polarimetric multiple scattering model for crops. *Remote Sensing of Environment*, 54:170–179.

Brancadoro, L. and Favilla, O. (2002). Un approccio sito-specifico alla coltivazione della vite. *L'informatore Agrario*, 1:22–45.

Brancadoro, L., Favilla, O., Dosso, P., and Serina, F. (2006). Use of satellite in precision viticulture: the franciacorta experience. *VI congrs international del Terrois Viticoles.*

Brisco, B. and Brown, R. (1998). *Manual of Remote Sensing*, volume 2, chapter 7, Agricultural Applications with Radar, page 393. F.M. Henderson and A.J. Lewis, Wiley,.

Brown, R., Brisco, B., Ahern, F., Bjerkelund, Manore, M., Pultz, T., and Singhroy, V. (1993). Sar application calibration requirements. *Canadian Journal of Remote Sensing*, 19:193–203.

Burini, A., Minchella, A., Del Frate, F., Fusco, L., Schiavon, G., and Solimini, D. (2006). Multi-temporal high resolution polarimetric L-band sar observation of a wine-producing landscape. In *Proceedings of IGARSS*. Denver, USA.

Burini, A., Minchella, A., and Solimini, D. (2005). Sar in agriculture: Sensitivity of backscattering to grapes. *Proceedings of IGARSS 2005, Seoul, Korea.*

Chanussot, J., Bas, P., and Lombrum, L. (2005). Airborne remote sensing if vineyards for detection of dead vine trees. *IEEE Transaction on Geoscience and Remote Sensing*, 44.

Cochrane, M. (2000). Using vegetation reflectance variability for species level classification of hyperspectral data. *International Journal of Remote Sensing*, 21:2075–2087.

Del Frate, F. and Solimini, D. (2004). On neural network algorithms for retrieving forest biomass from sar data. *IEEE Transaction on Geoscience and Remote Sensing*, 42:24–34.

Del Frate, F.and Schiavon, G., Solimini, D., Borgeaud, M., Hoekman, D., and Vissers, M. (2003). On the potential of multi-polarization and multi-temporal c-band sar data in classifying crops. In *IEEE International Geoscience and Remote Sensing Symposium*, pages 2195 – 2196.

Delenne, C., Rabatel, G., and Deshayes, M. (2008). An automatized frequency analysis for vine plot detection and delineation in remote sensing. *IEEE Geoscience and Remote Sensing Letters*, 5:341–345.

Della Vecchia, A., Ferrazzoli, P., Guerriero, L., Ninivaggi, L., Strozzi, T., and Wegmüller, U. (2008). Observing and modeling multifrequency scattering of maize during the whole growth cycle. *IEEE Trans. Geosci. Remote Sens.*, 46:3709–3718.

Dubois, P. C., Van Zyl, J. J., and Engman, T. (1995). Measuring soil moisture with imaging radars. *IEEE Transaction on Geoscience and Remote Sensing*, 33:915–926.

Ferrazzoli, P. (202). Sar for agriculture: Advances, problems and prospects. In *Proc. 3rd Int. Symp. on Retrieval of Bio- and Geophysical Parameters From SAR Data for Land Applications*, pages 47–56.

Ferrazzoli, P. and Guerriero, L. (1994). Interpretation and model analysis of maestro-1 flevoland data. *International Journal of Remote Sensing*, 15:2901–2916.

Ferrazzoli, P., Guerriero, L., and Schiavon, G. (1999). Experimental and model investigation on radar classification capability. *IEEE Transactions on Geoscience and Remote Sensing*, 37:960 – 968.

Ferrazzoli, P., Paloscia, S., Pampaloni, P., Schiavon, G., Sigismondi, S., and Solimini, D. (1997). The potential of multifrequency polarimetric sar in assessing agricultural and arboreous biomass. *IEEE Transaction on Geoscience and Remote Sensing*, 35:5–17.

Fiset, R. and Farhat, M. (2001). A low-cost polarimetric response tool using spreadsheets. In *Geoscience and Remote Sensing Symposium*, pages 1625–1627.

Freeland, R., Yoder, R., Ammons, J., and Leonard, L. (2002). Integration of real-time global positioning with ground-penetrating radar surveys. *Applied Engineering in Agriculture*, 18:647650.

Freeman, A. and Durden, S. (1998). A three-component scattering model for polarimetric sar data. *IEEE Transactions on Geoscience and Remote Sensing*, 36:963–973.

Hall, A., Louis, J., and Lamb, D. (2003). Characterising and mapping vineyard canopy using high-spatial-resolution aerial multispectral images. *Computers and Geosciences*, 29:813822.

Horn, R. (2005a). Bacchus-doc radar and optical campaign, data acquisition report. Technical report, ESA/ESRIN.

Horn, R. (2005b). Bacchus-doc radar and optical campaign, experiment plan. Technical report, ESA/ESRIN.

Huisman, S., Hubbard, S., D., R., and Annan, P. (2003). Monitoring soil water content with ground-penetrating radar: A review. *Vadose Zone Journal*, 2:476–491.

ITRES, R. L. (1996). Compact airborne spectrographic imager software manual. Technical report, ITRES technology.

Johannsen, C. (1996). Overview of precision farming. *Proceedings of Information Ag Conference*, 1:53–54.

Johnson, F. (2004). Toward the improved use of remote sensing and process modeling in california's premium industry. *Internet web page.*

Johnson, L., Herwitza, S.and Dunagana, S., Lobitza, B., Sullivana, D., and Slyea, R. (2003). Collection of ultra high spatial and spectral resolution image data over california vineyards with a small uav. *International Symposium on Remote Sensing of Environment.*

Johnson, L. and Pierce, L. (2003). Image-based decision tools for vineyard management. In *ASAE Annual International Meeting.* ASAE.

Johnson, L. F., Roczen, D., and Youkhana, S. K. (2004). Mapping vineyard leaf area with multispectral satellite imagery. *Computers and Electronics in Agriculture*, 38:33–34.

Johnson, R., Glasscum, R., and Wojtasinski, R. (1982). Application of ground penetrating radar to soil survey. *Soil Survey Horizons*, 23:1725.

Kamp, D. and Lynch, D. (2008). *The Wine's Dictonary*, volume 1, pages 125–141. Broadway.

Kitchen, N., Sudduth, K., Birrell, S., and Borgelt, S. (1996). Missouri precision agriculture research and education. *Proceedings of the 3rd International Conference on Precision Agriculture*, 1:1091–1100.

Knight, R. (2001). Ground penetrating radar for environmental applications. *Annual Review Earth Planet*, 29:229–280.

Krasnopolsky, V. M. and Schiller, H. (2003). Some neural network applications in environmental sciences. part i: Forward and inverse problems in geophysical remote measurements. *Elsevier Science Ltd.*

Lewis, A., McNeill, S., and Fowler, A. (1999). Interpretation of almaz-1 a sar imagery of the wairarapa, new zealand. *Geocarto Int.*, 14:77–78.

Mariani, L., Failla, O., Del Monte, G., and Facchinetti, D. (2007). Iphen, a model for real time production of grapevine phenological maps. In *Congress on Climate and Viticulture*, pages 272–278.

Mattia, F., Le Toan, T., Souyris, J. C., De Carolis, G., Floury, N., Posa, F., and Pasquariello, G. (1997). The effect of surface roughness on multifrequency polarimetric sar data. *IEEE Transaction on Geoscience and Remote Sensing*, 35:954966.

Moran, M., Inoue, Y., and Groeneveld, D. (1997). Opportunities and limitations for image-based remote sensing in precision crop management. *Remote Sensing of the Environment.*

More, J. J., Garbow, B. S., and Hillstrom, K. E. (1980). User guide for minpack-1. Technical report, Argonne National Lab.

Pearson, R., Grace, J., , and May, G. (1997a). Real-time airborne agricultural monitoring. *Remote Sensing of the Environment*, 44:271–290.

Pearson, R., Grace, J., , and May, G. (1997b). Real-time airborne agricultural monitoring. *Remote Sensing of the Environment*, 44:271–290.

Persaud, N., Gandah, M., and Ouattara, M. (1993). Estimating leaf area of pearl millet from linear measurements. *Agronomy Journal*, 85:10–12.

Pierce, F. and Nowak, P. (2000). Aspects of precision agriculture. advances in agronomy. *The agronomist*, 67:1–85.

Rosenqvist, A., Shimada, M., and Watanabe, M. (2004). Alos palsar: Technical outline and mission concepts. In *4^{th} International Symposium on Retrieval of Bio- and Geophysical Parameters from SAR Data for Land Applications*, pages 1–7.

Rubin, Y., Grote, K., and Hubbard, S. (2002). Mapping the volumetric soil water content of a california vineyard using high-frequency gpr ground wave data. *The Leading Edge*, 21:552–559.

Rubin, Y., Williams, K., Hubbard, S., and Peterson, J. (2005). Environmental and agricultural applications of gpr. *International Workshop on Ground Penetrating Radar.*

Springer, M. D. and Thompson, W. E. (1970). The distribution of products of beta, gamma and gaussian random variables. *Society for Industrial and Applied Mathematics.*

Srinivasan, A. (2006). Handbook of precision agriculture :principles and applications. *Food Products Pres*, 1:3–15.

Toan, T. L., Ribbes, F., Wang, L.-F., Floury, N., Ding, K.-H., Kong, J. A., Fujita, M., and Kurosu, T. (1997). Rice crop mapping and monitoring using ers-1 data based on experiment and modeling results. *IEEE Trans.Geosci. Remote Sens.*, 35:41–56.

Ulaby, F., Allen, C., Eger, G., and Kanemasu, E. (1984). Relating the microwave backscattering coefficient to leaf area index. *Remote Sensing of Environment*, 14:113–134.

Ulaby, F. and Dobson, M. (1989). *Handbook of Radar Scattering Statistic for Terrain*, pages 119–353. Artech House Publishers.

Ulaby, F. and Elachi, C. (1990). *Radar Polarimetry for Geoscience Application*, pages 10–45. Artech House.

Ulander, L. and Le Toan, T. (1999). Bragg-scattering resonance in vhf-sar forestry data. *IEEE Transaction on Geoscience and Remote Sensing*, 6:1886 – 1890.

Wassenaar, T., Andrieux, P., Baret, F., and Robbez-Masson, J. (2002). Vineyard identification and description of spatial crop structure by per-field frequency analysis. *International Journal of Remote Sensing*, 23:33113325.

Wassenaar, T., Andrieux, P., Baret, F., and Robbez-Masson, J. (2005). Soil surface infiltration capacity classification based on the bi-directional reflectance distribution function sampled by aerial photographs. the case of vineyards in a mediterranean area. *Catena*, 62:94–100.

Whitt, M. W. and Ulaby, F. T. (1994). Radar response of periodic vegetation canopies. *International Journal of Remote Sensing*, 15:1813 – 1848.

Williams, M. (2006). A coherent, polarimetric sar simulation of forests for polsarpro. Technical report, ESA.

Winkler, A. (1958). The ralation of lead area and climate to vine performance and grape quality. *Am. J. Enol. Viticulture*, 9:10–23.

Curriculum Vitae

ALESSANDRO BURINI

Work Experience

- From December 2008 to Present - CEOS ESA Cal/Val Portal Manager
  - Review of technical and scientific content (Sensors description, in-situ data, satellite data, documentation, information)
  - Coordination of the Calibration and Validation teams in order to support their projects with the portal and to promote the portal To gather requirements for optimization
  - Calibration Tool development
  - Collaboration with CEOS
- From March 2005 to December 2008 - Remote Sensing Engineer
  - Automatic Land Cover Products (Pixel Based and Object Oriented) by SPOT5, Ikonos, QuickBird, Landsat,Meris and MODIS Data
  - Object extraction and Recognition
  - Web Services for Precision Farming by Satellite Data and Ground Sensors
  - Multi-temporal change detection technique

  - Ship Detection and Monitoring, Neural Detection of Oil Spill (ERS 1-2, Envisat, RADARSAT-2)
  - Classification and Parameters Retrieval (L-C and X Band. ALOS, ERS/ENVISAT, TerraSAR-X/COSMO)
  - Neural Networks for retrieving vertical ozone profiles by GOME and SCIAMACHY data. Production of local concentration maps and global monitoring
  - Neural Network design and implementation for Remote Sensing

Education

- June 2009, Geoinformation PhD at University “Tor Vergata” of Rome.
- February 2005, MS degree in Telecommunications Engineering at University of Rome “Tor Vergata”, *magna cum laude.*
- November 2002, BS degree in Telecommunications Engineering at University of Rome “Tor Vergata”, *magna cum laude.*

List of Publications

- **A. Burini**, A. Minchella, D. Solimini, "SAR in agriculture: Sensitivity of Backscattering to Grapes", *Proc. IGARSS' 05*, Seoul, Korea, 2005

- **A. Burini**, F. Del Frate,A. Minchella, G. Schiavon,D. Solimini, R. Bianchi, L. Fusco, R. Horn, "Multi-Temporal High-Resolution Polarimetric L-Band SAR observation of a wine-producing landscape" , *Proc. IGARSS' 06*, Denver, USA, 2006

- **A. Burini**, F. Del Frate, A. Minchella, G. Schiavon, L. Fusco, D. Solimini, "Da immagini SAR informazioni per la viticoltura", *Mondo GIS*, Italy, Dic. 2006

- P. Sellitto, **A. Burini**, F. Del Frate, S. Casadio, "Neural Networks Algorithms for Ozone Profiles Retrieval from Satellite Measurements: Analysis with ESA-Envisat SCIAMACHY and NASA-Aura OMI data", *European Geosciences Union General Assembly 2007*, Wien, Austria, 2007

- P. Sellitto, F. Del Frate, **A. Burini**, "Neural Network Algorithms for the retrieva of Ozone Concentration Profiles from ENVISAT-SCIAMACHY measurements", *Envisat Symposium 2007*, Montreux, Switzerland, 2007

- P. Sellitto, **A. Burini**, F. Del Frate, S. Casadio, "Dedicated Neural Networks Algorithms for Direct Estimation of Tropospheric Ozone from Satellite Measurements", *Proc. IGARSS' 07*, Barcelona, Spain, 2007

- **A. Burini**, G. Schiavon, D. Solimini,"Sensitivity of multi-temporal high resolution polarimetric C and L-band SAR to grapes in vineyards", *Proc. IGARSS' 07*, Barcelona,Spain, 2007

- F. Pacifici, **A. Burini**, F. Del Frate, D. Solimini,"Urban land cover classification: potential of high and very-high resolution SAR imagery", *Proc. IGARSS' 07*, Barcelona,Spain, 2007

- **A. Burini**, C. Putignano, F. Del Frate, M. Del Greco, G. Schiavon, D. Solimini, "A neural approach for unsupervised classification of very-high resolution polarimetric SAR data", *Proc. IGARSS' 07*, Barcelona, Spain, 2007.

- **A. Burini**, G. Schiavon, D. Solimini, "Sensitivity of multi-temporal high-resolution polarimetric L-band SAR to grapes in vineyards", *5th International Symposium on Retrieval of Bio- and Geophysical Parameters from SAR Data for Land Applications*,Bari, Italy, 2007

- C. Putignano, **A. Burini**, F. Del Frate, D. Iasillo, G. Signorile, "Produzione di mappe tematiche da dati satellitari:integrazione tra metodologie neurali e ad oggetti", *11^a Conferenza Nazionale ASITA*, Torino, Italy, 2007

- **A. Burini**, C. Putignano, F. Del Frate, G. Licciardi, C. Pratola, G. Schiavon, D. Solimini, "TerraSAR-X/SPOT-5 fused images for supervised land cover classification", *Proc. IGARSS'08*, Boston , USA, 2008

- **A . Burini**, C. Putignano, F. Del Frate, M. Lazzarini, G. Licciardi, G. Schiavon, D. Solimini, F. De Biasi, P. Manunta, "TerraSAR-X imaging for unsupervised land cover classification and fire mapping", *Proc. IGARSS'08*, Boston , USA, 2008

- **A. Burini**, G. Schiavon, D. Solimini, "Fusion of high resolution polarimetric SAR and Multi-Spectral Optical Data for precision Viticulture", *Proc. IGARSS'08*, Boston , USA, 2008

- **A. Burini**, C. Solimini, R. Cossu, L. Fusco, D. Solimini, S. Argentini, "Solar Radiance estimation by means of Meteosat 2^{nd} generation and Neural Processing: a vineyard precision farming case", *Proc. IGARSS'08*, Boston , USA, 2008

- **A. Burini**, G. Schiavon, D. Solimini, "Near Real-Time Polarimetric C-Band SAR Observations of Vineyards: RADARSAT-2 watching the Italian Frascati wine area", *Proc. of PolInSar 2008*, ESRIN, Frascati, 2008

- C. Putignano, **A. Burini**, F. Del Frate, G. Schiavon and D. Solimini, "Very-High Resolution X-band SAR data for linear features extraction and classification", *Proc. of PolInSar 2008*, ESRIN, Frascati, 2008

- G. Schiavon, **A. Burini** and D. Solimini, "RADARSAT-2: Main Features and Near Real-Time Applications", *Proc. of EURAD 2009*, Rome, 2009

List of Tables

List of Figures